Mixed Matrix Membranes Consisting of Porous Polyimide Networks and Polymers of Intrinsic Microporosity for Gas Separation

A thesis submitted to the University of Manchester for the degree of Doctor of Philosophy in the Faculty of Science and Engineering

2016

Bann Dawood

School of Chemistry

Contents

List of Figures

List of Tables

List of Abbreviations

ATR-IR	Attenuated Total Reflectance-Infrared Spectroscopy
BET	Brunauer-Emmet-Teller
$CHCl_3$	Chloroform
CMP	Conjugated Microporous Polymers
COF	Covalent Organic Frameworks
D	Diffusion Coefficient
DMAc	Dimethyl Acetamide
DMF	Dimethylformamide
DMSO	Dimethylsulfoxide
EtOH	Ethanol
GPC	Gel Permeation Chromatography
HCP	Hypercrosslinked Polymers
IUPAC	International Union of Pure and Applied Chemistry
MeOH	Methanol
MMMs	Mixed Matrix Membranes
Mn	Number Average Molecular Weight Distribution
MOFs	Metal Organic Frameworks
Mw	Weight Average Molecular Weight Distribution
NMR	Nuclear Magnetic Resonance
P	Permeability Coefficient
PAF	Polyaromatic Frameworks
PDI	Polydispersity Index
PIM	Polymers of Intrinsic Microporosity
S	Solubility Coefficient
TFTN	Tetrafluoroteranapthylonitrile
TGA	Thermogravimetric Analysis
THF	Tetrahydrofuran
THSBI	5,5’,6,6’-tetrahydroxy-3,3,3’,3’-tetramethyl-1,1’-spirobisindane

Abstract

The University of Manchester

Bann Dawood

Doctor of Philosophy

Mixed Matrix Membranes Consisting of Porous Polyimide Networks and Polymers of Intrinsic Microporosity for Gas Separation

2016

This research aimed to develop the fabrication of mixed matrix membranes (MMMs) utilizing a polymer of intrinsic microporosity (PIM-1) with porous polyimide networks, and to explore their effect on gas transport properties. PIM-1 has been chosen as polymer matrix for its high surface area and high sorption of gases. It is also considered as interesting candidate for membrane gas separation. PIM-1 has been synthesized successfully using high temperature methods (40 min, 160 ^{o}C) and low temperature methods (72 h, 65 ^{o}C). Porous polyimide networks have been chosen as organic fillers as they have good chemical affinity to polymer matrix and can adhere much better than inorganic fillers. MPN-1 and MPN-2 were synthesized by condensation polymerization of A_2 (dianhydride) and B_4 (tetraamino). The polymer matrix (PIM-1) and network polyimide fillers were characterized using various characterization techniques, including FTIR, NMR spectroscopy, TGA and N_2 sorption analysis.

MMMs were fabricated successfully utilizing PIM-1 with 10, 20, and 30wt. % loadings of fillers. The MMMs prepared were homogenous on a macroscale. They characterized using different techniques, such as FTIR spectroscopy, powder x-ray diffraction, and scanning electron microscopy. The gas transport properties of MMMs were obtained using a time lag method. The treatment of MMMs with alcohol showed an increase in the permeability and diffusivity of gases. We aimed in this research to increase solubility of microporous polyimide network (MPN-1) by decreasing the extent of network structure. Different strategies have been utilized. First, using different molar ratios and second, using end-capping modification. The polymers were characterized using various techniques, including FTIR, NMR spectroscopy and TGA. Following this, their CO_2 uptake and solubility are also examined.

Declaration

No portion of the work referred to in the thesis has been submitted in support of an application for another degree or qualification of this or any other university or other institute of learning.

Copyright Statement

Acknowledgements

First of all I would like to thank my supervisor Prof. Peter Budd for your help and guidance over the years. I would like to have a special thanks to my sponsor, Kurdistan Region-Iraq, for funding during my PhD.

I would like to extend my gratitude to Dr. Johannes Jansen, Dr. Paola Bernardo, Dr. Gabriele Clarizia at ITM for providing the permeability measurements and to all technicians in the University of Manchester.

I would like to show my greatest appreciation to Muhanned Khdhayyer, Khaled Althumari and Raghidah Wagia for their friendship and words of encouragement.

All Prof. Budd Group have been extraordinarily helpful and supportive, Dr. Wayne Harrison, Dr. Rupesh Bhavsar, Lei Gao, Bekir Satilmis, Peter Youle, Rebecca Dey, Tom Raine, Nosheen, Bahare and Hosna. I owe my deepest gratitude for their support and encouragement.

My mum and all my family support encouragement and prayers were invaluable during my PhD time.

About the Author

Bann was born in Iraq and graduated in Chemistry (BSc) from Mosul University. Then, she did an MSc course in industrial chemistry at the same university in 2007. She started her PhD at Manchester University in 2012.

Chapter 1
Introduction

1.1 Aim and Objectives

Aim

The aim of this research is to develop nanocomposite membranes constituting of porous network polyimides (PNPs) in polymer of intrinsic microporosity (PIM-1), in order to enhance permeability and selectivity for gas separations. The aim of this work will be achieved through the following objectives:

Objectives

1. Synthesis and characterization of polymer matrix, PIM-1, (chapter 2)

2. Synthesis and characterization of porous network polyimides as dispersed phases (chapter 3).

3. Synthesis and characterization of PIM-1 membrane and PIM-1/PNPs mixed matrix membranes with various loadings of the fillers. (Chapter 4)

4. Investigate gas transport behaviour of PIM-1 and nanocomposite membranes (chapter 4)

5. Investigate using end capper in order to reduce the extent of network formation, by creating hyperbranched polyimides (chapter 5)

1.2 Carbon dioxide Separation Processes

Increasing the emission of carbon dioxide in the environment leads to global warming, which is considered as one of the major environmental problems that the world faces today.[1] Carbon dioxide comprises about 80% of greenhouse gases which absorb infrared radiation causing an increase in the earth's temperature. It is reported that CO_2 emissions which are produced from industry and power plants using fossil fuels are increasing, owing to a considerable expansion in the production of natural gas as an effective and environmentally clean fuel supply.[2] Many industrial separation processes are utilized to capture CO_2, which are listed below.

1.2.1 Cryogenic Process

Cryogenic separation is also known as low temperature distillation which utilizes a very low temperature to purify gas mixtures in the separation process. The main industrial application of the cryogenic process is separation and purification of gases. It is used to separate CO_2 from other gases through controlling the pressure and temperature, which results in solid or liquid CO_2, and also other contaminants are separated in the process.[3]

The cryogenic process has advantages of producing a liquid CO_2 ready for transportation by pipeline. On the other hand, the major problems of this method are the amount of energy that are required in cooling and the necessity to remove components that have freezing points over normal operating temperature to avoid freezing and blockage in the equipment.[4]

1.2.2 Absorption Process

Absorption is a unit process in which a gas mixture is contacted with the proper liquid, aiming to achieve preferential dissolving of one or more of the gas components. Therefore, these components are removed or partially removed from the

gas into the liquid. The solutes may either react chemically or physically with the liquid.[5]

Generally, absorption processes can be classified into two main classes. A chemical absorption process is one in which the solvent reacts chemically with dissolved gas.[6] the binding between sorbent and CO_2 molecules is strong and this can offer a fast and an efficient removal of most CO_2 in one stage of absorption. On the other hand, the strong binding between CO_2 and the sorbent molecules is considered as one of the reasons for high regeneration energy requirement. Another problem is controlling the impurities and minor components in the flue gas, involving SO_2, oxygen, etc., which may cause degradation of the sorbents. Finally, many sorbents are corrosive; in this case only diluted solutions can be used. Many basic sorbents are used to absorb CO_2 from flue gas such as alkali carbonate, aqueous ammonia and alkanolmines.[7]

Alkanolamines are utilized widely as absorbents for CO_2 capture. The structure of alkanolamines involves primary, secondary and ternary amines which have at least one OH and amine group, such as monoethanolamine (MEA) diethanolamine (DEA) and N-methlydiethanolamine (MDEA).[8]

The second class is physical absorption processes in which the solvent reacts physically with the dissolved gas. In physical absorption, the solvent is used as an absorbent with thermodynamic properties in which CO_2 is preferably absorbed over the other components of the gas mixture.[6] In physical absorption the interaction between CO_2 molecules and the absorbent molecules is weaker as compared to chemical absorption, reducing the requirement for energy on regeneration.[1] Physical Absorption occurs at high CO_2 partial pressure. As such, the main energy requirement is originated from flue gas pressurization. Therefore, physical absorption is not economic for gas streams when the partial pressure of CO_2 is less than 15 vol. %. The typical solvents that are used in physical absorption are Selexol (dimethyl ethers of polyethylene glycerol) and Restisol (methanol).[9]

1.2.3 Adsorption Process

Adsorption is a physical process which involves the attachment of a gas or liquid to a solid surface, [10] by either chemical or physical attraction.[11] Solid adsorbents such as activated carbon, zeolite and meso-porous silicates, alumina, metal oxides are used for gas separation.[12] In CO_2 capture by an adsorption process, a packed column is filled by a spherical adsorbent bed and a stream bearing CO_2 is passed through the column. CO_2 is attracted to the adsorbent and attached on its surface. After reaching equilibrium between the adsorbent phase and gas phase, desorption takes place to get a pure form of CO_2 and regenerated adsorbent can be used for further adsorption cycle.[13] Consequently, adsorptive separation process is composed of a cyclic sequence of adsorption and desorption steps.[14] Based on regeneration method, adsorption processes can be divided into pressure swing adsorption and temperature swing adsorption.

1.2.3.1 Temperature Swing Adsorption (TSA)

Thermal swing temperature adsorption process is widely utilized for purification processes like drying or removing of CO_2 from natural gas. In TSA, desorption is achieved by increasing the temperature of the adsorbent bed, either by applying a heat or by purging with hot purge gas. Thermal swing adsorption is very effective to separate minor components. The disadvantages of the TSA process is the adsorption cycle time which is required to cool down the bed. Other problems are the high energy requirement and large heat loss.[1]

1.2.3.2 Pressure Swing Adsorption (PSA)

Pressure swing adsorption is a well-established process for gas separation. The PSA process is recognized for CO_2 separation from gas streams containing methane. The separation of CO_2 from natural gas streams rely on materials with selective adsorption to CO_2 by difference in equilibrium capacities or by variations in uptake rates.[1]

In PSA, the gas mixtures flows through bed at high pressure and low temperature until the adsorption of CO_2 approaches the equilibrium condition at the exit bed. The

beds are then regenerated by stopping the flow of the feed mixture, decreasing the pressure, [13] which can be achieved either by using depressurization or by evacuation or by combination of both.[1]

1.3 Liquid Separation Processes

Recently, Biofuels have gained an attention in the industry as an emerging alternative to fossil energy sources.[15] Biofuels are of great importance as they replace petroleum fuels and they can be utilized as an alternative to fossil fuels for generation heat, power and chemicals. Additionally, they have many advantages for the environment, economy and consumers.[16] Biofuels are composed of biodiesel, bioalcohols, biogas and other minor components.[17] Bioalcohols (such as bioethanol and biobutanol) have been considered as a promising candidate to substitute fossil fuels. Many separation processes have been utilized to separate bioalcohol. Distillation is the most common process which is used to separate multi-component mixtures in chemical processes. Separation is based on the difference in the boiling points of the components. Nevertheless, the distillation process has disadvantages, which involve large scale equipment and low energy efficiency. Furthermore, the separation efficiency of a distillation process is restricted by the thermodynamic vapour-liquid equilibrium. The traditional distillation process is unable alone to produce fuel grade alcohols due to formation of zeotropic mixtures. Therefore, separation processes like ternary distillation, vacuum distillation and molecular sieve sorption are used in dehydration of bioalcohols in order to cope with the limitation of zeotropic mixtures.[18]

1.4 Membrane Technology

Membrane technology is a novel and promising separation process which is used widely, [19] in chemical, biochemical and food industries, [18] owing to its low energy consumption, simplicity, effectiveness, [19] high performance compared to traditional separation processes, [20] and high selectivity of separating materials.[21] A membrane can be defined as a permselective barrier between two phases, as is shown in Figure 1-1.

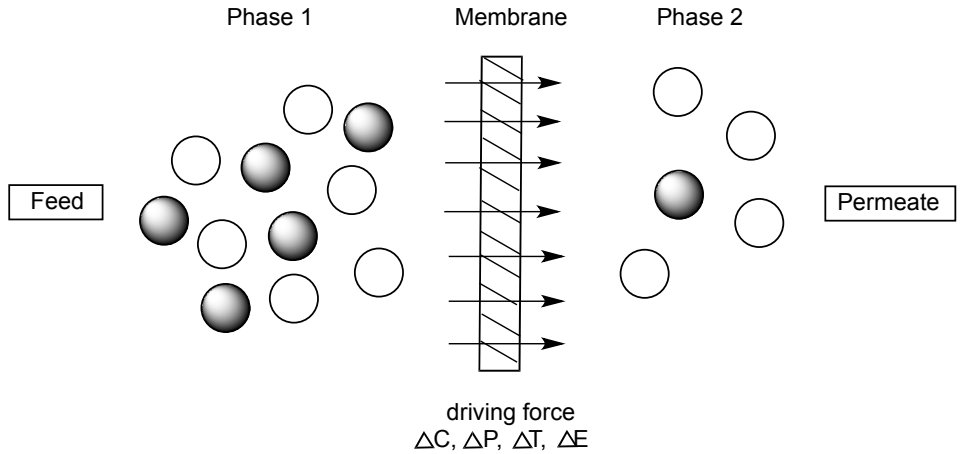

Figure 1-1: A schematic of two phases separated by membrane.[22]

Phase 1 is considered as a feed or upstream side of membrane whereas phase 2 is considered as a permeate or downstream side. Separation is accomplished as the membrane can transport one component from the feed mixture more easily than other components. Transport can be achieved by creating a driving force across the membrane, which might be a difference in concentration, pressure, temperature or electrical field.[22]

1.4.1 Membrane Separation Processes

One of the major problems in the chemical industry is separation, concentration and purification of the chemical species.[23] Over 50% of energy costs in the chemical industry are utilized to separate gaseous or liquid mixture.[24] Membrane separation processes offer many advantages over traditional separation processes, as they can be faster, more effective and more economic.[23] Membrane separation processes can be divided into three groups based on their separation properties.

1. Ultrafiltration and microfiltration utilize the size of solutes for separation the particles by a sieving action. The driving force is the difference in pressure. The pore size of membranes are used in ultrafiltration range from 1 to 50 nm, whereas in microfiltration the pore size ranging between 0.05 to 10μm.

2. Reverse osmosis, gas separation and pervaporation are associated with a dense membrane structure; the pore size is less than 1 nm. The separation is based on the difference in affinity between the feed components and the membrane, and also of the

difference in the diffusivity of components through membrane. The driving force of reverse osmosis and gas separation is a pressure difference and of pervaporation the driving force is the concentration gradient.

3. Electrodialysis uses anion and cation selective membrane for separation charged particles from uncharged ones. The ions can be transported through membrane by a diffusion mechanism which results by applying a potential difference.[25]

1.5 Pervaporation

Pervaporation is a membrane separation process which can be utilized for separation of liquid mixtures, [26] by partial vaporization through a dense membrane.[21] The term pervaporation is derived from two major integral operations which are involved in the separation process, namely, permeation and evaporation, because the feed is a liquid and the vapour permeates on the other side of membrane as shown in Figure 1-2.[27]

In pervaporation, the liquid feed is placed in a direct contact with one side of membrane, while the permeate is evolved in a vapour phase on the other side of membrane. Separation is achieved by applying a difference in partial pressure across the membrane by using either a vacuum pump or by sweeping an inert gas to decrease the total pressure on the permeate side of membrane.[21] Then the vapour is condensed and collected or can be released as desired.[28]

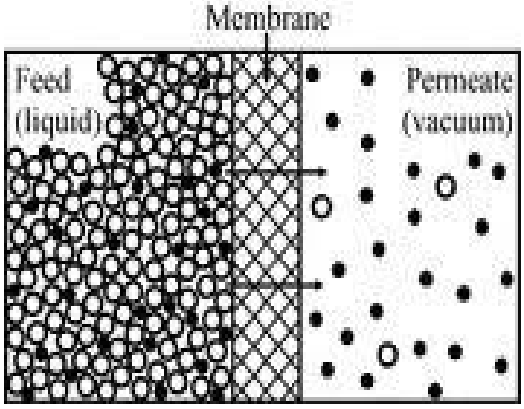

Figure 1-2: Overview of pervaporation across the membrane.[27]

1.5.1 Mass Transport in Pervaporation

The mass transport in pervaporation is usually described by the solution-diffusion model; according to this mechanism transport of components through membrane consists of three consecutive steps:

1. Sorption of component from the feed liquid to the upstream side of membrane.

2. Diffusion of the component through the membrane.

3. Desorption of the component under the low pressure to the downstream side of membrane. Hence, the permeability is a function of both solubility and diffusivity through the membrane.

Therefore, membrane selectivity is influenced by both the solubility (which is a thermodynamic property) and diffusivity (which is a kinetic property). The solubility of a compound is determined by the interaction of permeant-membrane, while the diffusivity is governed by the molecular size, shape, and the mass of permeant. When both the sorption and diffusion favour a given compound. As a result, very high pervaporation selectivity for this component can be achieved.[29]

1.5.2 Performance of Pervaporation Membrane

Pervaporation is considered as a rate-controlled separation process. In order to improve pervaporation membranes, three issues should be taken into account:

1. Membrane productivity

2. Membrane selectivity

3. Membrane stability

Membrane productivity is a measure of the quantity of a component which is permeated through a specific area of membrane in a given unit of time. Membrane productivity is determined by permeation flux, J, which relies on both intrinsic permeability and the effective thickness of membrane.

Membrane selectivity is characterized by separation factor which is defined as:

$\alpha = (Y/1-Y)\ (1-X/X)$

Where X and Y are the molar fractions of the more permeable component in the feed and permeate respectively.

Membrane stability is described as the capability of a membrane to maintain both selectivity and permeability under specific system conditions for an extended period of time. Membrane stability is influenced by the chemical, mechanical and thermal properties of the membrane.[30]

1.5.3 Pervaporation Membranes

The choice of membranes for pervaporation process is dependent on the liquid mixture. Membrane performance is characterized by the degree of separation of liquid mixtures and on the permeation rate (flux). Pervaporation membranes can be divided into three groups according to the nature of separation. Hydrophilic membranes are utilized to separate water from organic solutions. This kind of membrane is made of polymers having glass transition temperatures above room temperature. Polyvinyl alcohol (PVA) is an example of a hydrophilic membrane. Organophilic membranes are used to recover organics from solutions and typically are made of elastomer polymers which have glass transition temperatures below room temperature such as nitrile, butadiene rubber and styrene butadiene rubber.[31] Organo-selective membranes are utilized to separate different organic compounds from each other and most of their applications have been found in the separation of aromatics from aliphatic or in isomer separation.[32]

1.6 Porous Materials

Porous materials can be defined as solids which comprise of cavities, channels or interstices[33]. In general, porous materials occupy porosity (volume ratio of pore size to the total volume of the material) between 0.2-0.95. Pores are categorized into two main types: open pores which are connected to the surface of the material, and closed pores which are separated from the outside. Open pores are required in the separation,

catalysis, filtration and membrane applications. Whereas, closed pores are helpful in sonic and thermal insulation applications. Pores can be found in various shapes and morphology such as spherical, cylindrical and slit types. They can also have complex shapes like hexagonal shape. It can also be straight or curved or with different turns and twists, resulting in high tortuosity.[34] According to the International Union and Applied chemistry (IUPAC), pores can be classified based on their size into three categories:micropores which have width below 2 nm, mesopores with width between 2 and 50 nm and macropores have width greater than 50 nm.[33, 34]

1.7 Adsorption

Gas adsorption measurements are utilized for characterization a wide range of porous materials.[33] Adsorption can be defined as the enrichment of one or more of the components in an interfacial layer. It can be divided into chemical and physical adsorption based on the strength of interaction. Chemical adsorption arises through the formation of strong chemical bond between the surface of adsorbent and the sorbate molecule. Whereas, physical adsorption occurs when an adsorbate gas is brought into contact with the surface of the solid adsorbent. Physisorption is utilized for characterization of the surface area and pore size distribution of porous materials.[35] There are six types of adsorption isotherm as is shown in Figure 1-3. These isotherms are necessary as they provide an important information about the pore structure of the adsorbent.[36] Type I isotherm is concave to the P/P_o axis and the adsorbed amount approaches a limiting value as $P/P_o \rightarrow 1$.[35, 36] The type I isotherm is seen for microporous materials.[36] While, type II can be seen for nonporous or macro adsorbent as unrestricted monolayer-multilayer adsorption can be obtained. Point B confirms the completion of monolayer adsorption and beginning the adsorption of multilayer. Type III isotherm is convex to the P/Po axis. This type of adsorption isotherm is not common and on the contrary of type II isotherm, point B is not present due to weak adsorbate-adsorbent interactions. Type IV adsorption isotherm is obtained for mesoporous materials. The first type of isotherm is related to monolayer-multilayer adsorption similar to type I isotherm. The hysteresis loop of type IV isotherm can be attributed to the occurrence of pore condensation. Type V isotherm presents both pore condensation and hysteresis. The initial part of adsorption isotherm is similar to type III isotherm, implying weak adsorbent-adsorbate interactions. Type

VI is a different case, representing stepwise multilayer adsorption on a uniform, non-porous surface.[35]

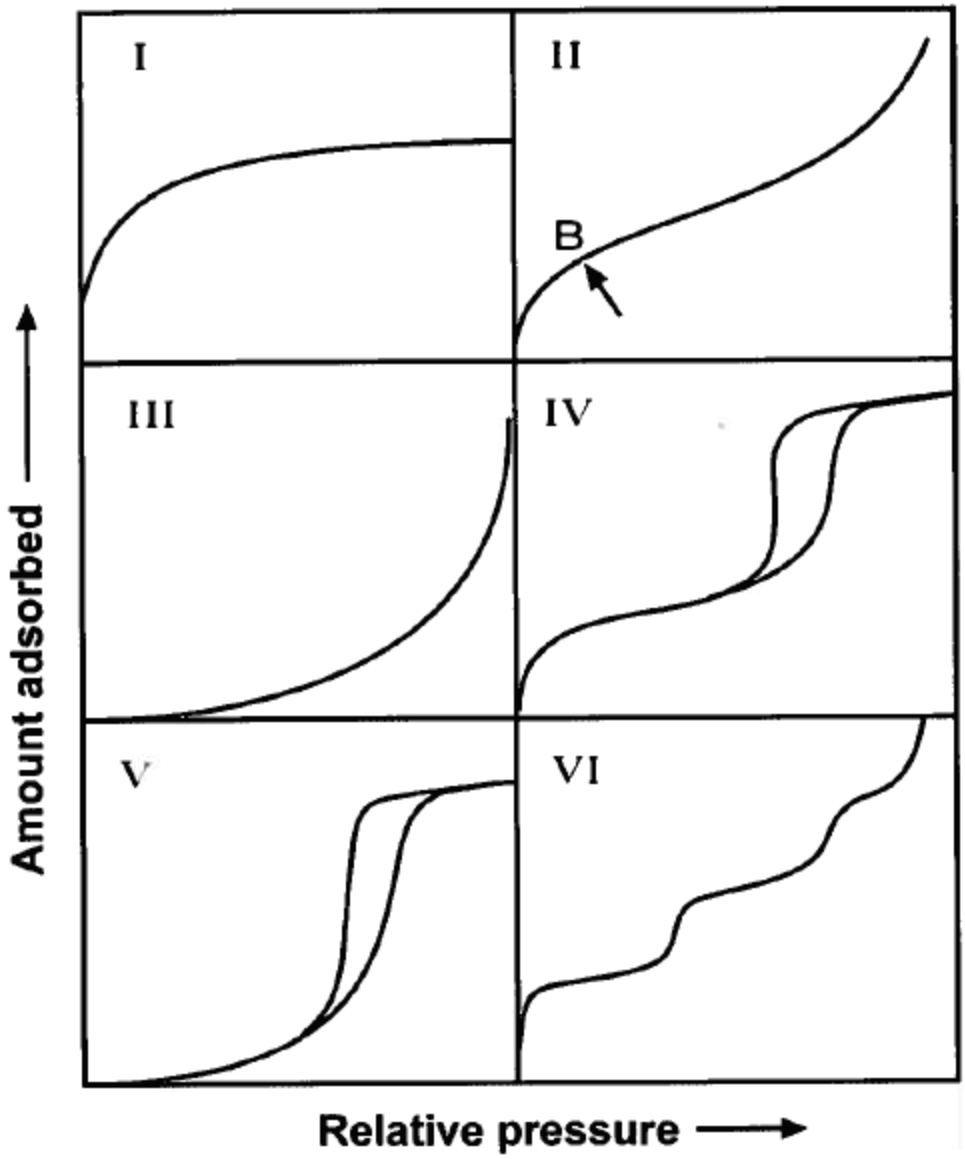

Figure 1-3: The IUPAC classification of adsorption isotherms[35].

Once the adsorption is produced, the surface area of a sample is calculated. Langmuir and Brauner-Emmett Teller (BET) are two well-known theories for determine the surface area. The Langmuir theory is applied to chemisorption adsorption than to physical adsorption. It assumed that gases form a monolayer on a solid. Furthermore, the collision of a gas molecule with a solid is inelastic, thus the gas molecule remains in contact with the solid for a period of time before returning to the gas phase. The

time of delay is responsible for adsorption phenomenon. The rate at which molecules strike a surface and leave it can be determined by equation (1.1).

$$V_a = \frac{V_m \mathrm{bp}}{1 + bP} \tag{1-1}$$

Where Va presents the quantity of gas adsorbed at pressure P, V_m is the quantity of gas adsorbed at the monolayer, and b is an empirical constant. The equation (1-1) can be arranged into a linear form (equation 1-2).

$$\frac{P}{V_a} = \frac{1}{Vmb} + \frac{P}{V_m} \tag{1-2}$$

When the values of P/Va are plotted against P values, a straight line should be produced. The slope and intercept of the line can be utilized to calculate b and V_m. The surface area s can then be calculated from V_m by equation (1-3).

$$s = \frac{V_m \sigma N_A}{\mathrm{m}\, V_0} \tag{1-3}$$

Where σ represents the area of surface occupied by a single adsorbed gas molecule ($16.2^* 10^{-20}$ for N_2), N_A is Avogadro constant, m the mass of the adsorbing sample, and V_o the molar volume of the gas (22414 cm^3). When nitrogen is the adsorptive, the Equation 1-3 is simplified into Equation 1-4:

$$s\,(m^2/g) = \frac{4.35\, V_m\ (cm^3\ at\ STP)}{\mathrm{m(g)}} \tag{1-4}$$

The Brunauer, Emmett, and Teller (BET) theory expands Langmuir theory by incorporating the concept of multilayer adsorption. It is assumed that the active forced in the condensation of gases are responsible for the binding energy in multilayer adsorption as can be described in Equation 1-5.

$$V_a = \frac{V_m\, CP}{(P_0 - P)[1 + (C-1)\frac{P}{P_0}]} \tag{1-5}$$

Where C is a constant, P_o presents the saturation pressure of the gas. Equation 1-5 can also be written in the linear form (equation 1-6):

$$\frac{P}{V_{a\,(P_0 - P)}} = \frac{1}{V_{mC}} + \frac{C-1}{V_{mC}}\left(\frac{P}{P_0}\right) \tag{1-6}$$

a plot of $P/[V_a (P_0-P)]$ vs. P/P_0 gives a straight line with intercept $1/V_mC$ and slope $(C-1)/V_m C$. This information can be utilized to calculate the surface area using Equation (1-3). In case of using nitrogen as adsorptive, the straight line is plotted using (P/P_0) values from 0.05 to 0.3.[37]

1.8 Porous Organic Network Polymers

In the past few years, porous organic polymers have gained an enormous interest and they have shown potential advantages in a wide range of applications, such as catalysis,[38] adsorption, carbon dioxide purification, hydrogen storage and membrane separation.[39] Firstly, they are comprised of solely light weight element through strong covalent bonding.[38,40] Secondly, there are a large number of synthetic routes which can introduce a large number of functionalities. For instance, moieties which can enhance binding affinities. Thirdly, they are scalable technology and there are already examples of systems (e.g., macroporous polymer resins for separations) which are produced commercially in a large scale. Additionally, they are chemically and physically stable owing to robust covalent bonds which connect the building blocks.[39, 40] There are two main classes of porous organic polymers are ordered, crystalline and disordered, amorphous.[41]

1.8.1 Crystalline Porous Organic Networks

1.8.1.1 Covalent Organic Frameworks (COFs)

Covalent organic frameworks are porous materials, shape- persistent zeolite analogues are composed of light elements (H, B, C, N and O) that can form strong covalent bonds.[42] For this reason, they have very light weight with remarkable thermal stability (up to 600 ^oC) make them useful for gas storage.[43] The first COFs (named COF-1) was prepared by self-condensation of 1,4-benzendiboronic acid (BDBA) to get a hexagonal layered which connected by a planar of boroxine rings (Fig. 1-4) which exhibited an apparent BET surface area of 711 $m^2 g^{-1}$.[43] A related boronate-ester linked structure (named COF-5) was prepared with similar condensation reaction between1, 4-benzendiboronic acid with hexahydroxytriphenylene (HHTP) to form a BC_2-O_2 linking ring,[43] displayed a BET surface area of 1590 $m^2 g^{-1}$**.** Further COFs

with considerable higher surface area were prepared using three-dimensional tetrahedral monomers. For instance, COF- 103 exhibited a high BET surface area of 4210m^2 g^{-1}.[41]

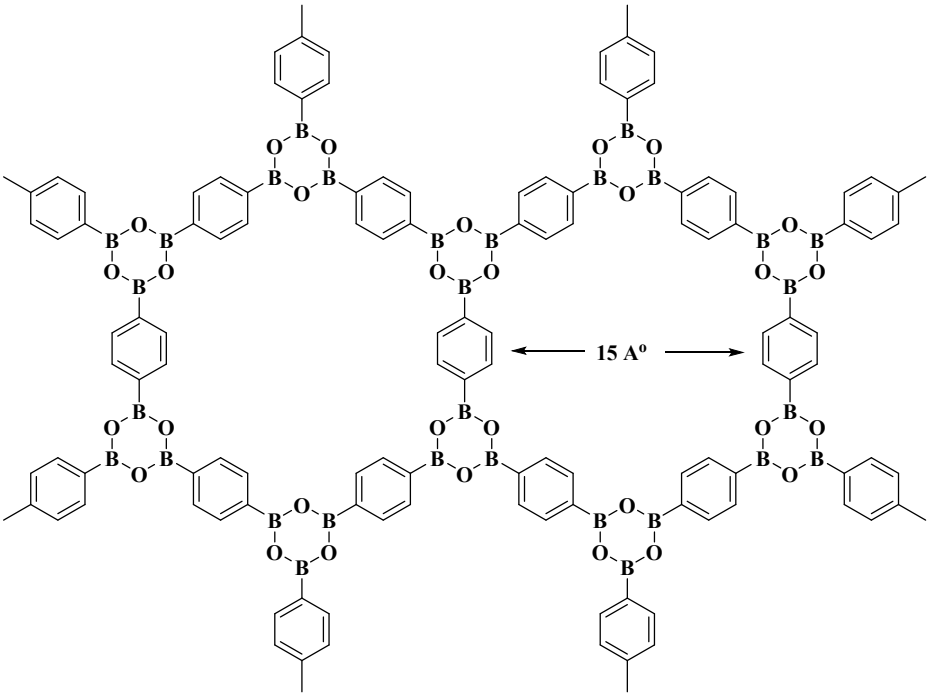

Figure 1-4: COF-1 structure.

1.8.1.2 Covalent Triazine Frameworks (CTFs)

Many of highly porous materials based on triazine networks have been produced by self-condensation of nitriles in the presence of $ZnCl_2$.[41] The first covalent triazine framework (named CTF-1) (Fig. 1-5) was prepared using 1,4-dicyanobenzene,[44] showed an apparent BET surface area of 791 m^2g^{-1} (nearly to that found in COF-1) . The molecular network structure of CTF-1 is an isoelectronic with the structure of COF-1.[42] Even though, the trazine in the CTF-1 is more thermally and chemically stable than the boroxine rings in the COF-1.[44]

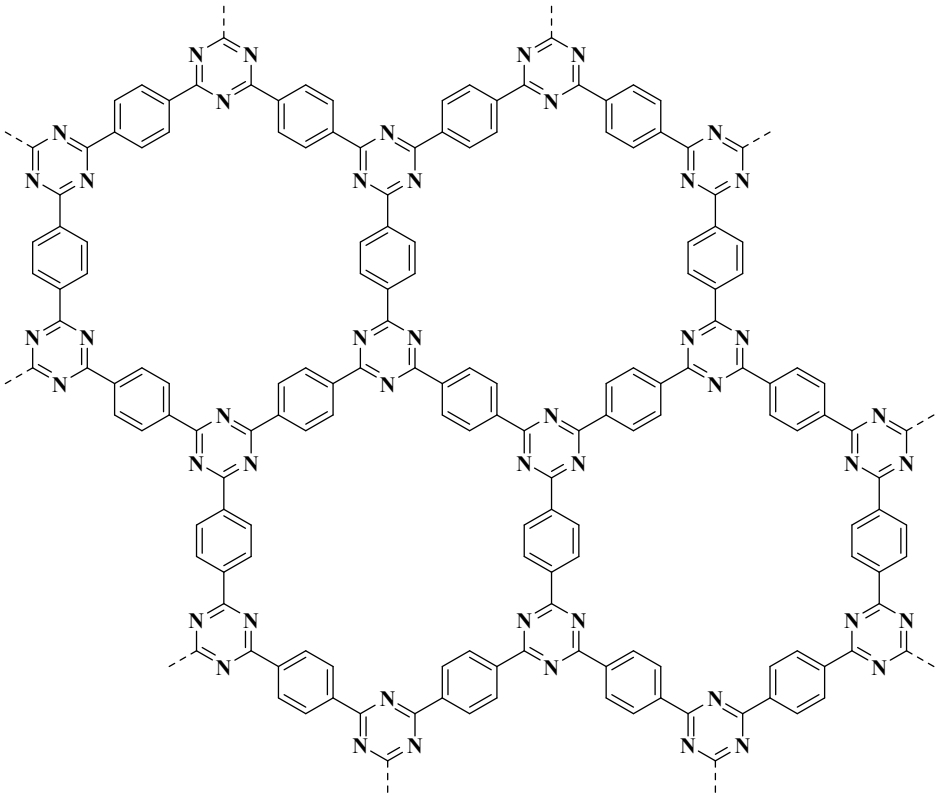

Figure 1-5: CTF-1 structure.[42]

1.8.2 Amorphous porous organic Networks

1.8.2.1 Polymers of Intrinsic Microporosity (PIMs)

There is another way of synthesizing nanoporous polymers is by using non-reversible condensation reactions to form polymers which pack ineffectively in the solid state.[41] Budd and McKeown introduced a new ladder of polymers which is referred as "polymers of intrinsic microporosity" (PIMs).[45] The porosity in PIMs is emerging from the rigid monomers which have tetrahedral carbon atom referred to as ' site of contortion'.[41] These site of contortion can force the backbone of the chains to twist and turn erratically, resulting in polymer chains that cannot pack efficiently in the solid state.[45] Consequently, free volume is introduced between the polymer chains. Polymers of intrinsic microporosity (PIMs) involves insoluble network PIMs which can potentially using as heterogeneous catalysts. Additionally, soluble PIMs (not crosslinked) which can be cast into membranes for many applications. Such as, liquid and gas separation.[46] The soluble PIM which is referred to as PIM-1 is synthesized by a polycondensation reaction which involves a double aromatic nucleophilic substitution between a tetrahydroxy monomer, [45] which is cheap and commercially

available and can introduce a site of contortion into the polymer chain,[41] with tetrafluoro monomer as shown in Figure 1-6.

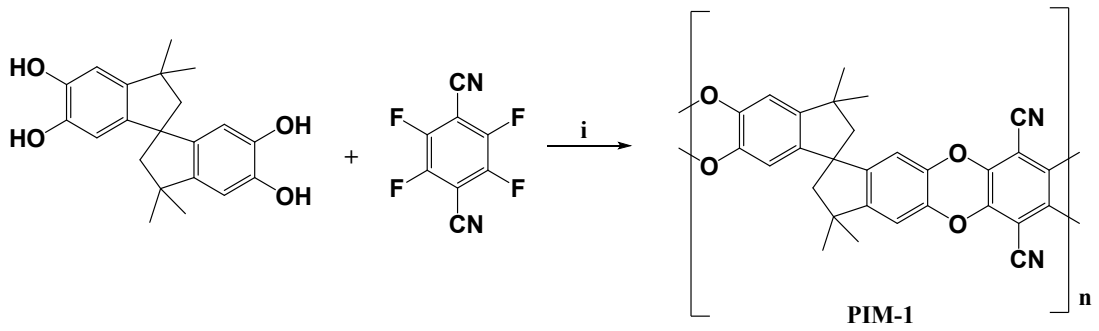

Figure 1-6:PIM-1 synthesis. The condition (i) are K_2CO_3, dimethylformamide, 50-70°C.[46]

In 2008, a Canadian research group aimed to improve the polymerization conditions for preparation of PIM-1 using high monomers concentration, less reaction time(40 min.) and high temperature (160 °C) in the mixture to Dimethylactemaide (DMAc) and toluene which can provide high molecular weight of PIM-1 with significantly decreasing the content of cyclic and crosslinking.[47]

PIM-polyimides (PIM-PIs) are polyimides with characteristic similar to PIM-1, considering the presence of spirobisidane and dibenzoixane in the repeat unit of polymers. They were prepared by imide forming reaction using a variety of aromatic diamine with bis (carboxylic anhydride) which incorporates a spirocentre (site of contortion) (Fig. 1-7). These polymers exhibited an apparent BET surface area up to 600 m^2 g^{-1}, and they are easily soluble in many solvents. Such as, chloroform, tetrahydrofuran, *m*-cresol and N-methylpyrrolidone so they can be cast from solution to form membrane. Furthermore, they demonstrated good performance in the separation of gases.[48]

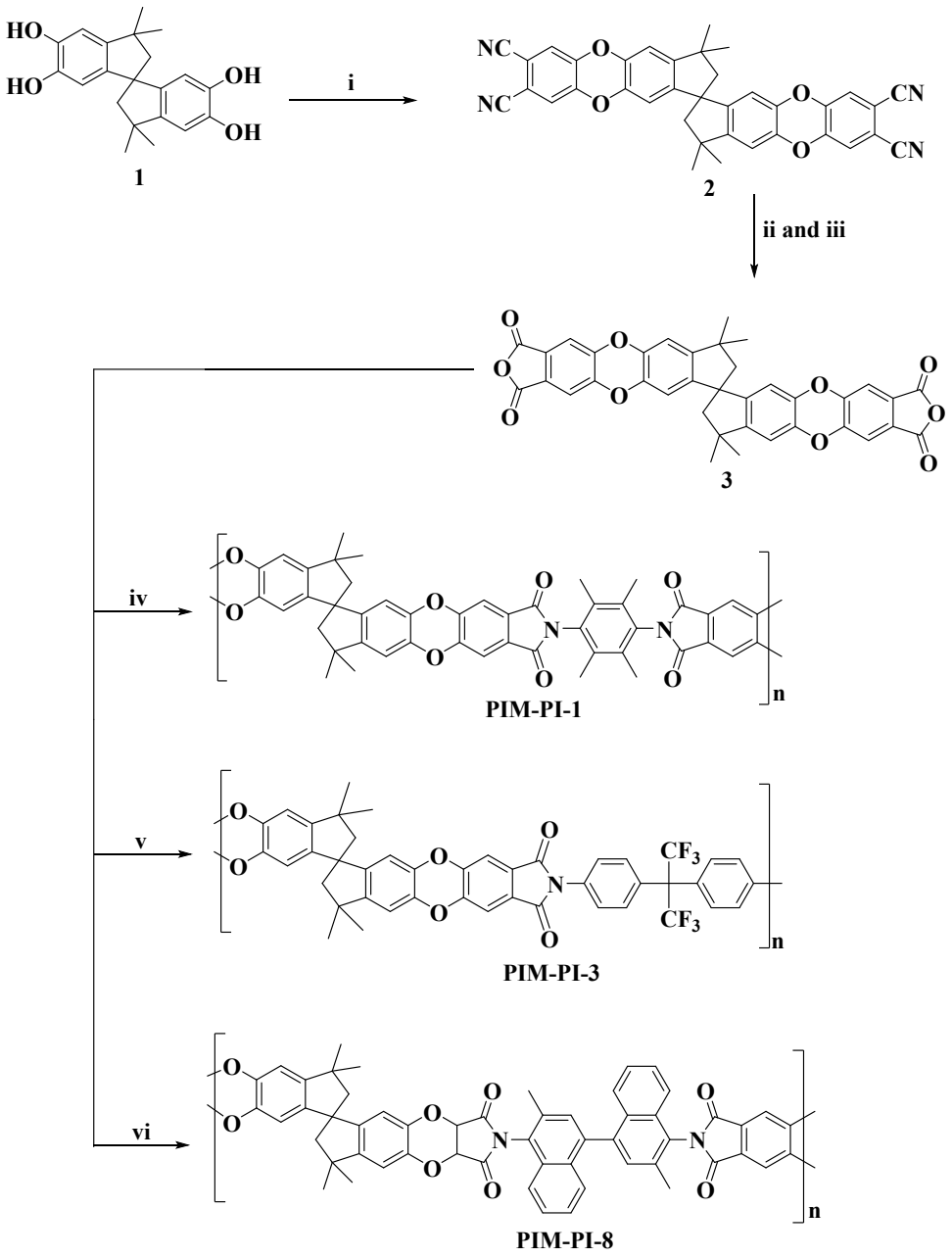

Figure 1-7: Preparation of PIM-polyimides PIM-1, PIM-3 and PIM-8. Reagents and conditions: (i) 4,5-dichlorophthalonitrile, K_2CO_3, N-N-dimethylformamide (DMF), 80 ^oC; (ii) KOH, EtOH/H_2O, reflux, 24h; (iii) acetic anhydride, reflux, 24h; (iv) 2,3,5,6-tetramethyl-1,4-phenylenediamine, *m*-cresol, quinoline,, toluene, reflux, 5h; (v) 4,4′ (hexafluoroisopropylidene)dianiline, *m*-cresol, quinoline, toluene, reflux, 5h; (vi) 3,3′-dimethylnaphthidine, *m*-cresol, quinolone, toluene, reflux, 5h.

PIMs network (Fig. 1-8) constructed using phthalocyanine and porphyrin fused rings that contain a spiro-centre. The spiro-centre would ensure that planar components are orthogonal. Thus, the network polymers cannot fill space efficiently, creating large amount of free volume. The resulting polymers which exhibited high BET surface area (up to 1000 $m^2 g^{-1}$) which can be used as heterogeneous catalysts.[49,50]

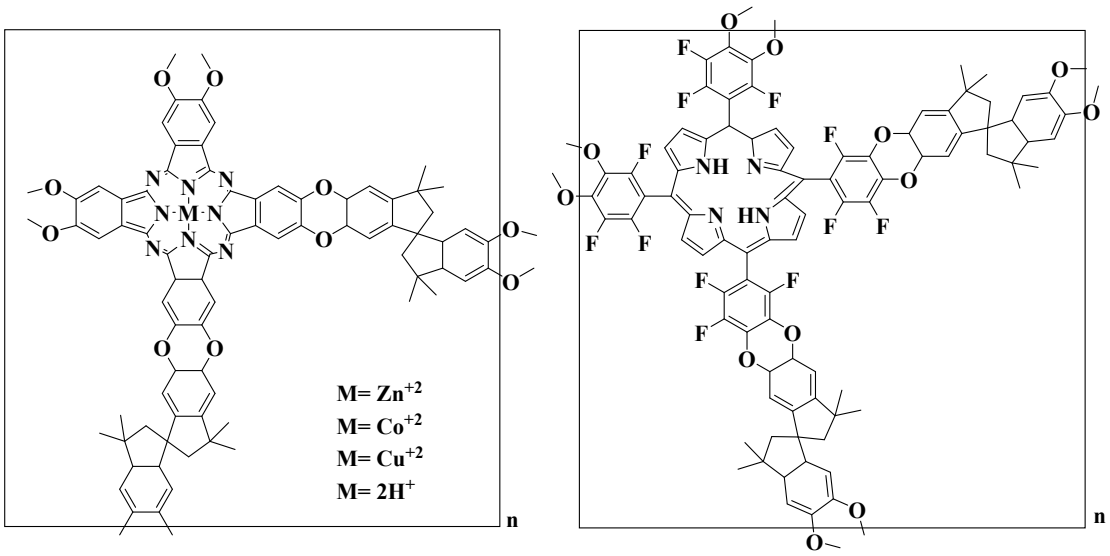

Figure 1-8: Structures of network PIMs based on phthalocyanine and porphyrin macrocycles with spiro-centre.

1.8.2.2 Hypercrosslinked Polymers (HCPs)

Hypercrosslinked polymers are considered as a novel class of porous materials, which can be prepared mainly by Friedel-Crafts alkylation reaction. HCPs have many characteristics. Firstly, they possess high thermal stability which is not commonly expected for other organic polymers because of their permanent porosity through extensive crosslinking reactions which prevent the polymer chain form collapsing into a dense, nonporous state. Secondly, HCPs can be regarded as a promising material for the gas storage applications. Particularly, in the field of clean energy and environmental issue. Such as, hydrogen storage and carbon dioxide capture owing to their light weight properties and high surface area.[51] Thirdly, HCPs have excellent chemical stability (e.g. to strong acids and bases), and they are quite readily produced on a large scale. Additionally, HCPs can be produced in a moulded monolithic form. Among the other various advantages of HCPs is their relative low heat of adsorption compared to other materials.[52] Among the most well- studied hypercrosslinked

materials are " Davanko- type" resins,[51] which are prepared by polymerization of vinyl benzyl chloride with a small amount of divinyl benzene as a crosslinker to form a lightly crosslinked copolymer, which is then swollen in a suitable solvent. After that, the copolymer can be hypercrosslinked by Friedel-Crafts alkylation reaction using a Lewis acid, like ferric chloride (Fig. 1-9).[41]

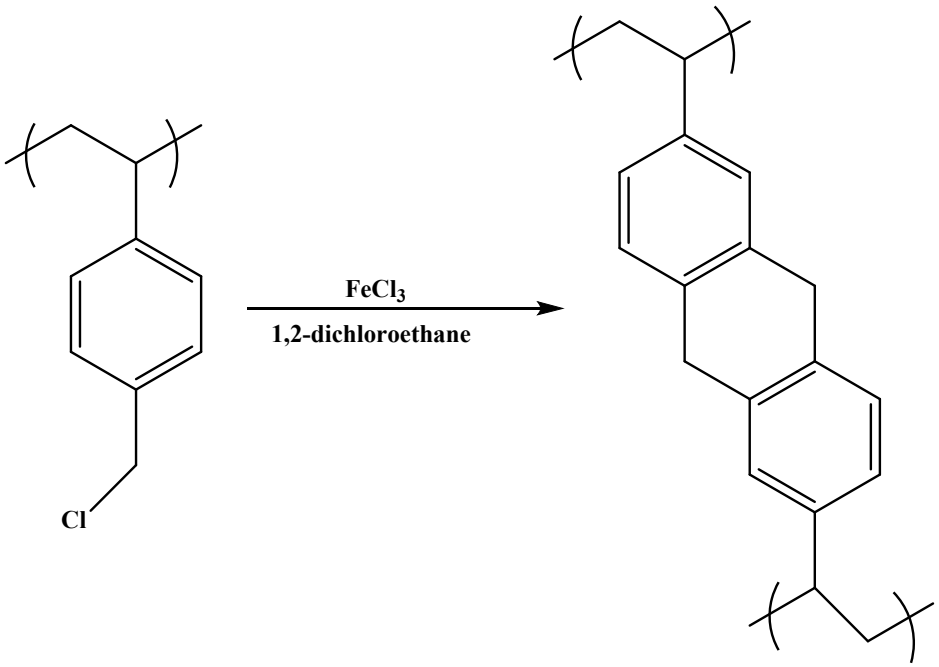

Figure 1-9: Hypercrosslinking of poly(chloromethyl)styrene using ferric chloride.

As a result of small differences in the synthetic procedures that are used to the precursor polymer, the apparent BET surface area of these polymers are various form about 600 m^2 g^{-1} up to 1466 m^2 g^{-1} and in most cases reported, the BET surface area can reach to 2090 m^2 g^{-1}.[41]

Recently, many porous networks have been prepared using imide bond forming reactions under relatively easy condition.[41] Among them; microporous polyimides with three-dimensional network structure have attracted great of interest in CO_2 capture applications due to their highly rigid heteroaromatic skeleton, superior thermal and chemical stabilities. Moreover, the imide rings are rich in nitrogen and oxygen atoms which may lead the polyimide networks to favour the interaction with CO_2 gas.[53] In 2008, Thomas *et al*. expanded the concept of PIM in preparation of aromatic polyimide and polyamide networks using of 2,2',7,7'-

tetraaminospirobifulorene. The polyimide network (named PI-1, Fig. 1-9) exhibited an apparent BET surface area of 982 m^2 g^{-1} as a result of incorporating a bulky and rigid spirobifluorne into the polymer backbone, yielding in inefficient packing of polymer chains and generating a high amount of free volume[54]. Later on, Farah *et al.*, Wang *et al.* and Rao *et al.* prepared ultamicroporous polyimide networks, which showed BET surface area of 750, 1407 and 2213 m^2 g^{-1}, respectively. The crosslinking polymerization was carried out using three different types of dianhydride with tetrakis(4-aminophenyl)methane as a crosslinker and inhibitor to chain packing, which result in high amount of free volume.[55-57]

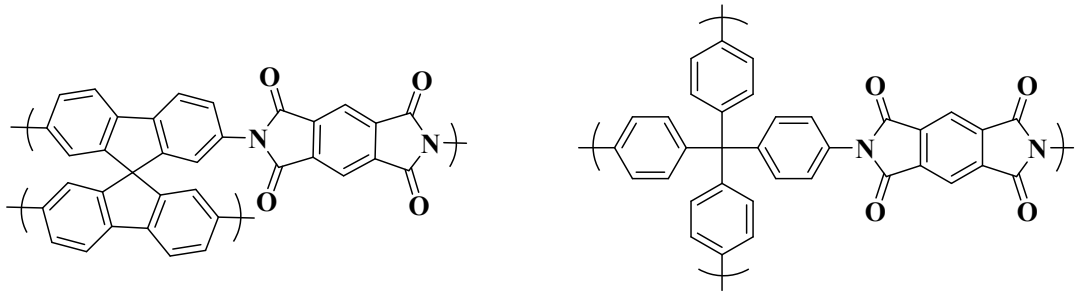

Figure 1-10: Structure of two different types of polyimide networks. PI-1 (left) and tetrahedral imide network (right).[41]

1.8.2.3 Conjugated Microporous Polymers (CMPs)

CMPs can be considered as a subclass of hyercrosslinked polymers. Nevertheless, they differ from other hypercrosslinked polymers in that they are composed of multiple carbon-carbon bonds and /or aromatic rings which can produce an extended conjugated network.[41] CMPs have attracted a great of interest owing to their porous structure which contain organic functionalities that enable a significant variation in the synthetic routes; these polymers can be utilized in a wide range of applications. For instance, gas sorption, molecular separation, electronic and catalysis.[58] In 2007, the first CMPs were prepared using Sonogashira-Hagihara palladium coupling to link aromatic halides to aromatic alkynes, producing poly (aryleneethynylene) (PAE) networks. A series of CMPs were prepared which exhibited different BET surface area. Among them, CAMP-0 (Fig. 1-11) displayed a high BET surface area of 1018 m^2 g^{-1}.[41]

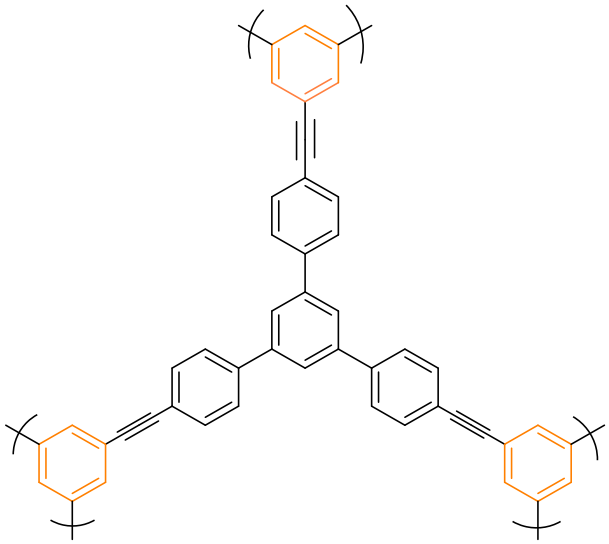

Figure 1-11: CAMP-0 structure.

1.9 Membrane Gas Separation

In the past few decades, membrane gas separation processes have been adopted rapidly in industrial processes as they offer many advantages over traditional separation processes,[54] like energy saving, ease of operation and environmentally.[59, 60] Membrane based-gas separations are of a great importance for a variety of industrial applications, such as air separation (> 99.5% nitrogen production and oxygen-enrichment), hydrogen recovery from ammonia purge stream, and carbon dioxide capture.[59,61]

In the membrane gas separation process, a feed mixture can separated into one or more gases, and thus generate a specific gas-enriched permeate or retentate. Separation is achieved by creating a driving force which is a pressure difference across the membrane.[62] In general, gas transport in dense membrane is occurred by solution-diffusion mechanism, [63] which is mentioned previously in chapter 1.

The performance of membrane based gas separation is characterized by two key parameters, namely permeability coefficient (P_A) and selectivity $\alpha_{A/B}$. Permeability coefficient can be defined as the product of gas flux and membrane thickness, which is divided by the pressure difference across the membrane. Gas selectivity is defined as the ratio of permeability coefficient of two gases ($\alpha_{A/B}=P_A/P_B$), where P_A represents

the permeability of the more permeable gas and P_B represents the permeability of the less permeable gas in the mixture of the binary gas pair. Polymers exhibiting both high permeability and selectivity are desired. Higher permeability is important to reduce the membrane area required to treat a given amount of gas, thus, reducing the cost of membrane units. Higher selectivity results in higher purity product gas.[64] Over the past two decades, studies have revealed a trade-off relationship between permeability and selectivity, polymers that exhibit high selectivity generally have low permeability and vice versa. This trend was analyzed by Robeson in 1991, who drew upper bounds in double logarithmic plots between selectivity versus permeability for a variety of gas pairs.[65] The permeation of gases through a polymer membrane is generally described by the solution-diffusion model in which separation of gas pairs can be accomplished not only by the diffusion of gases through polymer matrix but also by the solubility of a particular gas within the membrane. The permeability of a penetrant is the product of diffusivity, D, and the solubility, S, as shown in eq. (1-7):

$$P = S \times D \tag{1-7}$$

The selectivity of a membrane to a specific gas is dependent on the ability of the molecules to permeate through the membrane. The permselctivity, α, is the ratio of the permeabilities of two gases, A and B, which are separated:

$$\alpha_{A/B} = \frac{P_A}{P_B} = \frac{S_A}{S_B}\frac{D_A}{D_B} \tag{1-8}$$

As shown in eq. (1-8). The permselectivity is the product of diffusivity selectivity and the solubility selectivity.

Membranes can be classified into glassy and rubbery polymers, based on the polymer glass transition temperature. For permanent gases in conventional glassy polymers, diffusivity selectivity is dominated, with smaller gas molecules diffusing faster than larger molecules. For organic vapours and hydrocarbon gases in rubbery polymers, solubility selectivity is generally dominate, thus the permeability is higher for large vapour molecules than for smaller gas molecules and the solubility of gas in the polymer matrix follows Henry's law, so the concentration of gas, in a polymer, is linearly proportional to its partial pressure, as shown in eq. (1-9):

$$C = K_D P \tag{1-9}$$

Where K_D is the Henry's law coefficient.[59,65] On the contrary, glassy polymers show more complex behaviour. Glassy polymers below their glass transition do not attain thermodynamic equilibrium, which can result to inefficient chain packing and an excess of free volume is obtained in the polymer matrix. In this case, Langmuir sorption also takes place, increasing the gas solubility. Thus, the total concentration of sorbed gas, C, in a glassy polymer may be given by the dual-mode sorption model, which is a combination of Henry's law and Langmuir type adsorption, eq. (1-10):

$$\mathrm{C} = \mathrm{C}_D + C_H = K_D f + C_{H'} \frac{bf}{1 + bf} \quad (1\text{-}10)$$

Where C_H is the Langmuir type, C_H' is the maximum sorption capacity, and b is the ratio of adsorption and desorption rate coefficients. The maximum sorption capacity can also relate to the proportion and distribution of free volume elements. Free volume is defined as the fraction of volume which is not occupied by the polymer molecules. The occupied volume involves the van der Waals volume multiplied by a factor 1.3, related to the packing density of crystal molecules at 0 K. According to this concept, the distribution in chain packing is quantified by the fractional free volume (FFV) and can be calculated using the following equations, (1-11) and (1-12):

$$V_f = \left(V_{sp} - 1.3V_w\right) \quad (1\text{-}11)$$

$$FFV = \left(V_f / V_{sp}\right) \quad (1\text{-}12)$$

Where V_f represents free volume, V_{sp} is the specific volume and V_w is the specific van der Waals volume.[59]

Generally, all glassy polymers. Such as poly(trimethylsilylpropyne) (PTMSP), poly(4-methyl-2-pentyne) (PMP) and polymers of intrinsic microporosity (PIM-1) suffer from physical aging over time because the polymer chains relax towards an unachievable thermodynamic equilibrium causing loss in free volume and chain mobility.[66] Thus, gas permeability decreases and selectivity increases.[67] Many researches have been focused towards modification of polymeric membranes either by freezing the high fractional free volume in place using many approaches. For instance, mixed matrix membranes (MMS), polymer blends or organic fillers. Whereas, other techniques are aimed towards rigidifying the polymer structure in place. Such as,

surface plasma treatment, crosslinking or co-polymerization.[66] Mixed matrix membranes (MMMs) has emerged as a strong approach by combination the advantages of polymeric membrane materials and inorganic fillers. Such as, carbon molecular sieve, zeolite, metal oxides, carbon nanotubes, zeolite imidazole framework (ZIF) and metal organic framework (MOF) which are dispersed in a continuous polymer matrix results in its performance exceeding the upper bound limit. However, MMMs face many challenges with regard to interface morphology (e.g., chain rigidifaction, pore blockage and low adhesion) as well as poor dispersion of particle with the polymeric matrix (e.g., agglomeration or sedimentation of particles).[68,69] A number of approaches have been outlined the advantage of using purely organic dispersed phases composed of C, H, N, O atoms which can exhibit better compatibility with a continuous polymer matrix. Furthermore, they offer opportunity for modifying the physical properties via organic synthesis. In 2013, Rangel *et al.* [70]prepared MMMs by using porous polyimide networks as fillers which has small pore size and good compatibility with polyimide matrix. As a result, a good and very quick dispersion can be reached between two phases without agglomerates and void which have a major impact in facilitating of mixed matrix membranes preparation. Bushell *et al.*[71] prepared MMMs using porous organic cages as a dispersed phase with polymer of intrinsic microporosity (PIM-1) as a polymer matrix. The results revealed that the incoprating of porous organic crystalline into PIM-1 can significantly increase permeability, whereas maintaining good selectivity as well as enhancing resistance towards physical aging. Lau *et al.* [66] prepared nanocomposite membranes using a nanoporous aromatic framework particle with super glassy polymers, leading to freeze the polymer chain packing, thus stopping the aging process with increasing the gas permeability and selectivity.

1.10 References

1. C. M. White, B. R. Strazisar, E. J. Granite, J. S. Hoffman and H. W. Pennline, Separation and capture from large stationary sources and sequestration in geological formations-coalbeds and deep saline aquifers. *J. Air & Waste Manage. Assos.* 2003, **53**, 645-715.

2. M. H. Al-Mazouqi, S. A. M. Marzouk, M. H. El-Naas and N. Abdullatif, CO_2- CH_4 gas mixture using different solvents and hollow fiber membranes, *Ind. Eng. Chem. Res.* 2009, **48**, 3600-3605.

3. H. Al-Megren Advances in natural gas technology, In Tech, Croatia, 2012.

4. S. Wong and R. Bioletti, Carbon dioxide separation technologies, *Carbon & Energy Management,* Alberta Research Council, 2002.

5. A. R. Meyers, Chemical engineering .Encyclopedia of physical science and technology(3rdedition), *Ramtech, Inc*. California, 2001.

6. A. D. Ebner and J. A. Ritter, State-of-the-art adsorption and membrane separation processes for carbon dioxide emitting industries, *In Tech*. 2009, **44**, 1273-1421.

7. S. I. Plasynski and Z. Y. Chen, Review of CO_2 capture technologies and some improvement opportunities, Washington DC,45(4).

8. C. Yu, C. H and C. T, A review of CO_2 capture by absorption and adsorption, *Aerosol and Air Quality Research*, 2012, **12**,745-769.

9. M. W, A. Lawal, P. Stephenson, J. Sidders, C. Ramshaw and H.Teung, Post-combustion CO_2 capture with chemical absorption: A state-of-the-art review, *Chemical Engineering Research and Design*,2011, **89**, 1609-1624.

10. M. Songolzadeh, M. T. Ravanchi and M. Soleimani, Carbon dioxide capture and storage: A general review on adsorbents, World Academy of Science, *Engineering and Technology*, 2010, **70**.

11. S. Andderson and R. Newell, Prospects for carbon capture and storage technologies, *RFF*, 2003, DP: 02-68.

12. R. Thiruvenkatachari, S. Su, H. An and X. Yu, Post combustion CO_2 capture by carbon fiber monolithic adsorbents, *Progress in energy and Combustion Science*, 2009,**35** ,438-455.

13. M. K. Mondai, H. K. Balsora and P. Varshney, Progress and trends in CO_2 capture/separation technologies: A review, *Energy*, 2012, **46**, 431-441.

14. T. D. Burchell, R. R. Judkins, M. R. Rogers and A. M. Williams, A novel process and material for the separation of carbon dioxide and hydrogen sulfide gas mixtures, *Carbon*, 1997, **35**, 1279-1294.

15.M.Kohoutova,A.sikora,S.Hovorka,A.Randova,J.Schaur,M.Tisma,K.Setuickova,R. Petrickovic,S.Gueruik,N.Greenspoon and P. Izak, Influence of ionic liquid content on properties of dense polymer membranes, *European Polymer Journal*, 2009, **45**, 813-819.

16. M. F. Demirbas and M. Balat, Recent advances on the production and utilization trends of biofuels: A global perspective, *Energy Conversion and Management*, 2006, **47**, 2371-2381.

17. L. Y. Jiang, Y. Wang, T-S.Chung, X. Y. Qiao and J-Y.Lai, Polyimides membranes for pervaporation and biofuels separation, *Progress in Polymer Science*, 2009, **34**, 1135-1160.

18. Y. K. Ong, H. Wang and T-S. Chung, A prospective study on the application of thermally rearranged acetate-containing polyimide membranes in dehydration of biofuels via pervaporation, *Chem. Eng. Sci*, 2012, **79**, 41-53.

19. Q. G. Zhang, Q. L. Liu, Y. Chen and J. H. Chen, Dehydration of isopropanol by novel poly(vinyl alcohol)-silicone hybrid membranes*, Ind.Eng.Chem.Res*., 2007, **46**, 913-920.

20. S-L, Wee, C-T. Tye and S. Bhatia, Membrane separation process-pervaporation through zeolite membrane, *Sep. and Pur.Tech*, 2008, **63**, 500-516.

21. W. Kujawski, Application of pervaporation and vapor permeation in environmental, *Polish of Environmental Studies*, 2000, **9**, 13-26.

22. M. Mulder, Basic principle of membrane technology, (2ed edition), Kulwer Acdameic Publishers, Netherlands, 1996.

23. H. Strathmann, Membrane separation processes, *J. Membr.Sci.*, 1981, **9**, 121-189.

24. K. Hunger, M. Schmeling, H. B.T. Jeazet, C. Janiak, C. Staudt and K. Kleinermanns, Inverstigation of crosslinked and additive containing polymer materials for membranes with improved performance in pervaporation and gas separation, *Membranes*, 2012, **2**, 727-763.

25. G. B. Van den Berg and C. A. Smolders, Diffusional phenomena in membrane separation processes, *Jour. Membr. Sci*., 1992, **73**, 103-118.

26. A. Sharma, S. P.Tampi, S.V. Suggala and P. K. Bhattacharya, Pervaporation from a dense membrane: Roles of permeant-membrane interactions, Kelvin effects, and membrane swelling, *Langmuir*, 2004, **20**, 4708-4714.

27. L. K. Ling, M. G. Nawawi and A. N. Sadikin, Pervaporation of ethanol-water mixture using PVA zeolite-clay membranes, *Journal Teknologi*, 2008, **49**,167-177.

28. X.F and Y. M. Huang, Liquid separation by membrane pervaporation: A review, *Ind. Eng. Chem. Res.*, 1997, **36**, 1048-1066.

29. E .A. Fouad and X. Feng, Use of pervaporation to separate butanol from dilute aqueous solutions: Effects of operating conditions and concentration polarization, *J. Membr. Sci.*, 2008, **323**, 428-435.

30. S. A. Ahmaed and S. R. Lone, Hybrid process (pervaporation-distillation): A review, *International Journal of Scientific & Engineering Research*, 2012, **3**.

31. K. Nath, Membrane separation processes, Asoke K. Ghosh, New Delhi, 2001.

32. F. Heymes, P. M. Demoustier, F. Charbit, J. L. Fanlo and P. Moulin, Recovery of toluene from high temperature boiling absorbents by pervaporation, *J. Membr. Sci.*, 2006, **284**, 145-154.

33. J. Rouquerol, D. Avnir, C. W. Fairbridge, D. H. Everett, J. H. Haynes. N. Pernicone, J. D. F. Ramsay, K. S. W. Sing and K. K. Unger, *Pure& Appl. Chem*., 1994, 66, 1739-1758.

34. G. Q. Lu, X. S. Zhao, Nanoporous materials science and engineering, *Imperial College Press*, London, 2004,4, 1-13.

35. S. Lowell, J. E. Shields, M. A. Thomas and M. Thommes, Characterization of porous solids and powders: surface area, pore size and density, Kluwer Academic Publishers, Netherlands, 2004.

36. F. Rouquerol, J. Rouquerol, K. S. W. Sing, G. Maurin and P. Llewellyn, Adsorption by powders and porous: Principles, methodology and applications, 2nd, Academic Press, 2014.

37. P. A. Webb and C. Orr, Analytical methods in fine particle technology, Micromertitics Instrument Corporation, USA., 1997.

38. Y. Zhu, H. Long and W. Zhang, Imine-linked porous polymer frameworks with high small gas (H_2, CO_2, CH_4, C_2H_2) uptake and CO_2/N_2 selectivity, *Chem. Mater.*, 2013, **25**, 1630-1635.

39. G. Li and Z. Wang, Naphthalene-based microporous polyimides: Adsorption behavior of CO_2 and toxic organic vapors and their separation from other gases, *J. Phys. Chem.*, 2013, **117**, 24428-24437.

40. C. D. Wood, B. Tan, A. Trewin, F. Su, M. J. Rosseinsky, D. Bradshaw, Y. Sun, L. Zhou and A. I. Cooper, Microporous organic polymers for methane storage, *Adv. Mater*., 2008, **20**, 1916- 1921.

41. R. Dawson, A. I. Cooper and D. J. Adams, Nanoporous organic polymer networks, *Prog. Polym, Sci*., 2012, **37**, 530-563.

42. J-X. Jiang and A. I. Cooper, Microporous organic polymers: design, synthesis and functions, *Top Curr Chem.*, 2010, **293**, 1-33.

43. Y. Li and R. T. Yang, Hydrogen storage in metal-organic and covalent-organic frameworks by spillover,*AICHE*., 2008, **54**, 1.

44. P. Katekomol, J. Roeser, M. Bojdys, J. Weber and A. Thomas, Covalent triazine frameworks prepared from 1,3,5-tricyanobenzene, *Chem. Mater.,* 2013, **25**, 1542-1548.

45. P. M. Budd and N. B. Mckeown, Highly permeable polymers for gas separation membranes, *Polymer Chemistry*, 2010, **1**, 63-68.

46. M. Heuchel, D. Fritsch, P. M. Budd, N. B. Mckeown and D. Hofmann, Atomistic packing model and free volume distribution of a polymer with intrinsic microporosity(PIM-1), *J. Membr. Sci*., 2008, **318**, 84-99.

47. N. Du, G. P. Robertson, J. Song, I. Pinnah, S. Thomas and M.D. Guiver, Polymers of intrinsic microporosity containing trifluoromethyl and phenylsulfone groups as materials for membrane gas separation, *Macromolecules*, 2008, **41**, 965.

48. B. S. Ghanem, N. B. Mckeown, P.M. Budd, N. M. Al-Harbi, D. Fritsch, K. Heinrich, L. Starannikova, A. Tokarev and Y. Yampolskii, Synthesis, characterization and gas separation properties of a novel group of polymers with intrinsic microporosity PIM-polyimides, *Macromolecules*, 2009, **42**, 7881-7888.

49. N. B. Mckeown, S. Hanif, K. Msayib, C. E. Tattershall and P.M.Budd, Porphyrin-based nanoporous network polymers, *Chem. Commun*., 2002, 2782-2783.

50. N. B. Mckeown, S. Makhseed and P.M.Budd, Phthalocyanine-based nanoporous network polymers, *Chem Commun.*, 2002, 2780-2781.

51. S. Xu, Y. Luo and B. Tan, Recent development of hypercrosslinked microporous organic polymers, *Macromol. Rapid Commun*., 2013, **34**, 6.

52. C. F. Martin, E. Stockel, R. Clowes, D. J. Adams, A. I. Cooper, J. J. Pis, F. Ruberia and C. Pevida, Hypercrosslinked organic polymer networks as potential adsorbents for pre-combustion CO_2 capture, *J. Mater. Chem*., 2011, **21**, 5475- 5483.

53. G. Li and Z. Wang, Microporous polyimides with uniform pores for adsorption and separation of CO2 gas and organic vapors, *Macromolecules*, 2013, **46**, 3058-30066.

54. J. Weber, M. Antonietti and A. Thomas, Microporous networks of high-performance polymers: Elastic deformations and gas sorption properties, *Macromolecules*, 2008, **41**, 2880-2885.

55. O. K. Farah, A. M. Spokoyny, B. G. Hauser, Y-S. Bae, S. E. Brown. R.q. Snurr. C. A. Mirkin and J. T. Hupp, Synthesis, properties, and gas separation studies of a

robust diimide-based microporous organic polymer, *Chem. Mater.*, 2009, **21**, 3033-3035.

56. Z. Wang, B. Zhang, H. Yu, L. Sun, C. Jiao and W. Liu, Microporous polyimide networks with large surface areas and their hydrogen storage properties, *Chem. Commun*., 2010, **46**, 7730-7732.

57. K. V. Rao. R. Haldar, C. Kulkarni, T. K. Maji and S. J. George, Perylene based porous polyimides: Tunable, high surface area with tetrahedral and pyramidal monomers, *Cem. Mater*., 2012, **24**, 969-971.

58. Y. Xie, T-T. Wang, X-H. Liu, K.Zou and W-q. Deng, Capture and conversion of CO_2 at ambient conditions by a conjugated microporous polymer, *Nature Communications*, 2013.

59. N. D, H. B. Park, M. M. Dal-Cin and M. D. Guiver, Advances in high permeability polymeric membrane materials for CO_2 separation, *Energy & Environmental Science*, 2011.

60. A. F. Ismail, N. Ridzuan and S. Abdul Rahman, Latest development on the membrane formation for gas separation, *J. Membr. Sci*., 2002, **24**, 1025-1043.

61. C. R. Mason, L. M. Atem, N. M. Al-Harbi, P. M. Budd, P. Bernardo, F. Bazzarelli, G. Claizia and J. C. Jansen, Polymer of intrinsic microporosity incorporating thioamide functionality: Preparation and gas transport properties, *Macromolecules*, 2011, **44**, 6471-6479.

62. P. Benarado, E. Drioli and G. Golemme, Membrane gas separation: A review/ state of art, *Ind. Eng. Chem. Res*, 2009, **48**, 4638-46663.

63. L. Shao, B. T, Low, T-S. Chung, A .R. Greenberg, Review- polymeric membranes for the hydrogen economy: Contemporary approaches and prospects for the future, *J. Membr. Sci*., 2009, **327**, 18-31.

64. B. D. Freemen, Basis of permeability/selectivity tradeoff relations in polymeric gas separation membranes. *Macromolecules*, 1999, **32**, 375-380.

65. P. M. B, K. J. Msayib, C. E. Tattershall, B. S. Ghanem, K. J. Reynolds, N. B. Mckeown and D. Fritsch, Gas separation membranes from polymers of intrinsic microporosity, *J. Membr. Sci.*, 2005, **251**, 263-269.

66. C. H. Lau, P. T. Nguyen, M. R. Hill, A. W. Thornton, K. Konstas, C. M. Doherty, R. J. Mulder, L. Bourgeois, A.C.Y.Liu, D.J. Sprouster, J.P. Sullivan. T.J .Bastow, A. J. Hill, D.L.Gin and R. D. Noble, Ending aging in super glassy polymer membranes, *Angew. Chem. Int. Ed.*, 2014, **53**, 1-6.

67. P. Bernardo, F. Bazzarelli, J. C. Jansen, G. Clarizia, F. Tasselli, C. R. Mason et al, Physical aging study of post-treated PIM-1 membranes: Effect on gas transport properties, *Procedia Engineering*., **44** (2012) 874-876.

68. H. A. Mannan, H. Mukhtar, T. Murugesan, R. Nasir, D. F. Mohshim and A. Mushtaa, Recent applications of polymer blends in gas separation membranes, *Chem. Eng. Technol.*, 2013, **36**, No. 11, 1838-1846.

69. H. Mushardt, V. Kramer, D.Hülagü, T. Brinkmann and M. Kraume, Development of solubility selective mixed matrix membranes for gas separation, *Chemie Ingenieur Technik*., 2014, **86**, No. 1-2, 83-91.

70. E. R. Rangel, E. M. Maya, F. Sanchez, J. Abajo and J. G. Campa, Gas separation properties of mixed-matrix membranes containing porous polyimides fillers, *J. Membr. Sci.*, 2013, **447**, 403-412.

71. A. F. Bushell, P. M. Budd, M. P. Attfield, J. T. A. Jones, T. Hasell, A. I. Cooper, P. Bernardo, F. Bazzarelli, G. Clarizia and J. C. Jansen, Nanoporous organic polymer/cage composite membranes, *Angew. Chem. Int. Ed*., 2013, **52**, 1253-1256.

Chapter 2

Synthesis and Characterization of MMM Polymer Matrix PIM-1

2.1 Introduction

This chapter introduces PIM-1, which will be used as matrix for MMMs. The synthesis of PIM-1 is described for both low and high temperature methods, alongside their characterization techniques, including FTIR spectroscopy, ^{1}H-NMR spectroscopy, thermogravimetric analysis (TGA), N_2 sorption analysis and gel permeation chromatography (GPC).

2.1.1 Polymers of Intrinsic Microporosity (PIMs)

As described in chapter 1, PIMs are considered as highly microporous organic polymers, due to their rigid molecular structure, which arises from sites of contortion as well as rigid fused rings which prevent polymer chains from relaxation in the solid state, generating high free volume.[1-6]

2.1.2 Synthesis of PIM-1

PIM-1 was first prepared in 2004 by Budd *et al*.[2] The synthesis of PIM-1 was based on dibenzodioxane forming polymerization reaction between 5,5',6,6'-tetrahydroxy-3,3,3',3'-tetramethyl-1,1-spirobisindane (TTSBI) with tetrafluoroterephthalonitrile (TFTPN) in dimethylformamide (DMF) as reaction medium and potassium carbonate (K_2CO_3) as a base, for 72 h at 65 ^{o}C, as shown in Figure 2-1.

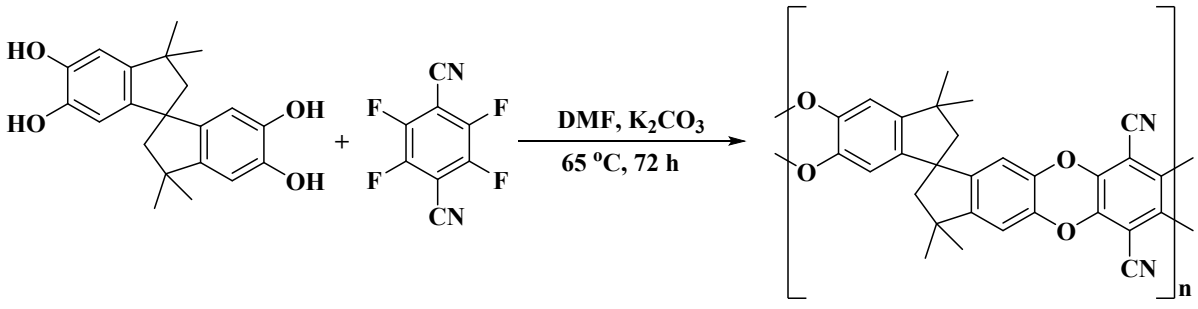

Figure 2-1: Synthesis scheme of PIM-1.

The product was a fluorescent yellow powder polymer which was soluble in polar aprotic solvents such as tetrahydrofuran (THF). Due to the rigid contorted structure of PIM-1, it exhibited high chemical and thermal stability with high BET surface area of 860 m^2 g^{-1}. PIM-1 was high molar mass, number-average molar mass, M_n=96000 Da,

weight-average molar mass, M_w=270 000 Da and PDI of 2.8. There was some oligmeric material. However, the group suggested dissolving PIM-1 in chloroform and precipitating in methanol in order to remove the low molecular weight oligomer.

Later on, in 2006 Kricheldorf *et al*.[6] investigated the condensation polymerization of TTSBI with TFTPN using four different solvents at 70 ^oC. It was found that cyclic polymers were formed when the reaction medium was dimethylformamide (DMF), N-methylpyrrolidone (NMP) and sulfone, as detected by Matrix Assisted Laser Desorption/Ionization-Time of Flight Mass Spectrometry (MALDI-TOF). However, the highest molecular weight, M_n= 18,000 Da and PDI of 5.2 was obtained in DMF at 70 ^oC different to the results of Budd *et al*.[2] . In dimethyl sulfoxide (DMSO), linear byproducts were formed due to side reactions and incomplete conversions. Temperature was increased, besides using different solvents, to get better results. Nevertheless, little influence was noticed.

In 2008, Song *et al*.[7] l investigated the polymerization conditions in order to get polymer with high molecular weight and less amount of crosslinking or branching species. The synthesis of PIM-1 was based on condensation polymerization between TTSBI with TFTPN using K_2CO_3 as base. The group found that purification of monomers plays an important factor in condensation polymerization and to get high molecular weight polymer. The group studied the effect of solvent, quality and molar ratio of K_2CO_3, temperature and time on the outcome of reaction. It was found that DMF was the best solvent in increasing the reaction rate, whereas fine powder K_2CO_3 had better effect on the reaction rate than granular K_2CO_3. Furthermore, it was noticed that the molar ratio of base greater than 2 % resulting in branched or crosslinked polymer. It was noticed that temperature had an effect on the reaction rate. The best temperature was between 50-55 ^oC, with higher temperature ($\geq$60 ^oC) forming crosslinked polymer, whereas the reaction temperature at 40 ^oC was too slow and produced polymer with very low molecular weight, increasing the polydispersity.

Afterwards, Du *et al*.[8] prepared PIM-1 with high molecular weight and less amount of cyclic or crosslinked compounds using new polymerization conditions. In this method, a high polymerization temperature of 160 ^oC and high monomer concentrations in DMAc solvent were applied, which was different to previously reported methods performed at lower temperatures. DMAc solvent was found to be a suitable solvent for both monomer salts and growing polymer chains. Furthermore,

toluene was added into the reaction mixture, not only to increase the rate of reaction by removing water but also to enhance the solubility of the polymer, which helps to reduce the amount of cyclic compounds. The reaction was carried out without the presence of toluene; a crosslinked polymer was formed in the last 10 min. Another important factor was the short time of 40 min to prepare PIM-1, compared to the original synthesis method[2]. The result was polymer with M_n= 55 000, M_w= 85 000 and PDI of 1.6.

In 2008, Du *et al*.[8] prepared high molecular weight PIM-1 by condensation polymerization of 5,5',6,6'-tetrahydroxy-3,3,3',3'-tetramethyl-1,1-spirobisindane with tetrafluoroterephthalonitrile in the presence of K_2CO_3 as base. The reaction was carried out in dimethyactemaide solvent (DMAc) at 155 ^oC for a few minutes. It was found that cyclic compounds were formed in the initial stages of reaction due to poor solubility of salts, which indicated that the rate controlling step in the polymerization is affected by the dissolution of the salts. As a result, the group found that use of a high-speed homogenizer increased the surface area of the salt, thus increasing its dissolution. Another important factor was addition of toluene during the reaction, which has two important roles: It increased the solubility of polymer, hence reduced the crosslinked compounds. Secondly, it removed water from the reaction.

In 2015, Zhang *et al*. [10] prepared PIM-1 using 5,5',6,6'-tetrahydroxy-3,3,3',3'-tetramethyl-1,1-spirobisindane with tetrafluoroterephthalonitrile as starting materials in the presence of K_2CO_3 as base. The reaction was based on solvent-free mechanochemical synthesis. In this method, the solid materials were ground manually without any solvents. The reaction was completed in a short time (15 min). The resulting was mixture washed with water, methanol and ethanol, producing a yellow powder which was soluble in organic solvents such as DMF and THF. PIM-1 synthesized by this method had high molecular weight and low polydispersity. The mechanochemical process was shown to be an effective and promising technique for synthesis of porous materials in terms of time, solvents and energy consumption.

In the present work, PIM-1 has been prepared according to Budd *et al*.[2] and Du *et al*.[8]

2.2 Experimental

2.2.1 Materials

5,5',6,6'-tetrahydroxy-3,3,3',3-tetramethyl-1,1'-spirobisindane (TTSBI), (97%, Alfa Aesar), was purified before use. TTSBI was dissolved in methanol and reprecipitated from dichloromethane. Tetrafluoroterephthalonitrile (TFTN, Apollo) was recrystallized by sublimation., anhydrous potassium carbonate (Fisher Scientific) was dried in oven at 100 ^{o}C overnight before use. Anhydrous dimethylformamide (DMF, Sigma Aldrich) and dimethylacetamide (DMAc, Sigma Aldrich) were used as received.

2.2.2 Apparatus

Molar mass values of PIM-1 were measured using a Viscotek VE2001 GPC solvent/sample module equipped with two Viscotek GMHHRM columns and a Viscotek TDA302 triple detector array (light scattering, viscosity and refractive index detectors).

PIM-1 powder (5 mg) was dissolved in filtered chloroform (5 ml) and left to stir overnight. The solution was then filtered into a vial using a 0.45 μm microfilter (Gelman Science). 100 μl of the filtered solution was injected using a Viscotek GPC VE2001. The data was then analyzed using OmnicSec software.

Gel Permeation Chromatography (GPC) separates particles based on their hydrodynamic volume. The polymer is first dissolved in solvent (mobile phase). Then, it passed through a packed column comprising of material of a known pore size and porosity (stationary phase). The particles with different size are passed through the stationary phase at different speed. The particles with small sizes have longer elution time while the larger particle sizes are eluted first from the column, i.e., the larger the particle size, the lower the retention volume. The calibration curve is performed by determine the retention volume of commercially standard polymer with a known molar mass and a narrow distribution. It is assumed that all polymers behave in a similar way, thus a value of molar mass is determined. The relationship between hydrodynamic volume and molar mass vary from polymer to polymer, hence the value calculated for molar mass can be related to a given standard.

^{1}H NMR spectra were recorded on a Bruker 400 MHz spectrometer. ^{1}H NMR samples were prepared by dissolving 10 mg of sample in 1ml of deuterated chloroform ($CDCl_3$) as solvent.

The Fourier transform infrared spectra of solids were recorded on a Bio-Rad FTS 6000 spectrometer equipped with an ATR setup, and annexed to a Whatman FTIR purge gas generator. The spectra were recorded in the attenuated total reflection (ATR) mode, with a resolution of 0.25 cm-1, a sensitivity of 1, and 16 scans in the range 4000 – 500 cm^{-1}.

The surface area measurement of polymers was carried out using a Micrometrics ASAP 2020 sorption analyser. A small amount of sample ~0.1 g was weighted in a sample tube and degassed automatically at 120 ^oC for 16 h. Once the sample tube was cooled, it was reweighed again, placed in the analysis port, and degassed manually for about 2 h at 120 ^oC. The analysis and free space of the sample were taken at 77 K and the BET surface area was calculated from N_2 adsorption data by multi-point Brunauer-Emmet-Teller (BET) analysis.

The thermogravimetric analysis (TGA) curves were recorded using a (Mettler Toledo Star @ System). The samples were heated to 800 ^oC, under N_2 with a flow rate of 10 ^oC/min.

2.2.3 Synthesis of PIM-1

2.2.3.1 Low temperature Method

PIM-1 was synthesized according to Budd *et al*.[2] The schematic synthesis of PIM-1 was shown in Figure 2-1.

Under a flow of nitrogen gas, 5,5',6,6'-tetrahydroxy-3,3,3',3'-tetramethyl-1,1'-spirobisindane (TTSBI) (5.10 g, 15 mmol) and tetrafluoroterephthalonitrile (TFTN) (3.00 gm, 15 mmol) were dissolved in dry dimethylformamide (DMF) (100 ml) at 65 ^oC. Then, anhydrous potassium carbonate K_2CO_3 (5.10 gm, 7.68 mmol) was added and the reaction mixture was left to stir for 72 h. Once the mixture was cooled down, the product was poured into water (250 ml) to remove any remaining salts or unreacted potassium carbonate. After that, the crude yellow product was filtered

under vacuum and dried in a vacuum oven at 110 °C overnight. In order to remove low molecular weight cyclic materials, the polymer was washed with the following solvents[11]: 1,4-dioxane (250 ml), acetone(100 ml), water (100 ml) and acetone (100 ml). Finally the product was dried in a vacuum oven at 110 °C overnight, giving a yield 6.95 g (68.5%) of PIM-1.

2.2.3.2 High Temperature Method

In this method, PIM-1 was prepared based on the procedure of Du *et al*.[8] The schematic synthesis of PIM-1 in shown in Figure 2.2.

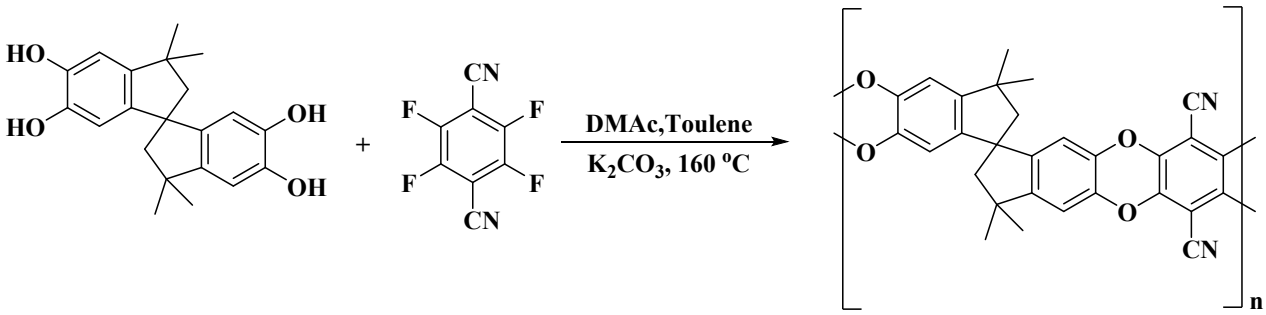

Figure 2-2: Synthesis of PIM-1 using high temperature method

In a dry 500 ml three-neck round bottom flask fitted with a mechanical stirrer, Dean-Stark trap and condenser, 5,5',6,6'-tetrahydroxy-3,3,3',3'-tetramethyl-1,1-spirobisindane (TTSBI) (20 g, 58.75 mmol), tetrafluoroterephthalonitrile (TFTN) (11.7560 g, 58.75 mmol), anhydrous potassium carbonate (24.35 g, 176.25 mmol), dimethylacetamide (DMAc) (117 ml), toluene (58 ml) were added under nitrogen atmosphere. The mixture was refluxed at 160 °C for 40 min. The resulting viscous solution was poured into methanol, turned to a solid-like structure. Then, the crude polymer was dissolved in chloroform and reprecipitated from methanol. After that, the polymer was refluxed with deionized water overnight to remove any remaining salts. The solid was then filtered off and dried under vacuum at 100 °C for 48 h, yield 20 g (74%).

2.3 Results and Discussion

2.3.1 Synthesis of PIM-1

Two batches of PIM-1, BD-1 and BD-2 have been synthesized, based on Budd *et al.*[2] and Du *et al*.[8] as described previously. BD-1 was prepared at low temperature (65 ^{o}C) for 72 h. whereas; BD-2 was synthesized at higher temperature (160 ^{o}C) and shorter time (40 min). In terms of short reaction time and less energy consumption, the high temperature method can be considered as more convenient method compared to low temperature method.

In both methods, PIM-1 was prepared based on condensation polymerization of 5,5',6,6'-tetrahydroxy-3,3,3',3'-tetramethyl-1,1-spirobisindane (TTSBI) with tetrafluoroterephthalonitrile (TFTN) using potassium carbonate as base. However, in the high temperature method, the monomer: base molar ratio was 1:1:3, higher than the low temperature method (1:1:0.5). The high concentration of potassium carbonate can have advantages to increase the rate of polymerization reaction and get high molecular weight polymer. However, the elevated temperature and high concentration can result in crosslinked and branched polymer. A high intensity blender mixing was applied to increase the surface area of salt and, as a result, increase its dissolution[12].

Purification of polymer was another difference between the two methods. It was noticed that in the low temperature method, more amount of solvents were needed in order to purify polymer from low molecular weight or cyclic compounds. Whereas, in high temperature method, less amount of solvents was used to remove oligomeric compounds. Hence, the low temperature method can be considered as a less practical method to prepare large scale of PIM-1, in comparison with the high temperature method.

2.3.2 FTIR Spectroscopy

The chemical structure of PIM-1 was characterized using FTIR spectroscopy, as shown in Figure 2-3. PIM-1 for low and high temperature methods shows the same chemical structure. The absorption band at 2239 cm^{-1} is related to the nitrile group, whereas the absorption band at 1263 cm^{-1} belongs to the ether linkage.

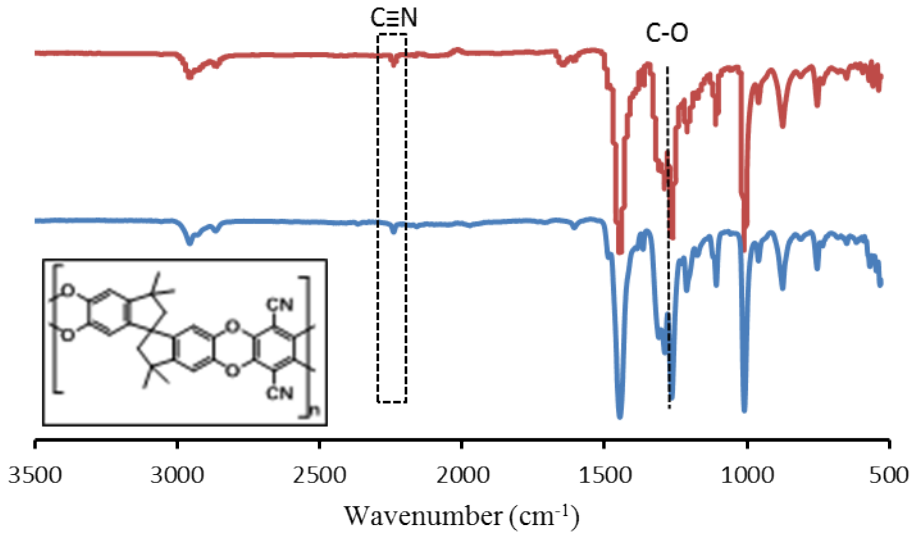

Figure 2-3: FTIR Spectroscopy of BD-1 (top, red) and BD-2 (bottom, blue).

2.3.3 ^{1}H- NMR Spectroscopy

The chemical structure of PIM-1 samples was further examined using ^{1}H-NMR spectroscopy (Fig.2-4). The spectrum shows that BD-1 and BD-2 have four different proton environments. The peaks at 1.32 and 1.37 ppm are related to hydrogens of the methyl groups in the spirocentre. Whereas, the peaks at 2.15 and 2.35 ppm correspond to protons of CH_2 in the spirocentre. The peaks at 6.43 and 6.81 ppm are assigned to protons of aromatic rings.

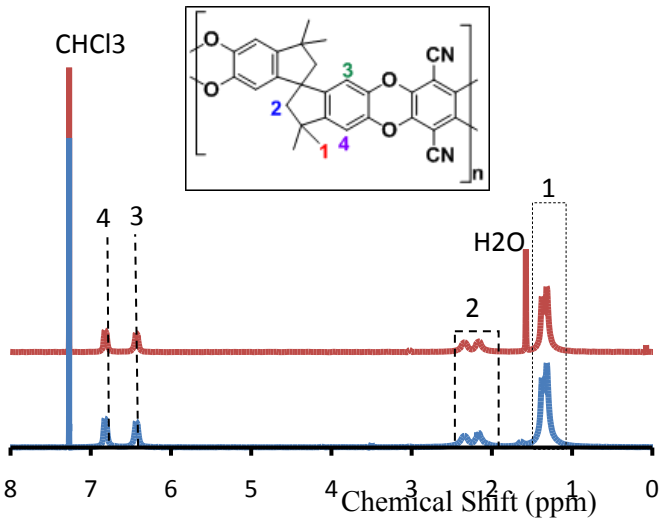

Figure 2-4: ^{1}H- NMR spectroscopy of BD-1 (top, red) and BD-2 (bottom, blue).

2.3.4 Thermogravimetric Analysis (TGA)

The thermal stability of PIM-1 for both methods was examined using thermogravimetric analysis (TGA). As can be seen in Figure 2-5, BD-1 and BD-2 exhibit high thermal stability up to 400 °C, which was compatible with data reported by Budd *et al.*[2] and Du *et al.*[8] The excellent thermal stability of PIM-1 can be attributed to the contorted structure (spirocentre) as well as the presence of fused rings which increase the rigidity of backbone chains.

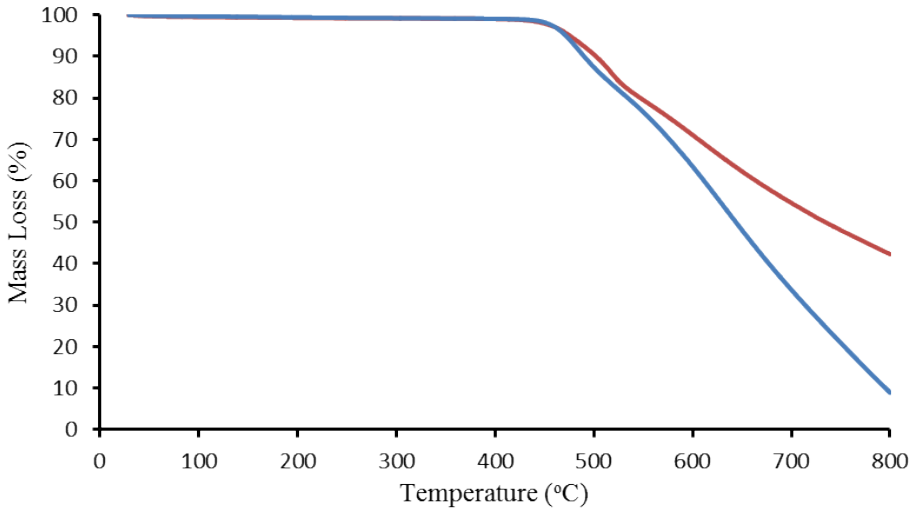

Figure 2-5: TGA of BD-1 (blue) and BD-2 (red).

2.3.5 N_2 sorption Analysis

The porosity of PIM-1for both methods was evaluated using N_2 sorption analysis at 77 K. Figure 2-6 shows a steep uptake of N_2 gas at very low relative pressure, characteristic of the microporous nature of the polymer.[13-15] It can be seen that the unclosed loop of the desorption curve lies above the adsorption curve, which can be related to swelling of the polymer structure caused by penetrant or defomation of the microporous structure.[14-17] The BET surface areas of both samples are presented in table 2-1. The high BET surface areas of BD-1 and BD-2 result from its contorted structure incorporated with its high rigidity, preventing the efficient packing of polymer chains in the solid state, generating high microporosity.[1, 2]

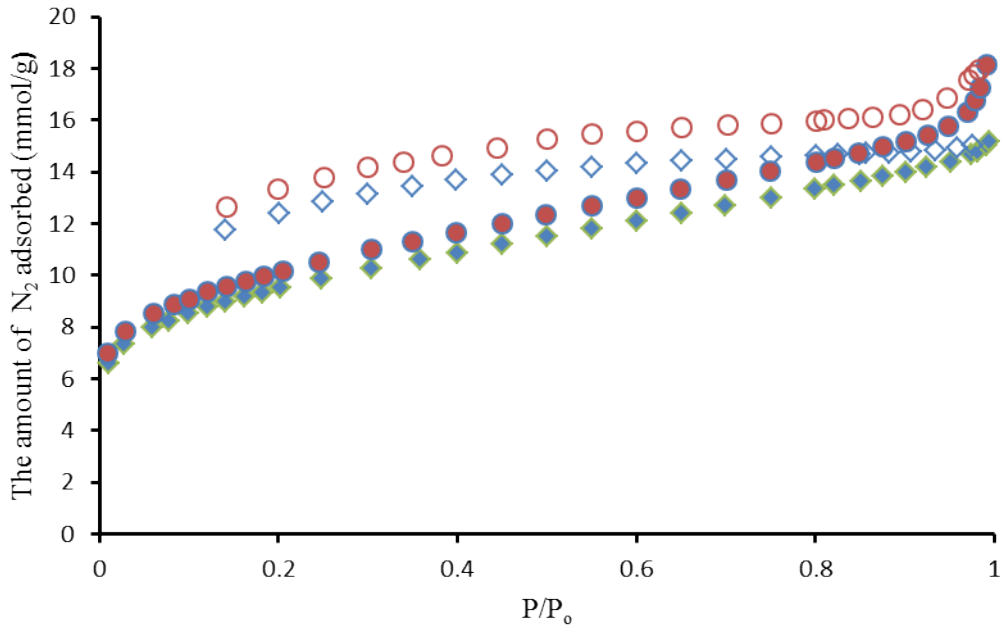

Figure 2-6: N_2 adsorption (filled symbols) and desorption (empty symbols) isotherms at 77 K. BD-1 (diamond symbols) and BD-2 (circular symbols).

Table 2-1: BET surface area of PIM-1 for both methods

Polymer	BET surface area (m^2 g^{-1})
BD-1	743
BD-2	800

2.3.6 Gel Permeation Chromatography (GPC)

The molar mass averages were obtained using multi detector gel permeation chromatography instrument. The GPC results for PIM-1 prepared by low and high temperature methods are presented in Figure 2-7 and table 2-2.

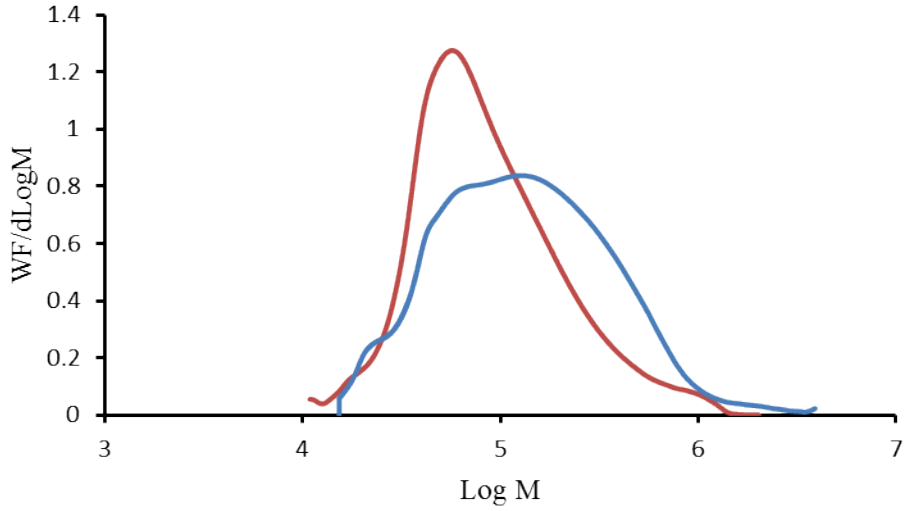

Figure 2-7: Weight distribution of log (molar mass) of PIM-1 samples: BD-1 (red) and BD-2 (blue).

Table 2-2: GPC results of the synthesized PIM-1 samples.

PIM-1 Batch	Molecular weight, M_w (Daltons)	Molecular weight, M_n (Daltons)	M_w/M_n Polydispersity
BD-1	131,000	64,000	2
BD-2	217,000	85,000	2.5

From the GPC results shown in Table 2-2, it can be seen that BD-2 batch prepared by high temperature method shows higher molecular weights compared to BD-1 prepared by the low temperature method which can be attributed to the reaction conditions. Such as, the high polymerization temperature of 160 ^oC which increase the growing of polymer chains to a greater extent compared to low temperature method. Furthermore, high monomer concentrations play an important factor in increasing the molecular weight of polymer. Moreover, the rate controlling step in the reaction is the dissolution of salts. Thus, a high speed homogenizer was applied to increase the surface area of salts[12]. As a result, high molecular weights were obtained in a short time.

In this research, PIM-1 prepared by the high temperature method was utilized as matrix for MMM preparation.

2.4 Summary

PIM-1 has been successfully synthesized using two different synthetic methods. The chemical structure of PIM-1was similar for both methods, as confirmed using FTIR spectroscopy and ^{1}H-NMR spectroscopy. PIM-1 prepared by high and low temperature methods showed high thermal stabilities up to 400 ^{o}C. The surface areas and molecular weights of PIM-1 samples are summarized in Table 2-3 which reveal that both samples show comparable surface areas. Whereas, PIM-1 prepared using high temperature method has higher molecular weight in comparison to low temperature method which can relate to reaction conditions.

Table 2-3: Summary of surface area and molecular weights of PIM-1 for high and low temperature methods.

PIM-1 samples	BET surface area (m^2 g^{-1})	Molecular weight, M_w (Daltons)	Molecular weight, M_n (Daltons)
BD-1	743	131,000	64,000
BD-2	800	217,000	85,000

2.5 References

1. P. M. Budd, B. S. Ghanem, S. Makhseed, N. B. Mckeown, K. J. Msayib and C. E. Tattershall, polymers of intrinsic microporosity (PIMs): robust, solution-processable, organic nanoporous materials, *Chem. Commun*., 2004, 230-231.
2. P. M. Budd, E. S. Elabas, B. S. Ghanem, S. Makhseed, N. B. Mckeown, K. J. Msayib, C. E. Tattershall and D. wang, Solution-processed, organophilic membrane derived from a polymer of intrinsic microporosity, *Adv. Mater*., 2004, **16**, 456.
3. N. B. Mckeown, P.M. Budd, K. J. Msayib, B. S. Ghanem, H. J. Kingston, C. E. Tattershall, S. Makhseed, K. J. Reynolds and D. Fritsch, Polymers of intrinsic microporosity (PIMs): Bridging the void between microporous and polymeric materials, *Chem. Eur. J*., 2005, **11**, 2610-2620.
4. P. M. Budd, N. B. Mckeown and D. Fritsch, Free volume and intrinsic microporosity in polymers, *J. Mater. Chem*., 2005, **15**, 1977-1986.
5. P. M. Budd and N. B. Mckeown, Highly permeable polymers for gas separation membranes, *Polym. Chem*., 2010, **1**, 63-68.
6. H. R. Kricheldorf, N. Lomadze, D. Fritsch and G. Schwarz, Cyclic and telechelic ladder polymers derived from tetrahydroxytetramethylspirobisindane and 1,4-dicyanotetrafluorobenzene, *J. Polym. Sci. Part A Polym. Chem*., 2006, **44**, 5344-5352.
7. J. Song, N. Du, Y. Dai, G. P. Robertson, M. D. Guiver, S. Thomas and I. Pinnau, Linear high molecular weight ladder polymers by optimized polycondensation of tetrahydroxytetramethylspirobisindane and 1,4-dicyanotetrafluorobenzene, *Macromolecules*, 2008, **41**, 7411-7417.
8. N. Du, G. P. Robertson, J. Song, I. pinnau, S. Thomas and M. D. Guiver, Polymers of intrinsic microporosity containing trifluoromethyl and phenylsulfone groups as materials for membrane gas separation, *Macromolecule.*, 2008, **41**, 9656-9662.
9. N. Du, J. Song, G. P. Robertson, I. Pinnau and M. D. Guiver, Linear high molecular weight ladder polymer via fast polycondensation of 5,5',6,6'-tetrahydroxy-3,3,3',3'-tetramethylspirobisindane with 1,4- dicyanotetrafluor obenzene, *Macromol. Rapid Commun*., 2008, **29**, 783-788.

10. P. Zhang, X. Jiang, S. Wan and S. Dai, Advancing polymers of intrinsic microporsity by mechanochemistry, *J. Mater. Chem. A*., 2015, **3**, 6739-6741.
11. P. M. Budd, N. B. Mckeown, B. S. Ghanem, K. J. Msayib, D. Fritsch, L. Starannikova, N. Belov, O. Sanfirova, Y. Yampolskii and V. Shantarovich, Gas permeation parameters and other physicochemical properties of a polymer of intrinsic microporosity: Polybenzodioxane PIM-1, *J. Membr. Sci*., 2008, **325**, 851-860.
12. K. Miyatake, A. R. Hill and A. S. Hay, High molecular weight aromatic polyformals free of macrocyclic oligomers. A condensative chain polymerization reaction, *Macromolecules*, 2001, **34**, 4288-4290.
13. P. M. Budd, K. J. Msayib, C. E. Tattershall, B. S. Ghanem, K. J. Reynolds, N. B. mckeown and D. Fritsch, Gas separation membranes from polymers of intrinsic microporosity, *J. Membr. Sci.*, 2005, **251**, 263-269.
14. N. B. Mckeown and P. M. Budd, Exploitation of intrinsic microporosity in polymer-based materials, *Macromolecules*, 2010, **43**, 5163-5176.
15. N.B. Mckeown and P. M. Budd, polymers of intrinsic microporosity., Materials Science., 2012, doi:10.5402/2012/513986.
16. P. M. Budd, A. Butler, J. Selbie, K. Mahmood, N. B. Mckeown. B. Ghanem, K. Msayib, D. Book and A. Walton, the potential of organic polymer-based hydrogen storage materials, *Phys. Chem. Chem. Phys*., 2007, **9**, 1802-1808.
17. H. Yu, C. Shen, M. Tian, J. Qu and Z. Wang, Microporus cynate resins: synthesis, porous structure, and correlations with gas and vapor adsorptions, *Macromolecules*, 2012, **45**, 5140-5150.

Chapter 3

Synthesis and Characterization of Network Polyimide Fillers

3.1 Introduction

In this research, the network polyimide fillers were utilized in the formation of MMMs. MPN-2, which incorporates a spiro-centre, has not previously been reported. This chapter introduces the synthetic methods for polyimide network (MPN-1) reported by other groups. The synthesis of fillers was investigated using different synthetic methods, and the products characterized using various techniques, including FTIR, ^{13}C solid-state NMR spectroscopy, TGA and N_2 sorption analysis.

3.1.1 Microporous Polyimide Networks

Porous polyimide networks have gained a great interest for gas storage, [1-5] and separations, [6-9] owing to their highly porous and rigid network frameworks as well as the presence of a large number of oxygen and nitrogen atoms in the backbone of the polymer, [5, 8] as described in chapter 1.

The condensation polymerization of multifunctional monomers is quite a complex process and may produce different topological structures. Generally, the polyimide network is composed of two types of linking unit, which are derived from the competitive reactions: ring-forming and branching. The percentage contents of these linking units in the structure of the network are significantly affected by many factors: chemical structure of monomers, reactivity of functional groups, as well as polymerization conditions such as solvent, concentration and temperature.[10]

3.1.1.1 Synthesis of Microporous Polyimide Network (MPN-1)

MPN-1, as can be seen in Figure 3-1, has a three-dimensional network which is constructed from the rigid tetrahedral shape of tetra(*p*-aminophenyl)methane TAPM, with four phenyls rings stretching outward from a carbon core, connected by rigid benzene struts of PMDA via five- membered imide rings, which prevent the network

chains from tight packing, generating a large amount of pore space and high surface area.[2, 8]

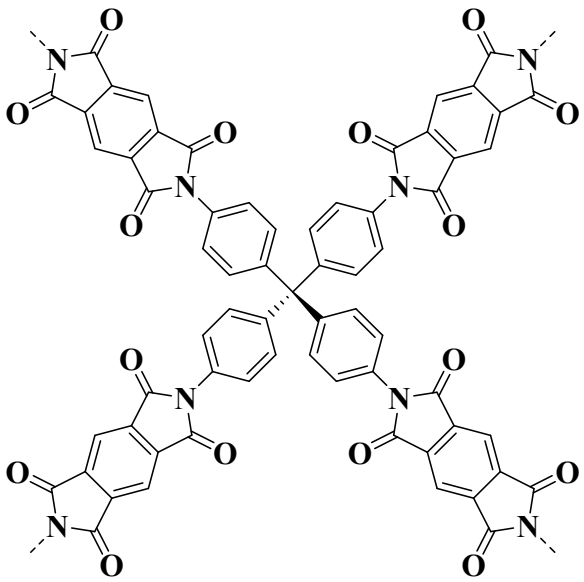

Figure 3-1: Structure of MPN-1

In 2010, Wang *et* al. [2] first prepared MPN-1 by a condensation polymerization of tetra(*p*-aminophenyl)methane (TAPM) with pyromellitic dianhydride (PMDA), using *m*-cresol as reaction medium and isoquinoline as catalyst.

The condensation reaction between A_2 (dianhydride) and B_4 (tetraamino) may undergo several stages, including oligomerization, branching, gelation and finally formation of a hypercrosslinked network[2]. The rapid gelation in the initial stage could prevent the approach of residual unreacted groups towards each other, due to the restriction of crosslinked points, which can result in imperfect crosslinking. Accordingly, the polymerization was first carried out at ice bath temperature for 24 h, then the temperature was increased gradually and the reaction mixture was allowed to polymerize at 80 ^{o}C for 4 h, 180 ^{o}C for 6 h and 200 ^{o}C for 8 h, so there was enough time for the branched or slightly crosslinked intermediate precursors to change their conformations for formation of a fully imidized network. The resulting solid was washed with methanol several times and then refluxed again with methanol in a Soxhlet extraction to remove any residual monomers, solvent and catalyst.

In 2013, a similar synthesis was reported by Li *et al*.[8] The one-pot polymerization reaction was carried out in *m*-cresol with isoquinoline as catalyst. As mentioned previously, due to the complex reaction of (A_2+B_4), the monomers were first dissolved at ice bath temperature for 2 h. Then the temperature of the reaction was increased gradually and left to polymerize at 30 ^oC for 8 h, 80 ^oC for 4 h, 160 ^oC for 4 h, 200 ^oC for 10 h and 220 ^oC for 4 h. The solid was washed successively with DMF, methanol and THF to remove solvent and catalyst. Further purification was done with THF in a Soxhlet apparatus for 24 h. The BET surface area of MPN-1 synthesized by Li *et al* [8] was 1454 m^2 g^{-1}, which was similar to the BET surface area reported by Wang *et al* [2] of 1407 m^2 g^{-1}. The slightly higher surface area may be due to a programmed temperature which allowed the intermediate branches to crosslink with each other and form a fully imidized network. Furthermore, the subsequent washing of polymer with DMF, methanol and THF can wash from the pores any remaining unreacted group, solvent and catalyst, resulting in high surface area. The synthesis used in this work was taken from Li *et al* [8].

3.1.1.2 Synthesis of Microporous Polyimide Network (MPN-2)

MPN-2, as shown in Figure 3-2, has a rigid three-dimensional structure. Tetra(*p*-aminophenyl)methane (TAPM) was used to direct the polymer into a three-dimensional geometrical shape. Furthermore, the dianhydride has a similar structure to PIM-1 and PIM-PIs, as described in chapter 1, [11, 12] in terms of the presence of spirobisidane (site of contortion) and dibenzodioxane, which can help to prevent the efficient packing of polymer chains. Consequently, large amounts of pore space can be generated with high surface area.

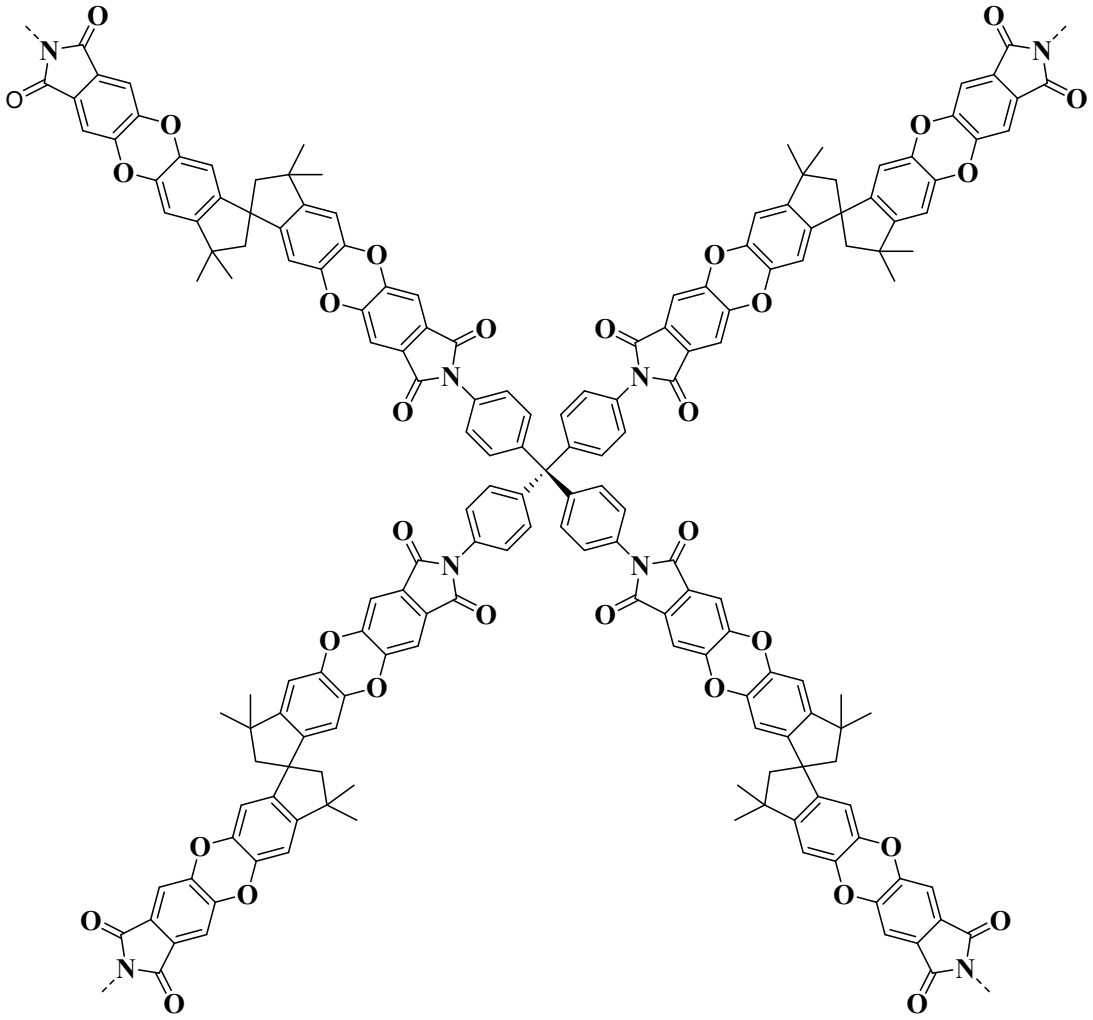

Figure 3-2: Structure of MPN-2.

To the best of our knowledge, a network polyimide with spiro-centre containing dianhydride has never been synthesized before. In this work, MPN-2 was prepared by two different polymerization methods. The first synthetic method was based on the procedure of Li *et al*.[8], as described previously. The second synthetic method was according to Weber *et al*[1], in this method, the condensation polymerization between tetra(*p*-aminophenyl)methane (TAPM) and bis dianhydride was carried out using *m*-cresol as reaction medium and isoquinoline as catalyst. The reaction mixture was first polymerized at room temperature for 1 h. Then, the temperature was raised to 80 ^{o}C for another 1 h. After that, the temperature was increased slowly to 200 ^{o}C and allowed to polymerize for 5 h. The resulting yellow/ brown solid could not dissolve in any common solvents, indicating the network structure.

3.2 Experimental Section

3.2.1 Chemicals

5,5',6,6'-Tetrahydroxy-3,3,3',3'-tetramethyl-1,1'-spirobisindane, (97%, Alfa Aesar) was recrystallized from methanol and reprecipitated from dichloromethane. Anhydrous potassium carbonate (Fisher Scientific), 4,5-dichlorophthalonitrile (Alfa Aesar), potassium hydroxide (Fisher Scientific), trityl chloride (97%, Aldrich), pyromellitic dianhydride (97%, Aldrich), raney-nickel (Aldrich), anhydrous dimethylformamide (Aldrich), acetic anhydride (Aldrich), aniline (≥ 99.5%, Sigma-Aldrich), fuming nitric acid (≥ 99.5%, Sigma-Aldrich), isopentyl nitrile (96%, Sigma-Aldrich), hydrazine hydrate solution (78-82%, Sigma-Aldrich), hypophosphorous acid solution (50 wt. % in H_2O, Sigma-Aldrich), *m*-cresol (99%, Sigma-Aldrich) and isoquinoline (97%, Aldrich) were used as received.

3.2.2 Apparatus

^{1}H and ^{13}C NMR spectra were recorded on a Bruker 400 MHz spectrometer. ^{1}H NMR samples were prepared by dissolving 10 mg of sample in 1 ml of deuterated chloroform ($CDCl_3$) or deuterated dimethyl sulfoxide (DMSO) as solvents. Due to the low sensitivity of ^{13}C compared to ^{1}H, 20 mg of sample was dissolved in 1 ml of deuterated chloroform or deuterated dimethylsulfoxide. High powered decoupling (Hpdec) magic angle spinning (MAS) solid state ^{13}C NMR spectra were collected using a Bruker Avance lll 400 MHz instrument, using admantane as a reference. Powder samples were packed into a 4 mm zirconia rotor and run at a spinning rate of ~ 12000 Hz. The spectra were collected with 6000 scans, using a repetition time of 10 seconds and a spectral width of 600 ppm.

The Fourier transform infrared spectra of solids were recorded on a Bio-Rad FTS 6000 spectrometer equipped with an ATR setup, and annexed to a Whatman FTIR purge gas generator. The spectra were recorded in the attenuated total reflection

(ATR) mode, with a resolution of 0.25 cm-1, a sensitivity of 1, and 16 scans in the range 4000 – 500 cm^{-1}.

The surface area measurement of polymers was carried out using a Micromeritics ASAP 2020 and Micromeritics ASAP 2010 sorption analyzer. A small amount of sample, ~0.1 g, was weighed in a sample tube and degassed automatically at 120 ^oC for 16 h. Once the sample tube was cooled, it was reweighed again, placed in the analysis port, and degassed manually for about 2 h at 120 ^oC. The analysis and free space of the sample were taken at 77 K and the BET surface area was calculated from N_2 adsorption data by multi-point Brunauer-Emmet-Teller (BET) analysis.

The thermogravimetric analysis (TGA) curves were recorded using a (Mettler Toledo Star @ System). The samples were heated to 800 oC, under N_2 with a flow rate of 10 ^oC/min.

3.2.3 Synthetic Procedures

Tetra (p-aminophenyl)methane (TAPM), as shown in Figure 3-3, was used in the synthesis of network fillers. There are three steps for synthesis of TAPM, described below.

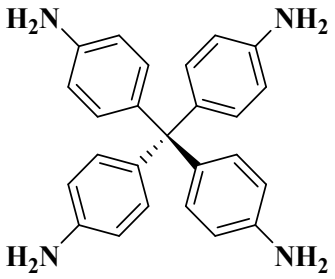

Figure 3-3: Structure of TAPM.

3.2.3.1 Synthesis of Tetraphenylmethane (TPM)

TPM was synthesized according to a procedure of Lu *et al*.[13] The schematic synthesis of TPM is presented in Figure 3-4.

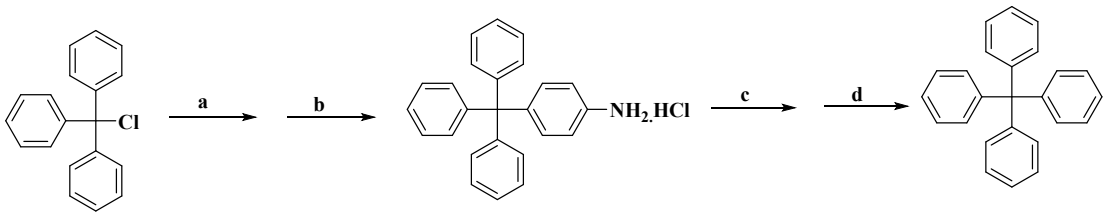

Figure 3-4: Synthesis of TPM. Reagents and conditions: a. treated with aniline at 190 ^{o}C, b. reflux with 2 M HCl/MeOH, c. -15 ^{o}C H_2SO_4/isoamylnitrile, d. heated with phosphoric acid at 50 ^{o}C.

Chlorotriphenylmethane (25.0 g, 89.67 mmol, 1 equiv) and aniline (21.7 g, 21.2 ml, 233.15 mmol, 2.6 equiv) were added into a 500 ml three-neck round bottom flask equipped with mechanical stirrer and condenser. The reaction mixture was heated slowly to 190 ^{o}C with vigorous stirring. After 15 min, the reaction mixture was cooled to room temperature. Then a solution of aqueous HCl (2 M, 100 ml) and methanol (150 ml) were added to the pulverized solid and refluxed for 30 min. After cooling to room temperature, the solid was filtered off, washed with water (250 ml), and dried in vacuum at 70 ^{o}C for 18 h. The dry solid was then suspended in 250 ml of DMF and cooled to -15 oC. At this temperature, sulfuric acid (96%, 27.5 ml) and isoamyl nitrile (20.4 ml, 17.8 g, 152.44 mmol, and 1.7 equiv) were added slowly and left to stir for 1 h. Then, hypophosphoric acid (30%, 75 ml) was added drop wise. After the addition was completed, the reaction mixture was heated to 50 ^{o}C until the evolution of gas had ended. After that, the solid was filtered off and washed subsequently with DMF (250 ml), water (250 ml) and ethanol (250 ml). The washing procedure was repeated twice. Finally, the solid was dried in vacuum at 70 ^{o}C for 18 h. The TPM was obtained as a pale yellow powder (22.79 g, 88.16%). An NMR spectrum of TPM was obtained using deuterated DMSO. 1H NMR (DMSO-d6; 400 MHz) δ (ppm): 7.14 ppm (8H, d, J= 7.57 Hz), 7.21 ppm (4H, d, J= 6.31 Hz), 7.29 ppm (8H, t, J= 7.60 Hz). 13C NMR (CDCl3; 400 MHz) δ (ppm): 64.95 ppm (Cq), 125.86 ppm (Ar-CCq), 127.43 ppm (Ar-Cortho), 131.16 ppm (Ar-Cmeta), 146.76 ppm (Cpara). FT-IR (thin film, cm-1): (3084, 3056, 3030) (=C-H stretching in aromatic ring), (1679, 1592,

1491) (C=C stretching in aromatic ring). Elemental analysis calculated for $C_{25}H_{20}$: C, 93.71; H 6.29%. Found: C, 89.34; H, 6.17%.

3.2.3.2 Synthesis of Tetra (p-nitrophenyl) methane (TNPM)

TNPM was synthesized in accordance to Wang *et al*.[2] The schematic synthesis of TNPM is shown in Figure 3-5.

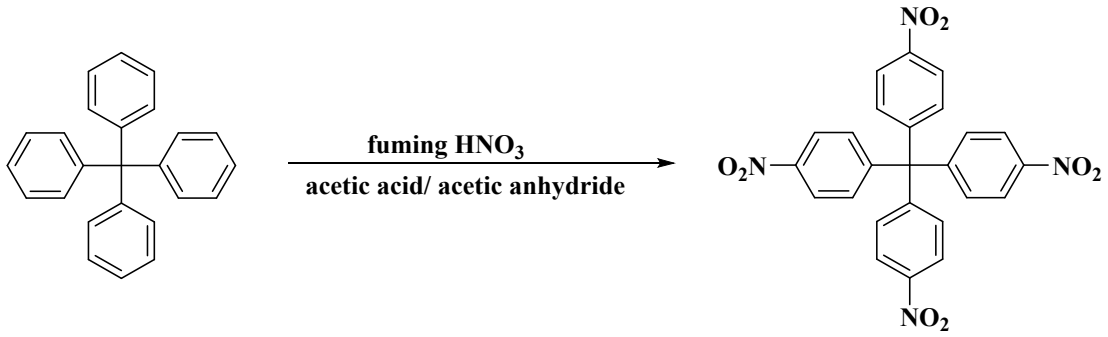

Figure 3-5: Synthesis of TNPM.

TPM (7.4 g, 23 mmol) was added in small portions to fuming nitric acid (40 ml) while being stirred vigorously in an ice/salt bath (-10 to -5 ^{o}C). Then, a mixture of acetic anhydride (12.5 ml) and glacial acetic acid (25 ml) was added slowly and left to stir for 1 h. After that, the reaction mixture was filtered off and recrystallized with THF. The solid was dried in vacuum to afford a light yellow crystal, yield 3 g (41.45%)**.** ^{1}H NMR (DMSO-d_6; 400 MHz) δ (ppm): 7.61 ppm (8H, d, *J*= 9.08 Hz, Ar -H), 8.23 ppm (8H, d, *J*= 8.83 Hz, Ar-H).^{13}C NMR (DMSO-d_6; 400 MHz) δ (ppm): 67.47 ppm (Cq), 124.22 ppm (Ar-C_{ortho}), 131.95 ppm (Ar-C_{meta}), 146.47 ppm (Ar-C_{para}), 151.48 ppm (Ar-CCq). FT-IR (thin film, cm^{-1}) 1512 (asymmetric N-O stretching), 1338 (symmetric N-O stretching). Elemental analysis calculated for $C_{25}H_{16}N_4O_8$: C, 60.00; H, 3.22; N, 11.20%. Found: C 60.22; H 3.22; N 10.60%.

3.2.3.3 Synthesis of tetra(p-aminophenyl)methane (TAPM)

TAPM was synthesized according to Farha *et al*.[6] The schematic synthesis of TNPM is presented in Figure 3-6.

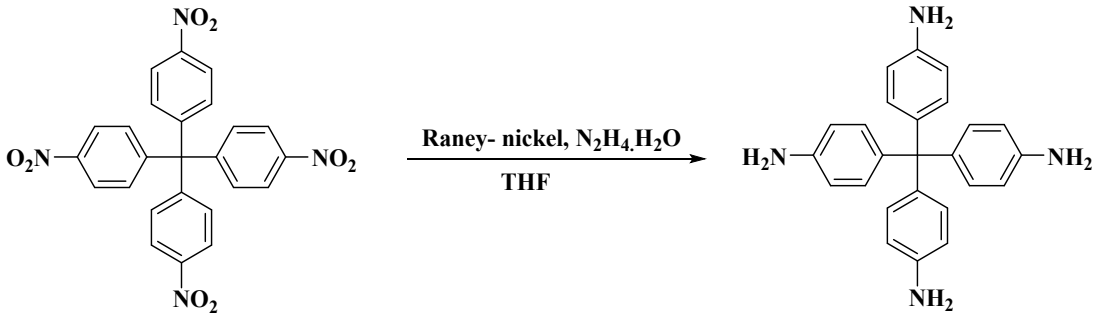

Figure 3- 6: Synthesis of TAPM.

Raney Ni (20 g) was added to TNPM (3 g, 6 mmol) dissolved in THF (200 ml), while being stirred under nitrogen. Then, hydrazine hydrate (4 g) was added dropwise via syringe and refluxed for 4 h. After that, the reaction mixture was hot filtered and washed with hot ethanol (100 ml). The solid was then precipitated by evaporation of solution. After filtration, the solid was washed with ethanol and dried in vacuum to afford TAPM as a white solid, yield 1.4 g (46.96%). ^{1}H NMR (DMSO-d_6; 400 MHz) δ (ppm): 4.85 ppm (8H, s, NH_2), 6.38 ppm (8H, d, *J*= 8.83Hz, Ar-H), 6.67 ppm (8H, d, *J*= 8.58Hz, Ar-H). ^{13}C NMR (DMSO-d_6; 400 MHz) δ (ppm): 61.32 ppm (Cq), 112.79 ppm (Ar-C_{ortho}), 131.27 ppm (Ar-C_{meta}), 136.05 ppm (Ar-CCq), 145.90 ppm (Ar-C_{para}). FT-IR (thin film, cm^{-1}): 3448 (asymmetric, N-H, stretching), 3394 (symmetric, N-H, stretching), 1269 (C-N stretching), Elemental analysis calculated for $C_{25}H_{24}N_4$: C, 78.92; H, 6.36; N, 14.73%. Found: C, 78.67; H, 6.46; N, 14.72%.

3.2.3.3 Synthesis of Network Polyimide (MPN-1)

MPN-1 was prepared according to Li *et al*.[8] The schematic synthesis of MPN-1 is presented in Figure 3-7.

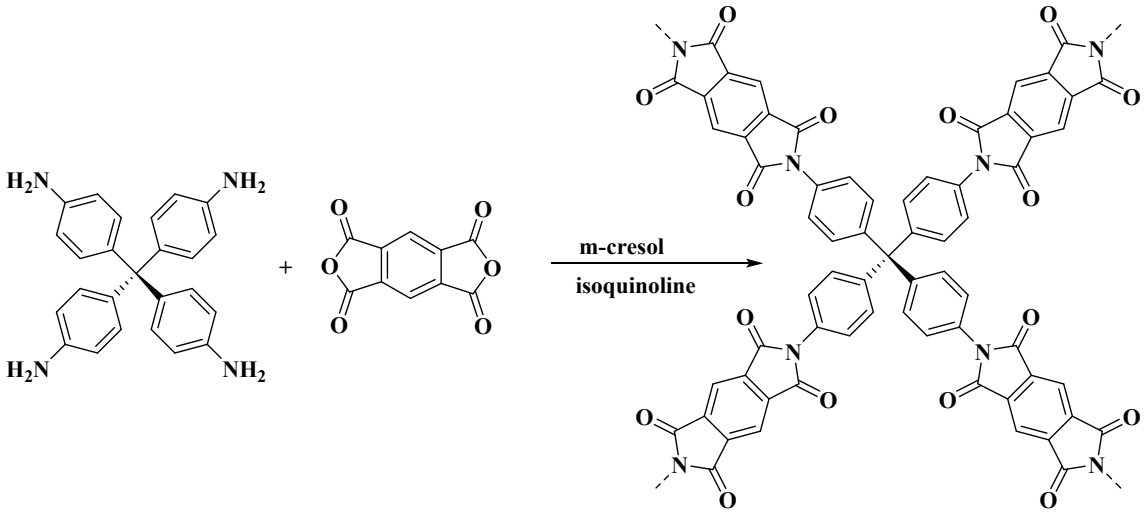

Figure 3-7: Synthesis of MPN-1.

To a dry three-neck round bottom flask equipped with a mechanical stirrer and a condenser, in an ice-bath, under a flow of nitrogen gas, tetra(*p*-amino phenyl)methane (TAPM) (0.400 g, 1.05 mmol), pyromellitic dianhydride (PMDA) (0.45 g, 2.10 mmol), and m-cresol (50 ml) were added and stirred for 2 h. Then, the reaction mixture was slowly heated to room temperature and a catalytic amount of isoquinoline (5 drops) was added. The temperature of reaction was increased and allowed to polymerize at 30 ^{o}C for 8 h, 80 ^{o}C for 4 h, 160 ^{o}C for 4 h, 200 ^{o}C for 10 h and 220 ^{o}C for 4 h. Once the reaction mixture was cooled down, the solid was isolated by filtration and washed successively with DMF, methanol and THF in order to remove any residual monomers, low molecular weight oligomers, solvent and catalyst. Further purification was done using THF in a soxhlet apparatus for 24 h. The product was then dried at 120 ^{o}C under vacuum for 24 h.

3.2.3.4 Synthesis of Network Polyimide (MPN-2)

In the synthesis of MPN-2, the dianhydride which is shown in Figure 3-8 was produced in three steps, as described below.

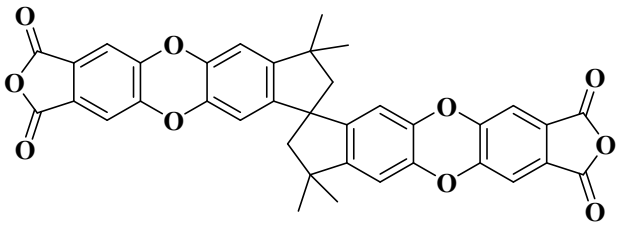

Figure 3-8: Structure of dianhydride.

3.2.3.5 Synthesis of bis(phthalonitrile)

Bis(phthalonitrile) was synthesized in accordance with the procedure of Maffei *et al*.[14] The schematic synthesis of bis(phthalonitrile) is shown in Figure 3-9.

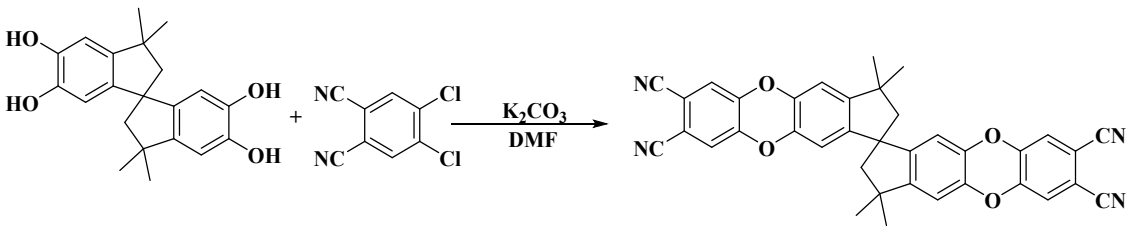

Figure 3-9: Schematic synthesis of bis(phthalonitrile).

To a dry two-neck round bottom flask, under a stream of nitrogen gas, were added 4,5-dichlorophthalonitrile (9.26 g, 47 mmol), 5,5',6,6'-tetrahydroxy,3,3,3',3'-tetramethyl,1',1,-spirobisidane (8 g, 23.5 mmol) and anhydrous dimethylformamide (DMF) (100 ml). Then, an excess of potassium carbonate (20.4 g, 0.1477 mmol) was added slowly with stirring. The mixture was heated at 80 ^{o}C for 3 h. Once the mixture was cooled, it was washed with distilled water (500 ml). After that, the product was collected by filtration and dried. The solid was recrystallized from methanol and dichloromethane. Finally, the product was dried in a vacuum oven at 100 ^{o}C

overnight, yield 10.7 g (77.4%). ^{1}H NMR ($CDCl_3$, 400 MHz): 1.32 (6H, s, CH_3), 1.37 (6H, s, CH_3), 2.16 (2H, d, *J*= 13.4 Hz, CH_2), 2.34 (2H, d, *J*= 13.1 Hz, CH_2), 6.34 (2H, s, Ar-H), 6.71 (2H, s, Ar-H), 7.10 (2H, s, Ar-H), 7.19 (2H, s, Ar-H). FT-IR (thin film, cm^{-1}): 2235 (C ≡ N stretching), 1332 (C-O stretching).

Elemental analysis calculated for $C_{37}H_{24}N_4O_4$: C, 75.50; H, 4.11; N, 9.52%. Found: C, 74.85; H, 3.88; N, 9.67%.

3.2.3.6 Synthesis of bis (dicarboxylic acid)

The next two steps were synthesized according to the procedure of Ghanem *et al*.[11] The schematic synthesis of bis(dicarboxylic acid) is shown in Figure 3-10.

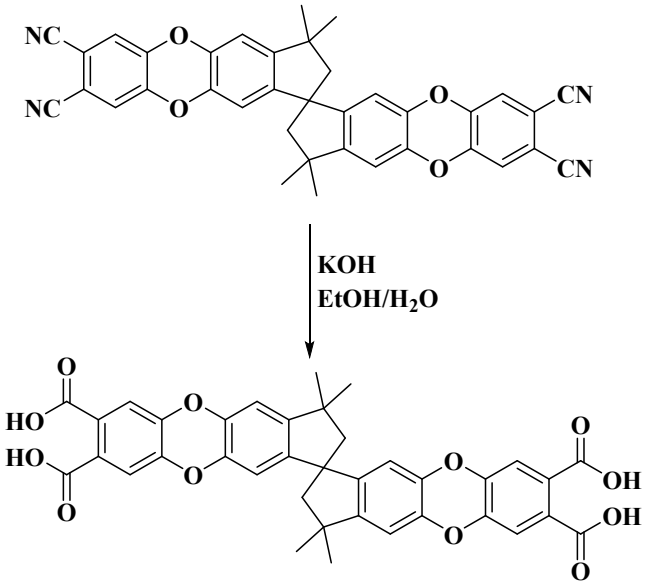

Figure 3- 10: Schematic synthesis of bis(dicarboxylic acid).

KOH (15.25 g, 272.02 mmol) was added to a mixture of ethanol-water (1:1 volume; 112 ml) in a one-neck round-bottom flask, with stirring to ensure complete dissolution. Then, bisphthalonitrile (8 g, 13.6 mmol) was added to the mixture. The mixture was heated to reflux with stirring overnight. After that, the solution was hot filtered in order to remove any insoluble particles. Once the mixture was cooled, the solution was acidified drop by drop with 3 M HCl; during the acidification a white gas could be seen, which is ammonia gas releasing from the solution, with white precipitate crashing from the solution. The precipitate was filtered under vacuum and washed with distilled water (1000 ml) in order to remove any remaining salts. The

product was dried in a vacuum oven at 100 °C overnight, yield, 7.56 g, (83.68%).^{1}H NMR (DMSO-d_6, 400 MHz): 1.27 (6H, s, CH_3), 1.34 (6H, s, CH_3), 2.12 (2H, d, *J*= 13.11 Hz, CH_2), 2.27 (2H, d, *J*= 13.11 Hz, CH_2), 6.35 (2H, s, Ar-H), 6.92 (2H, s, Ar-H), 7.37 (2H, br.s, Ar-H),7.44 (2H,br. s, Ar-H).). FT-IR (thin film, cm^{-1}): 3362 (OH), 1712 (C=O stretching), 1319 (C-O-C stretching). Elemental analysis calculated for $C_{37}H_{28}O_{12}$: C, 66.87; H, 4.25%. Found: C, 59.97; H, 3.44%.

3.2.3.7 Synthesis of bis (dianhydride)

The schematic synthesis of the dianhydride is presented in Figure 3-11.

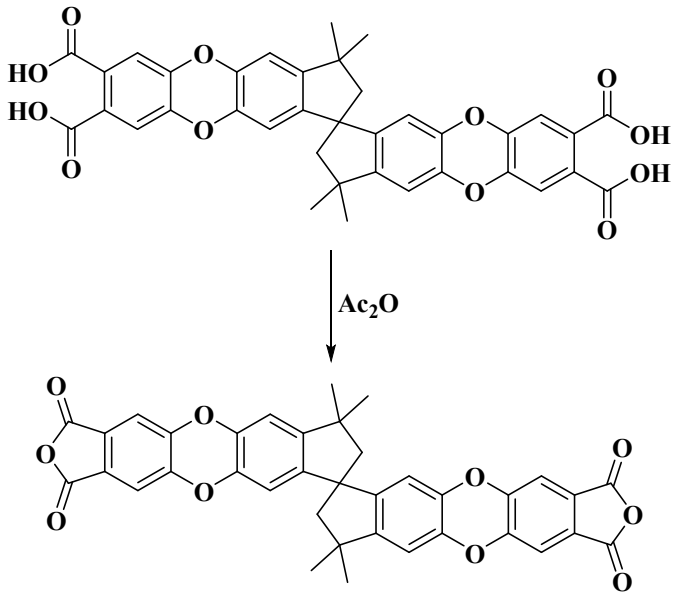

Figure 3-11: Schematic synthesis of bis(dianhydride).

To a one-neck round bottom flask were added bis(dicarboxylic acid) (3.5 g, 5.26 mmol) and anhydrous acetic anhydride (58.5 ml) under a nitrogen atmosphere. The mixture was heated and refluxed at 80°C for 24 h. Once the mixture was cooled, the yellow precipitate was collected by vacuum filtration, washed with acetic acid and toluene and dried in an oven at 80 °C overnight. Then, the solid was recrystallized from toluene and dried in a vacuum oven at 100 °C overnight, yield 2.6 g (74.2%).^{1}H NMR ($CDCl_3$, 400 MHz): 1.33 (6H, s, CH_3), 1.39 (6H, s, CH_3), 2.18 (2H, d, *J*= 13.4 Hz, CH_2), 2.35 (2H, d, *J*= 12.9 Hz, CH_2), 6.39 (2H, s, Ar-H), 6.74 (2H, s, Ar-H), 7.28 (2H, s, Ar-H),7.38 (2H, s, Ar-H). FT-IR (thin film, cm^{-1}): 1842 (asymmetric, C=O,

stretching), 1769 (symmetric, C=O, stretching), 1323 (C-O stretching). Elemental analysis calculated for $C_{37}H_{24}O_{10:}$ C, 70.70; H, 3.85%. Found: C, 70.44; H, 3.62%.

3.2.3.8 Synthesis of Network Polyimide (MPN-2-1)

MPN-2 was first prepared in accordance with a procedure of Li *et al*.[8] The schematic synthesis of MPN-2 is shown in Figure 3-12.

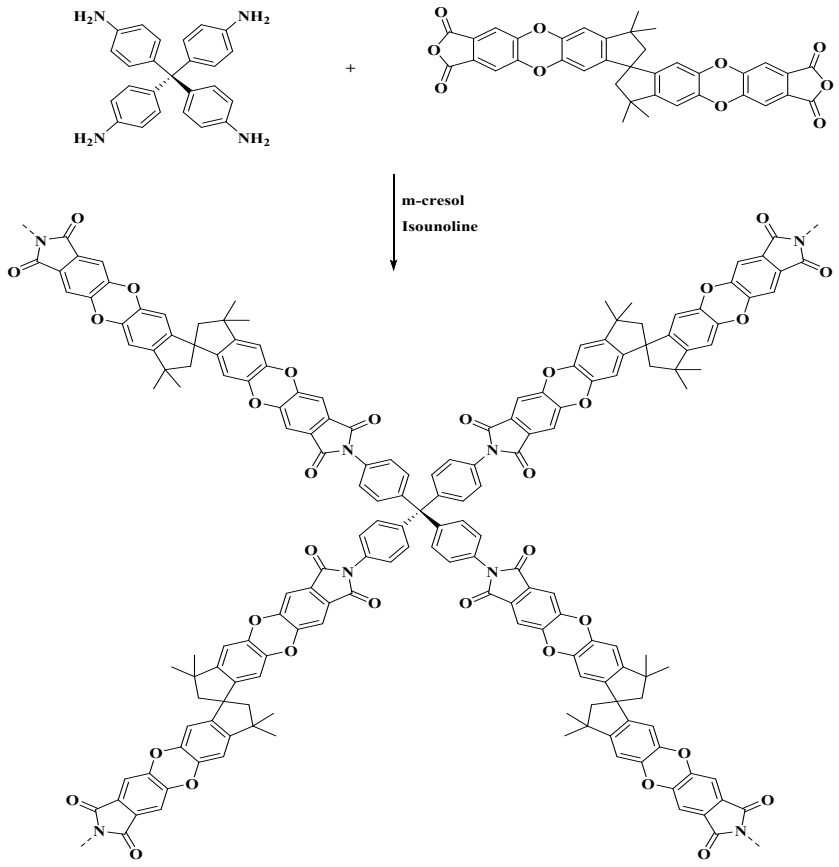

Figure 3- 12: Schematic synthesis of MPN-2.

To a dry three-neck round bottom flask equipped with a mechanical stirrer and a condenser, in an ice-bath, under a flow of nitrogen gas, tetra(*p*-amino phenyl)methane (TAPM) (0.09 g, 0.2 mmol), bis-dianhydride (0.3 g, 0.4 mmol), and *m*-cresol (15 ml) were added and stirred for 2 h. After that, the reaction mixture was slowly heated to room temperature and a catalytic amount of isoquinoline (5 drops) was added. Then, the temperature of reaction was increased and allowed to polymerize at 30 ^{o}C for 8 h, 80 ^{o}C for 4 h, 160 ^{o}C for 4 h, 200 ^{o}C for 10 h and 220 ^{o}C for 4 h. Once the reaction mixture was cooled down, the solid was isolated by filtration and washed

successively with DMF, methanol and THF. Further purification was done using THF in a soxhlet apparatus for 24 h. The product was then dried at 120 ^{o}C under vacuum for 24 h.

3.2.3.9 Synthesis of Network Polyimide (MPN-2-2)

MPN-2 was also prepared according to Wang *et al*.[1] Under a nitrogen atmosphere, in a three-neck round bottom flask equipped with a mechanical stirrer, and a condenser, were added tetra(*p*-amino phenyl)methane (TAPM) (0.09 g, 0.2 mmol), bis dianhydride (0.3 g, 0.4 mmol), and *m*-cresol (15 ml). The reaction mixture was stirred at room temperature for 1 h. A catalytic amount of isoquinoline (4-5 drops) was added and the temperature of polymerization was increased and kept at 80 ^{o}C for an additional 1 h. Then, the temperature was increased to 200 ^{o}C and allowed to polymerize at this temperature for a further 5 h. After cooling, methanol was added to the reaction mixture. The precipitate was filtered, washed with DMF and methanol. The solid was extracted with THF in a Soxhlet apparatus overnight and dried in a vacuum oven at 120 ^{o}C for 24 h.

3.3 Results and Discussion

3.3.1 MPN-1

MPN-1 was prepared by condensation polymerization according to Li *et al.*[8] as described previously. However, the amount of solvent in this method was insufficient to dissolve the monomers. Therefore, an extra amount of *m*-cresol solvent (40 ml) was added to complete the dissolution of all monomers. The MPN-1 was obtained as a brown powder which could not dissolve in any solvents, indicative of the network structure. Thus, the structure of polymer was characterized using FTIR and solid-state ^{13}C NMR spectroscopy.

3.3.1.1 FTIR Spectroscopy

The chemical structure of MPN-1 was confirmed using FTIR spectroscopy, as shown in Figure 3-13. The strong absorption bands at 1780 and 1726 cm^{-1} are attributed to asymmetric and symmetric vibration, respectively, of the carbonyl group of the imide ring. The absorption band at 1339 cm^{-1} is related to (-C-N-C) stretching of the five membered imide ring. The disappearance of the bands of the amino group at 3394 cm^{-1} and the anhydride group at around 1841 cm^{-1} confirm that a high degree of polymerization is achieved and the imidized network is formed successfully.

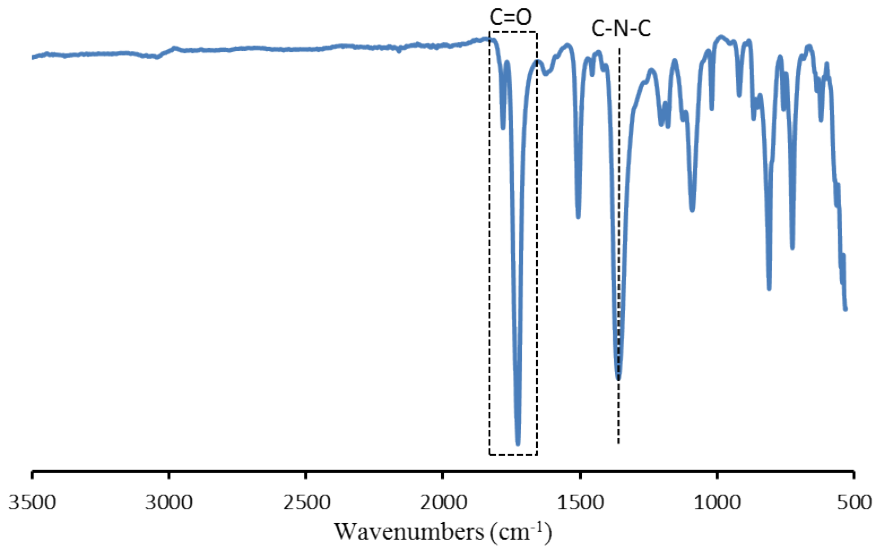

Figure 3-13: FTIR spectrum of MPN-1.

3.3.1.2 Solid State ^{13}C-NMR Spectroscopy

Solid-state ^{13}C NMR spectra provided further evidence of the chemical structure of MPN-1 (Fig. 3-14). The peak at 63 ppm corresponds to the aliphatic carbon of the tetrahedral unit, whereas the peak at 164 ppm is related to the carbonyl carbon of the imide ring. The peak at 145 ppm belongs to the N- substituted phenyl carbon of the imide ring, confirming the complete polymerization and formation of imide ring in the polymer structure. The overlapping peaks at 118.96, 129.94 and 136.30 ppm are assigned to other aromatic carbon atoms in the polymer backbone.

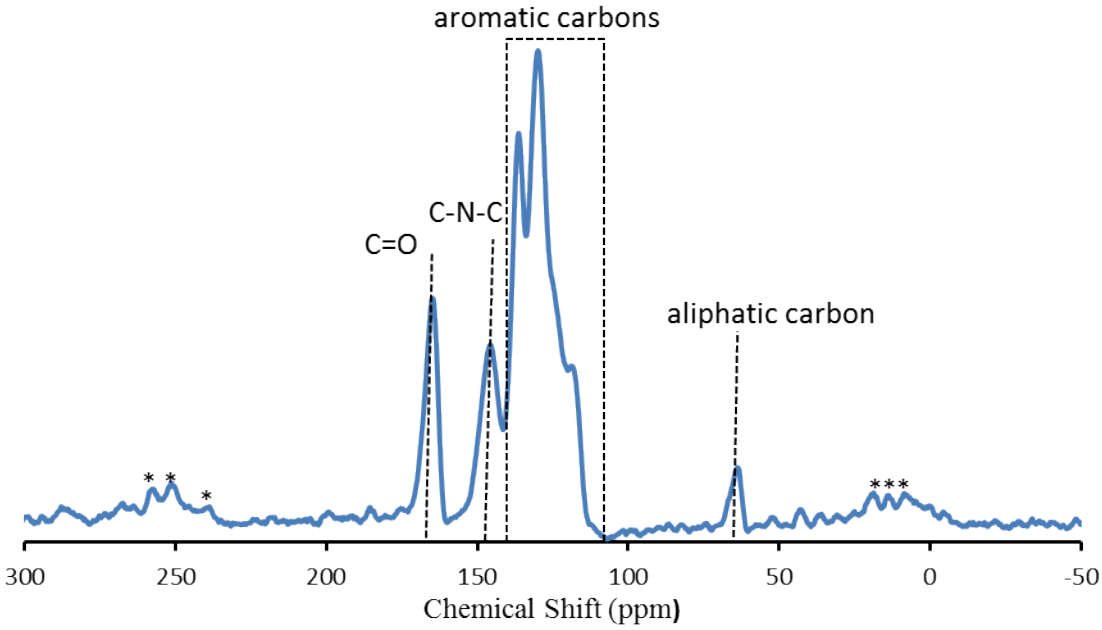

Figure 3-14:^{13}C Solid-state NMR spectra of MPN-1. Asterisks indicate peaks arising from spinning side bands.

3.3.1.3 Thermal Gravimetric Analysis (TGA)

The thermal stability of MPN-1 was examined using thermogravimetric analysis (TGA) under nitrogen atmosphere. As can see in Figure 3-15, MPN-1 shows high thermal stability up to 500 ^{o}C retaining about 52% of weight at 800 ^{o}C. The high

thermal stability of MPN-1 could be attributed to the high content of imide rings in the polymer structure and high crosslinking density. However, a small degradation after 300 °C can be seen, which may be related to the degradation of residual end groups. The small weight loss (< 6%) below 100 °C is due to the removal of moisture upon heating. [15]

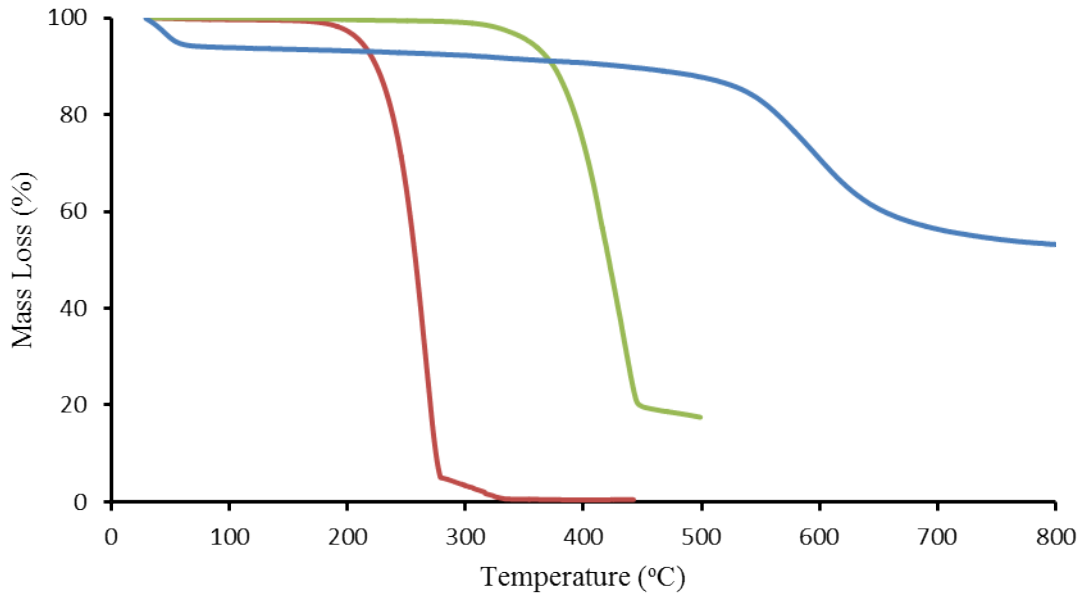

Figure 3-15: TGA of MPN-1 and monomers: (PMDA, red), (TAPM, green) and (MPN-1, blue).

3.3.1.4 Nitrogen Adsorption and BET Surface Area of MPN-1

The porosity of MPN-1 was analysed using N_2 sorption analysis at 77 K (Fig. 3-16). The high uptake of nitrogen gas at very low relative pressure indicates the microporous nature of the polymer. The unclosed hysteresis loop of the desorption curve above the adsorption curve can be related to the swelling of the polymer skeleton in liquid nitrogen.[7, 10, 16] The BET surface area of MPN-1 was measured as 1121 $m^2 g^{-1}$, lower than the BET data reported by Li *et al*. [8] (1454 $m^2 g^{-1}$). The lower surface area of MPN-1 might be because of changes in the polymerization conditions, such as concentration, which can result in a polymer that contains short branch units. The small remaining branches may have two different roles: they might open up the

network, thus increasing the swelling of MPN-1 in liquid nitrogen (Fig.3-16), or the presence of small end groups may fill up the pore space, which decreases the surface area of the MPN-2.[10]

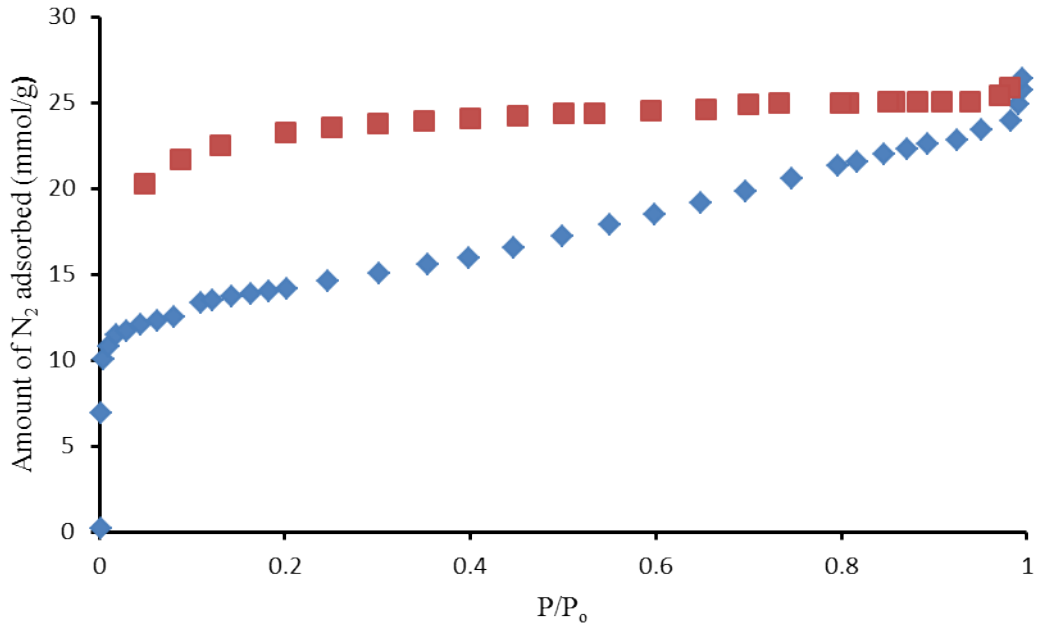

Figure 3-16: N_2 adsorption/desorption isotherm of MPN-1 at 77 K. Adsorption (blue diamonds) and desorption (red squares).

3.3.2 MPN-2

Two batches of MPN-2 (MPN-2-1 and MPN-2-2) were prepared according to Li *et al*. [8] and Weber *et al* [1], respectively. The resulting yellow/ brown solid was not soluble in any solvents. Due to the network structure of polymers, FTIR spectroscopy and solid-state ^{13}C NMR spectroscopy were utilized for analyzing the chemical structure of the polymers.

3.3.2.1 FTIR Spectroscopy

The structure of MPN-2 for both methods was confirmed by FTIR spectroscopy, as shown in Figure 3-17. The absorption bands at 1778 and 1720 cm^{-1} are characteristic of asymmetric and symmetric vibrations of the (-C=O) group of the imide ring, whereas the band at 1352 cm^{-1} is assigned to (-C-N-C-) stretching of the five membered imide ring, indicating the formation of imide ring in the polymer. The disappearance of bands at 3394 and 1842 cm^{-1} relating to N-H stretching of TAPM monomer and carbonyl group of dianhydride monomer, respectively, indicate complete condensation polymerization and successful formation of the imidized network.

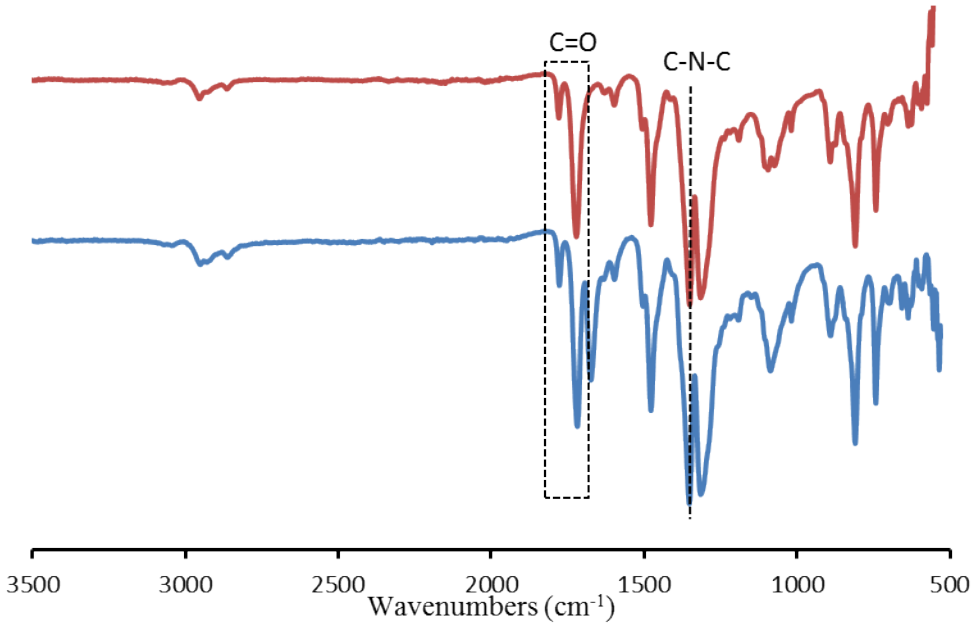

Figure 3-17: FTIR spectrum of MPN-2-2 (top, red) and MPN-2-1 (bottom, blue).

3.3.2.2 ^{13}C Solid-State NMR Spectroscopy

The chemical structure of MPN-2-1 and MPN-2-2 was further examined using solid-state ^{13}C NMR spectroscopy (Fig. 3-18). The peaks at 29, 42 and 56 ppm are related to CH_3, CH_2 groups and sp^3 carbon in the spiro-centre of the dianhydride monomer,

respectively. The peak at 64 ppm is assigned to the quaternary carbon of the tetrahedral centre, which confirms the presence of both monomers in the structure of the polymer. The peak at 164 ppm is attributed to the carbonyl carbon of imide ring, whereas the peak at 146 ppm is correlated to C-N substituted phenyl ring, indicating the successful polymerization and formation of imidized network. The overlapping peaks at 110, 127 and 140 ppm are related to other aromatic carbon atoms in the backbone of the polymer. The presence of a small peak at 35 ppm belongs to THF residual solvent trapped inside the network during soxhlet extraction, which can often be seen in porous organic polymers.[17, 18]

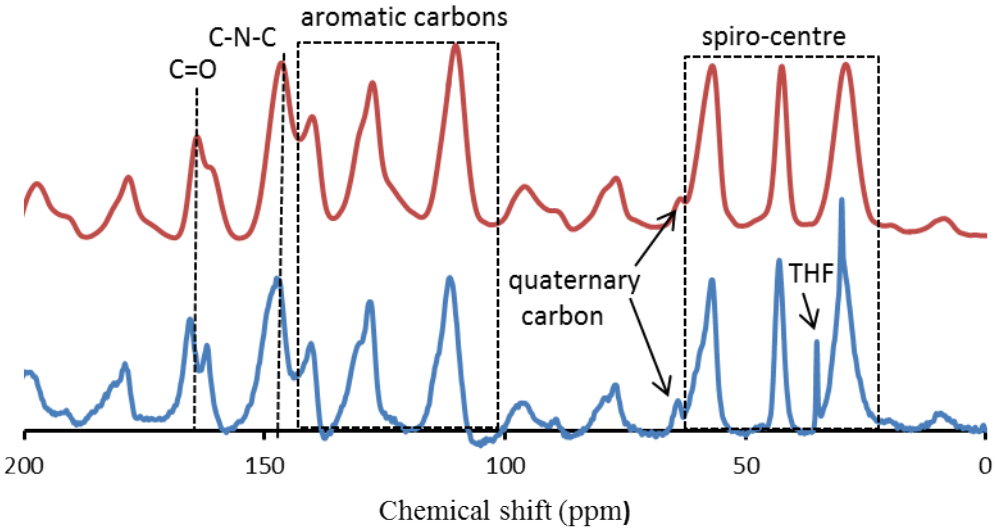

Figure 3- 18: Solid-state ^{13}C NMR spectra of MPN-2-1 (top, red) and MPN-2-2 (bottom, blue).

3.3.2.3 Thermal Gravimetric Analysis (TGA)

The thermal stability of MPN-2 prepared by different methods was investigated using thermogravimetric analysis (TGA). As shown in Figure 3-19, MPN-2 for both methods exhibits no decomposition in the backbone up to 500 ^{o}C which is comparable to reported network polyimides.[2-10] The high thermal stability of MPN-2 can be attributed to rigid tetrahedral shape. Furthermore, the presence of a spiro-centre (site

of contortion) and aromatic fused rings in the polymer structure can rigidify the polymer chains.

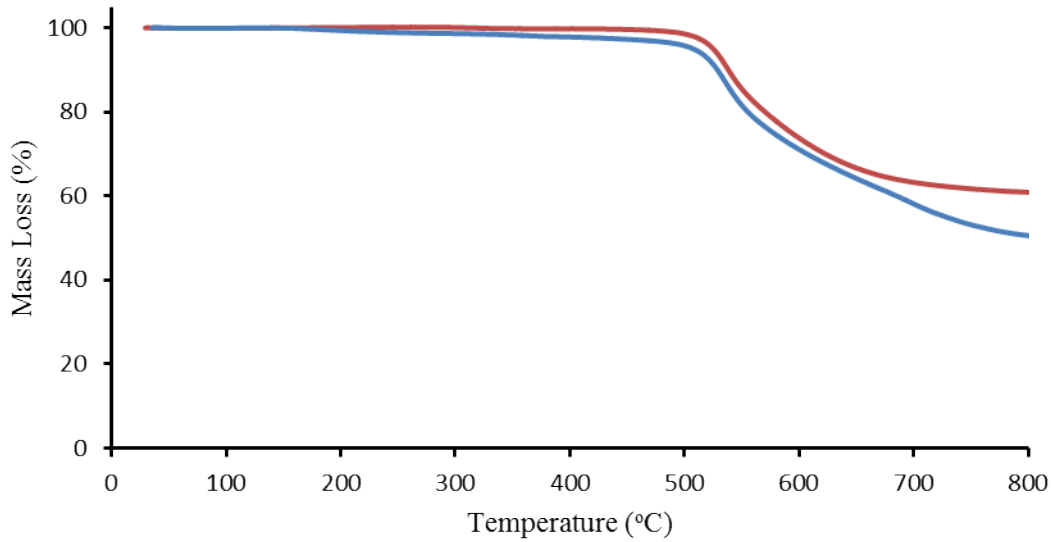

Figure 3-19: TGA of MPN-2-1 (blue) and MPN-2-2 (red).

3.3.2.4: N_2 Adsorption and BET Surface Area Measurement

The porosity of MPN-2 for both methods was analysed using N_2 sorption analysis at 77 K (Fig. 3-20). The isotherm shows a high uptake of N_2 gas at very low relative pressure, indicative the existence of microporosity in the polymer network. The unclosed loop of the desorption curve above adsorption curve can result from swelling of the network by liquid nitrogen.[7, 10, 16] The BET surface areas of MPN-2 polymer for both methods are presented in Table 3-1.

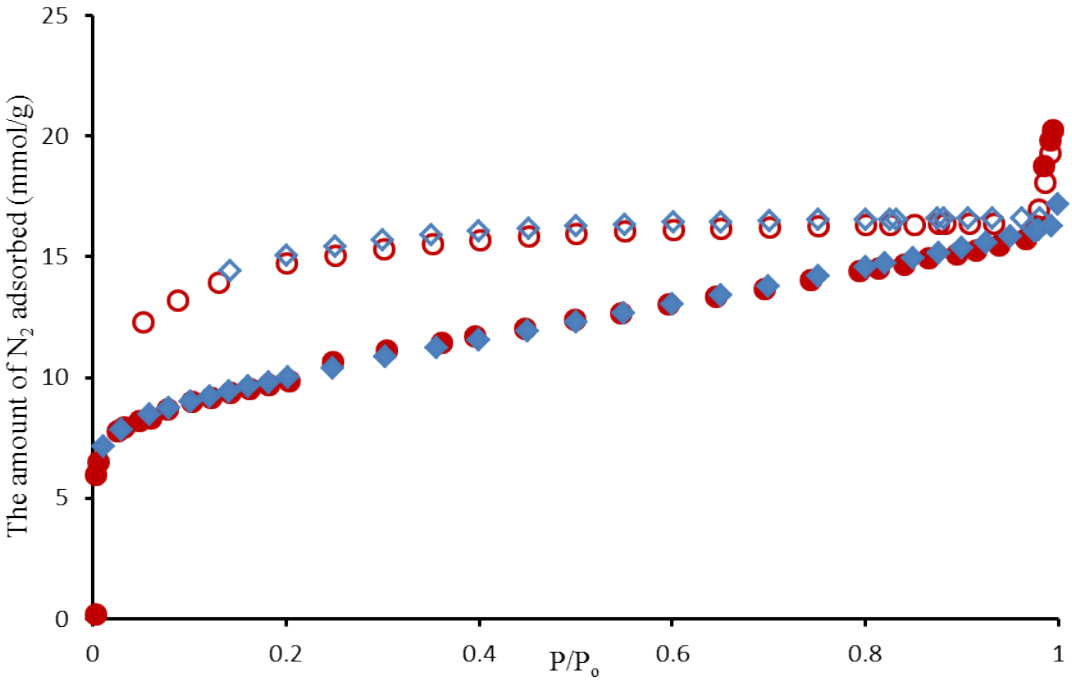

Figure 3-20: N_2 adsorption (filled symbols) and desorption (empty symbols) isotherms at 77 K. MPN-2-1 (circular symbols) and MPN-2-2 (diamond symbols).

Table 3-1: BET surface area of MPN-2 for both methods.

Polymer	BET surface area ($m^2\ g^{-1}$)
MPN-2-1	799
MPN-2-2	790

The high BET surface area of both polymers can be attributed to the rigid tetrahedral core with spirocentre (site of contortion), which could prevent the network polymer from packing efficiently. The surface areas of MPN-2 polymers are similar, which indicate that the change in the polymerization conditions has no effect on the surface area.

3.4 Summary

In this chapter, it has been shown that network polyimide fillers MPN-1 and MPN-2 have been prepared successfully. Both polymers were insoluble in common organic solvents, which indicate their network structure. The chemical structures of the polymers were characterized using FTIR spectroscopy and solid-state ^{13}C NMR spectroscopy. The thermal stability and porosity were evaluated using TGA and N_2 sorption analysis, respectively.

MPN-1 was prepared based on literature. However, a change in polymerization conditions, such as concentration, might have an effect on the surface area of the polymer. On the other hand, MPN-2 was prepared for the first time using two different methods. The data revealed that the chemical structure and BET surface area of MPN-2 prepared by both methods were comparable.

3.5 References

1. J. Weber, M. Antonietti and A. Thomas, Microporous networks of high-performance polymers: Elastic deformations and gas sorption properties, *Macromolecules.*, 2008, **41**, 2880-2885.

2. Z. Wang, B. Zhang, H. Yu, L. Sun, C. Jiao and W. Liu, Microporous polyimide networks with large surface areas and their hydrogen storage properties, *Chem. Commun*., 2010, **46**, 7730-7732.

3. Y. Luo, B. Li, L. Liang and B. Tan, Synthesis of cost-effective porous polyimides and their gas storage properties, *Chem. Commun*., 2011, **47**, 7704-7706.

4. C. Shen, Y. Bao and Z. Wang, Tetraphenyladamantane-based microporus polyimide for adsorption of carbon dioxide, Hydrogen, organic and water vapors, *Chem. Commun.*, 2013, **49**, 3321.

5. K. V. Rao, R. Haldar, T. K. Maji and S. J. George, Porous polyimides from polycyclic aromatic linkers: selective CO_2 capture and hydrogen storage, *Polymer*, 2014, **55**, 1452-1458.

6. O. K. Farah, A. M. Spokoyny, B. G. Hauser, Y-S. Bae, S. E. Brown. R.Q. Snurr. C. A. Mirkin and J. T. Hupp, Synthesis, properties, and gas separation studies of a robust diimide-based microporous organic polymer, *Chem. Mater.*, 2009, **21**, 3033-3035.

7. G. Li and Z. Wang, Naphthalene-based microporus polyimides: Adsorption behavior of CO2 and toxic vapors and their separation from other gases, *J. Phys. Chem*., 2013, **117**, 24428-24437.

8. G. Li and Z. Wang, Microporous polyimides with uniform pores for adsorption and separation of CO2 gas and organic vapors, *Macromolecules.*, 2013, **46**, 3058-3066.

9. Y. Yang, Q. Zhang, Z. Zhang and S. Zhang, Funtional microporus polyimides based on sulfonated binaphthalene dianhydride for uptake and separation of carbon dioxide vapors, *J. Mater. Chem. A*., 2013, **1,** 10368-10374.

10. Z. Wang, B. Zhang, H. Yu, G. Li and Y. Bao, Synthesis control of network topology and pore structure in microporus polyimides based on triangular triphenylbenzene and triphenylamine units, *Soft Matter*, 2011, **7**, 5723-5730.

11. B. S. Ghanem, N. B. Mckeown, P.M. Budd, N. M. Al-Harbi, D. Fritsch, K. Heinrich, L. Starannikova, A. Tokarev and Y. Yampolskii, Synthesis, characterization and gas separation properties of a novel group of polymers with intrinsic microporosity PIM-polyimides, *Macromolecules*, 2009, **42**, 7881-7888.

12. B. S. Ghanem, N. B. Mckeown, P. M. Budd, J. D. Selbie and D. Fritsch, High-performance membranes from polyimides with intrinsic microporosity, *Adv. Mater*., 2008, **20**, 2766-2771.

13. W. Lu, D. Yuan, D. Zhao, C. I. Schilling, O. Plietzsch, T. Muller, S. Brase,J. Guenther, J. Blumel, R. Krishna, Z. Li and H-C. Zhou, Porous polymer networks: Synthesis, porosity, and applications in gas storage separation, *Chem. Mater.,* 2010, **22**, 5964-5972.

14. A. V. Maffei, P. M. Budd and N. B. Mckeown, Adsorption studies of microporous phthalocyanine network polymer, *Langmuir*., 2006, **22**, 4225-4229.

15. P. Arab, M. Gulam. Rabbani, A. K. Sekizkardes, T. Islamoglu and H. M. El-Kaderi, Copper (I)-catalysed synthesis of nanoporous azo-linked polymers: Impact of textural properties on gas storage and selective carbon dioxide capture, *Chem, Mater*., 2014, **26**, 1385-1392.

16. P. M. Budd, A. Butler, J. Selbie, K. Mahmood, N. B. Mckeown, B. Ghanem, K. Msayib, D. Book and A. Walton, The potential of organic polymer-based hydrogen storage materials, *Phys. Chem. Chem. Phys.*, 2007, **9**, 1802-1808.

17. P. Pandey, A. P. Katsoulidis, I. Eryazici, Y. Wu, M. G. Kanatzidis and S. T. Nguyen, Imine-linked microporus polymer organic frameworks, *Chem. Mater*., 2010, **22**, 4974-4979.

18. A. Laybourn, R. Dawson, R. clowes, J. A. Iggo, A. I. Copper, Y. Z. Khimyak and D. J. Adams, Branching out with aminals: Microporus organic polymers from difunctional monomers, *Poly. Chem*., 2012, **3**, 533-537.

Chapter 4
Gas Transport Properties of MMMs

4.1 Introduction

This chapter will investigate the preparation of MMMs, and their characterization using different techniques including FTIR, PXRD, and SEM. This chapter will also explore the effect of Wt. % loading of filler particles on the gas permeation properties through a membrane where the fillers NP-1 and NP-2 are used. The permeability and selectivity of MMMs for different gas pairs is analyzed using the time lag method. The time lag method also is utilized to determine the diffusion coefficient, which with the permeability coefficient enables the solubility coefficient to be calculated.

Conventional mixed matrix membranes (MMMs) are comprised of a bulk polymer matrix (continuous phase) and inorganic particles (dispersed phase) as shown in Figure 4-1.[1-4] From the combination of both components properties has emerged a new generation of membrane for gas separation applications.[1, 3]

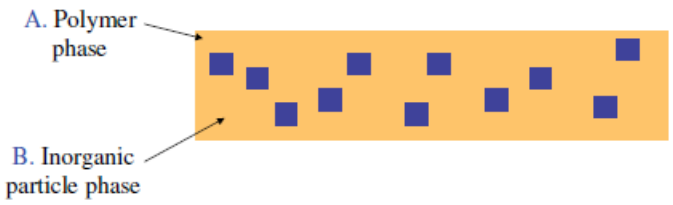

Figure 4-1: Schematic of a mixed matrix membrane (MMM).[2]

In an ideal mixed matrix membrane structure, polymer chains come into an intimate contact with the filler particle's surface, with a clearly transparent interface[5]. However, due to the difference in the properties between polymer and inorganic particles, as well as the tendency of inorganic particle fillers to agglomerate, fabrication of an ideal mixed matrix membrane with no defects in the polymer-inorganic particle interface is challenging and defects can form at the polymer-inorganic interface as a result of weak polymer-particle adhesion. These defects have a great impact on the membrane performance. The polymer-inorganic interface defects can be categorized as follow:[6]

1. Interface voids

2. Polymer chain rigidification

3. Particle pore blockage

As can see in Figure 4-2, case 1 presents the ideal morphology of mixed matrix membranes. Case 2 shows the interface voids around the filler particles as a result of low adhesion between the filler particles and polymer chains. Case 3 exhibits the region of rigidified polymer chains which are in direct contact with particle surface in which their mobility are decreased in comparison to bulk polymer chains. The formation of interface voids and rigidified polymer chains are related to stress which arise during the formation of membrane as a result of solvent evaporation or removal[6]. Case 4 shows the situation which is correlated to filler pore blockage in which the surface pores of fillers has been partially blocked by polymer chains[2].

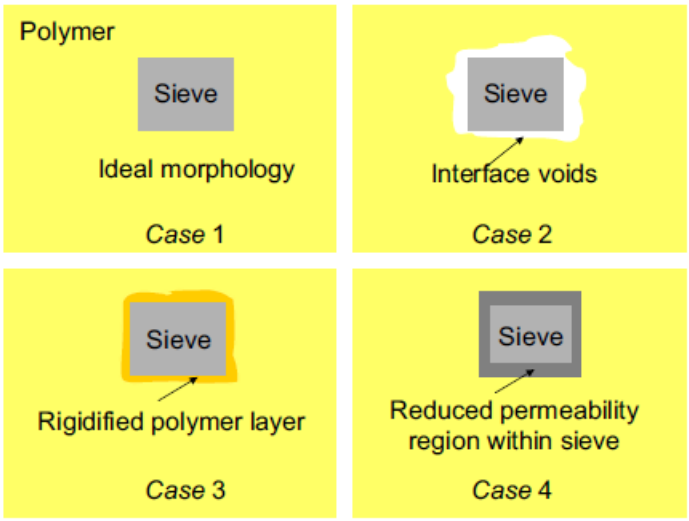

Figure 4-2: Schematic representation of various morphology of MMMs structure.[2]

Particle agglomeration is another problem which may arise during the fabrication of mixed matrix membranes. The agglomeration of inorganic particles result from the differences in density, polarity or other physio-chemical properties between filler and polymer, which cause precipitation of filler, resulting in the formation of an inhomogeneous phase between particle and polymer.[2,7] The agglomeration of inorganic particles can cause voids that are difficult to reach by polymer chains,

forming non-selective defects in the mixed matrix membranes. Especially, when increasing the loading of inorganic filler particles.[2,7, 8]

4.1.1 Fabrication of Mixed matrix Membranes

Fabrication of mixed matrix membranes is greatly affected by weak interaction between inorganic particles and polymer chains as well as a poor distribution of the particles in the polymer matrix phase. Furthermore, the properties of mixed matrix membranes are influenced by the pore size of particles, loading of particles and polymer type. Preparation of a homogenous solution between inorganic particles and polymer is an important factor in the first step of mixed matrix membranes fabrication. For this purpose, there are different methods that can be utilized:

1. The inorganic particles are dispersed into the solvent and left to stir for a period of time. This is followed by the addition of polymer to the solution, as shown in Figure 4-3a
2. Dissolving the polymer in the solvent. Then, the inorganic particles are added to the polymeric solution (Fig. 4-3b).
3. Dispersion of particles into the solvent. While, the polymer is dissolved separately in a solvent. Then, the particle suspension is added to the polymer solution (Fig. 4-3c).

The first and third methods are preferred for better distribution of inorganic particles as in a dilute suspension solution; the agglomeration is avoided by high shear rate during stirring. The second method is often used for distribution of nanoparticles in the polymer matrix.[6]

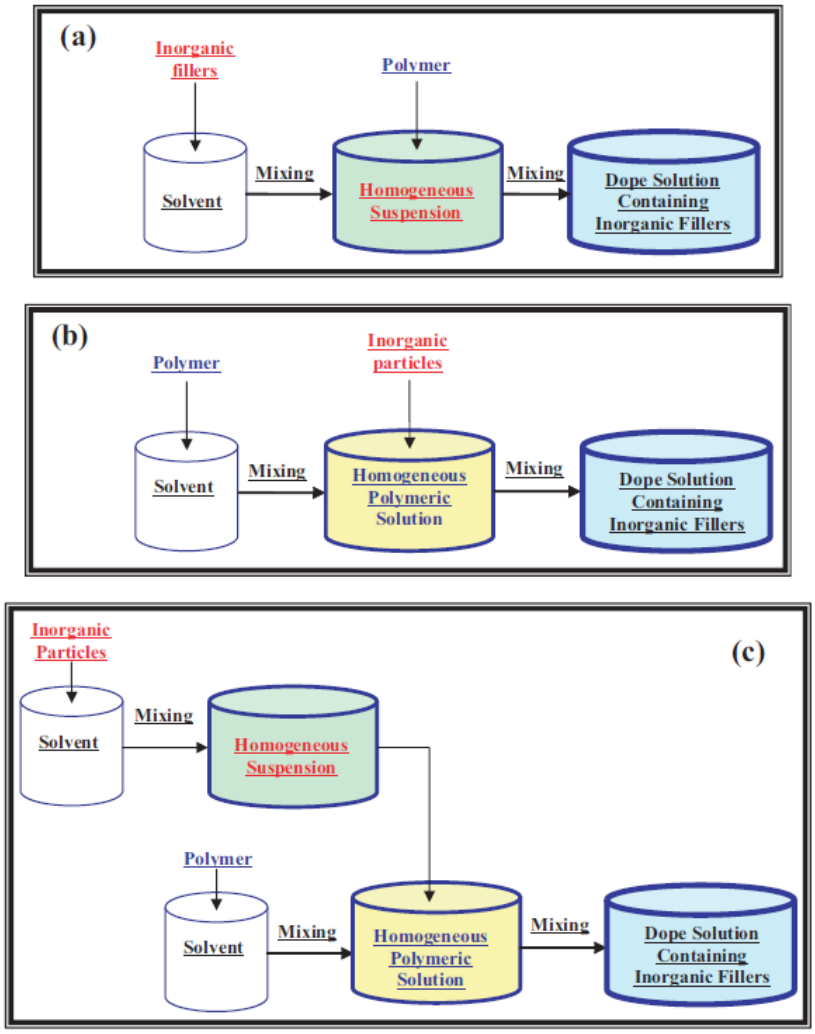

Figure 4-3: Different methods of mixed matrix membranes fabrication.[6]

4.1.2 Gas Transport of Polymeric Membranes

As mentioned previously, a membrane acts as a selective barrier by allowing the permeation of certain components while it retains the other components. In gas separation membranes, permeability and selectivity are two important factors to assess the performance of a membrane.[9] The efficiency of a membrane for gas separation is determined by its permeance, which is a measure of permeate that passes through a certain area of membrane in a given time for a particular pressure difference. When multiplying the permeance by the thickness of the membrane, the permeability coefficient, P, is obtained (Equation 4-1).

$$P = J.I/\Delta P \quad (4\text{-}1)$$

Where J is the flux, I is the membrane thickness and ΔP is the pressure difference.

In principle, the permeability is independent of membrane thickness for a homogenous membrane. Practically, permeability coefficient is affected by the thickness of the membrane and its history. The unit of permeability coefficient, P, is Barrer (1 Barrer = 10^{-10} cm^3 [STP] cm cm^{-2} s^{-1} cm Hg^{-1}.[10]

The permeation of gases through polymer membranes is described by solution-diffusion model, where permeability coefficient is the product of diffusion coefficient or diffusivity, D_A, a kinetic parameter which is governed by the size of penetrant, polymer chain mobility and free volume, and solubility coefficient, S_A, which is a thermodynamic parameter, relying on physicochemical interactions between the gas molecules and the polymer segments.[11, 12]

$$P_A = S_A D_A \quad (4\text{-}2)$$

Selectivity can be defined as the ability of a membrane to separate the mixture components. The ideal selectivity is determined by dividing the permeability of single gases and can be decoupled into solubility-selectivity and diffusivity-selectivity, Equation 4-3. [13, 14]

$$\alpha_i/_j = P_i/_{P_j} = D_i/_{D_j} \cdot S_i/_{S_j} \quad (4\text{-}3)$$

Where P is permeability and $\alpha_i/_j$ represents the selectivity of gas i and j in the mixture.

The sorption of gas molecules onto a polymer membrane is described by the dual mode sorption model. It is assumed that the penetrant can be fitted into two categories: molecules adsorbed directly into the polymer membrane, C_D is the concentration which follows Henry's law, C_H, associated with holes or microvoids in the polymer matrix, C'_H is the Langmuir capacity Equation 4-4.

$$C_D = K_D P, \qquad C_H = \frac{C'_{HbP}}{1 + bP} \tag{4-4}$$

Where K_D is the Henry's law coefficient, C'_H represents the hole saturation constant, p is the pressure and b is the hole affinity constant.[15, 16]

By combination of the two equations, the total concentration is obtained, Equation 4-5.[10, 12, 16]

$$C = K_D P + \frac{C'_{HbP}}{1 + bP} \tag{4-5}$$

4.1.3 Effect of Interfacial defects on the membranes gas separation

The interfacial region between the continuous phase and dispersed sieve phase plays an important role in the successful formation of mixed matrix membranes. The type of morphology that forms at the interfacial region has a great impact on the separation performance of the membrane.[17]

As described previously, due to poor adhesion in the interface phase between polymer bulk and inorganic particles, non-selective interfacial voids can be formed that are larger than the penetrating molecules. These voids allow the permeation of both the slow and fast molecules. As a result, the selectivity of mixed matrix membranes is decreased. While, the permeability is increased as the gas molecules pass through the less resistant interfacial voids rather than passing through the inorganic phase. Hence, the inorganic particles become ineffective for separation. On the other hand, if the interfacial adhesion between the polymer matrix and the particles is good, a reduction can occur near the filler particles surface, which is termed as polymer rigidification.[6, 17] It is believed that the rigidified polymer layer near the filler particles can result in the decrease of permeability and enhancement in the diffusivity selectivity as the mobility of polymer chains is decreased. Thus, higher selectivity around the filler particles with a decrease in gas permeability can be obtained in overall mixed matrix membranes.[2]

The pore blockage of filler particles with solvents and contaminants can also have an impact on the gas transport of mixed matrix membranes.[17] The effect is related to pore

size of fillers as well as the molecular diameter of gases. Generally, pore blockage of fillers decreases the gas permeability of mixed matrix membranes. The effect of pore blockage on selectivity is accompanied by the pore diameter of fillers. The selectivity decreases when the pore size of fillers is close to the molecular diameter of gases, while an enhancement in the selectivity can be achieved when the pore size of fillers is larger than the molecular diameter of gases.[2, 6]

4.1.4 Gas Transport properties of PIM-1

PIM-1 has been known as an interesting candidate for membrane gas separation.[18] PIM-1 has combined both high gas permeability and selectivity, [19] which placed PIM-1 above Robeson's upper bound for important gas pairs such as O_2/N_2 and CO_2/CH_4.[20] The high performance of PIM-1 over Robeson's upper bound can be related to high solubility, enhancing the permeability while the selectivity is maintained. The high solubility of PIM-1 for gases can be attributed to the microporous structure of PIM-1, which can provide high capacity for gas uptake, integrated with chemical functionalities of PIM-1 such as the polar cyano group which strengthens intermolecular interactions, thus improving sorption.[21]

4.1.5 Alcohol Treatment of PIM-1

Treating high free volume polymers such as poly(1-trimethylsilyl-1-propyne) (PTMSP) with alcohol has been studied previously.[22] Methanol has been utilized to erase any prior thermal and aging histories from PTMSP polymer. It was noted that treating PTMSP film with methanol increases the free volume and permeability compared to untreated films.[22] This is also true with polymers of intrinsic microporosity (PIMs) such as PIM-1 which can be treated with methanol (Fig. 4-4). The polymer chains swell reversibly in methanol which opens up the voids, thus increasing the free volume.[23] Furthermore; methanol treatment allows removing any residual solvent and allows relaxation of chains.[20]

The permeability coefficients of PIM-1 are greatly affected by the casting and treatment procedure of membrane. Budd *et al*.[24] has studied the effect of film casting

and treatment of PIM-1 on the gas permeability parameters. Three samples of PIM-1 have been tested after different treatments: The first sample of PIM-1 (GC1) was dissolved in THF solvent and after casting the solution on the surface of cellophane bottom in the casting cup; a weak stream of water was applied to peel off the film. The second sample (GC2) was first reprecipitaed in methanol and washed with acetone to get rid of adsorbed water or impurities. Then the PIM-1 solution was cast. Later on, it was peeled without contacting with water. The sample GC3 was prepared by immersing PIM-1 membrane in the methanol. The gas permeation results are shown in Table 4-1. It can be seen that treatment of PIM-1 membrane with methanol leads to increase in free volume. As a result, there is an increase in the diffusion of gas molecules in the membrane. The increase in the diffusion, boosting the gas permeability by three times for all gases tested, especially with the values of $P(O_2)$ and $P(CO_2)$, which shows that PIM-1 can be considered as a remarkably permeable membrane. Thomas *et al*.[25] studied PIM-1 membranes after treatment with methanol and drying at 70 ^{o}C in air. The alcohol treated samples of PIM-1 prepared by Budd *et al.*[24] and Thomas *et al.*[25] surpass the 1991 Robeson's upper bound and fall on or above the 2008 upper bound.[26]

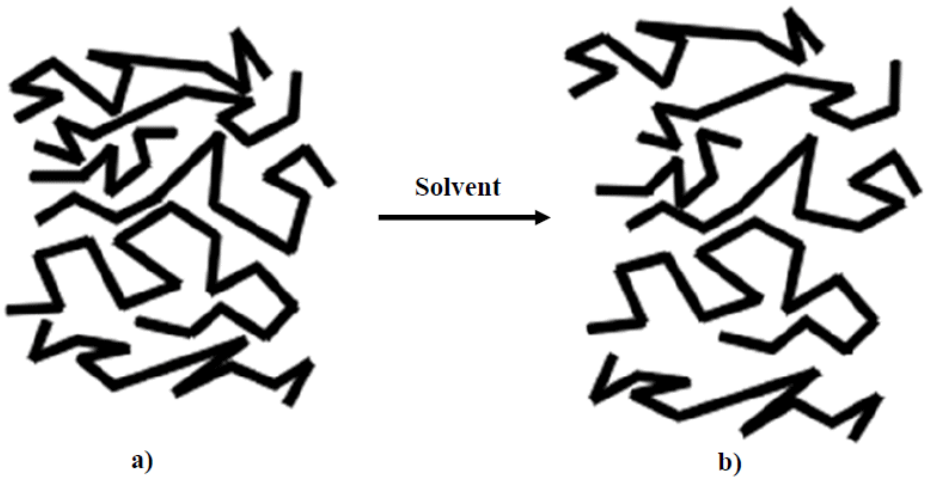

Figure 4-4: A schematic showing the swelling effect of alcohol treatment on polymers of intrinsic microporosity such as PIM-1, (a) before treatment with alcohol and (b) after treatment.

Table 4-1: Permeability (P), diffusion (D) and solubility (S) of PIM-1 membrane after different treatments.[24]

Sample		Gases			
		CH_4	O_2	N_2	CO_2
GC1	P	114	150	45	550
	D	-	9.3	5.7	3.5
	S	-	14	9.1	270
GC2	P	310	580	180	4390
	S	1.3	15	4.3	4.5
	D	160	40	35	770
GC3	P	740	1610	500	12600
	D	7.1	39	16	16
	S	163	39	37	700

P = Barrer = 10^{-10} cm^3 (STP) cm/cm^2 s cm Hg

D (× 10^7 cm^2/s) S (× 10^3 cm^3 (STP) / cm^3 cm Hg)

4.1.6 Mixed Matrix Membranes comprising of Porous Organic Fillers

As mentioned previously, mixed matrix membranes (MMMs) may combine the advantages of polymeric membrane materials and inorganic fillers, such as carbon molecular sieve, zeolite, metal oxides, carbon nanotubes, zeolite imidazole framework (ZIF) and metal organic framework (MOF), to enhance the performance of the membrane.[27] However, MMMs face many challenges with regard to interface morphology (e.g., chain rigidification, pore blockage and low adhesion) as well as poor dispersion of particles with the polymeric matrix (e.g., agglomeration or sedimentation of particles).[28] In most cases, a good dispersion between inorganic filler and polymer matrix requires hours or days to achieve homogenization or using high speed mixing or even sonication and coupling agents.[29] A number of approaches have been outlined with the advantage of using purely organic dispersed phases composed of C, H, N, O atoms which can exhibit better compatibility with a continuous polymer matrix.[30] In 2013, Rangel *et al*.[29] prepared MMMs by incorporating organic porous fillers with good chemical affinity to polymer matrix as both phases contained a polyimide skeleton. They assumed that the organic fillers with polyimides structure can bond strongly to the matrix phase through secondary linkages, aiming to achieve better adhesion to the matrix than inorganic or carbon fillers and reducing the formation of non-selective interface voids between the filler and polymer matrix. The group found that a good and very quick dispersion can be achieved without agglomerates and voids, which improves the preparation of mixed matrix membranes, thus enhancing the gas permeation performance of the membrane. Bushell *et al*. [30] prepared MMMs using porous organic cages as a dispersed phase with a polymer of intrinsic microporosity (PIM-1) as a polymer matrix. It was noticed that the incorporating of porous organic crystalline material into PIM-1 can significantly increase permeability and maintain good selectivity, as well as enhancing resistance towards physical aging. In 2014, Lau *et al*.[31] prepared mixed matrix membranes using a porous aromatic framework (PAF), tetrakis (4-bromophenyl)-methane (PAF-1) as dispersed phase with super glassy polymers such as poly (trimethylsilypropyne) (PTMSP), poly(4-methyl-2-pentyne) (PMP) and polymer of intrinsic microporosity (PIM-1). The study revealed that adding PAF-1 to super glassy polymers can freeze the chain packing of polymers. Thus, stopping the aging process and permeability

decline over time. This approach makes microporous organic polymers attractive materials for long time use in gas separation applications. In 2015, Lau *et al*.[32] prepared PIM-1/PAF-1 nanocomposite membranes. They aimed to study the effect of adding porous aromatic frameworks such as PAF-1 on the gas transport properties of the membrane over time. The good interaction of PAF-1 pores with the bulky moieties of PIM-1 offer the opportunity to control the physical aging of PIM-1 over time. Furthermore, an enhancement in the H_2 permeability while maintaining high selectivity of H_2/N_2 is an important factor for the usage of ammonia as a H_2 storage medium.

4.2 Experimental Section

4.2.1 Preparation of PIM-1 Membrane

PIM-1 powder (0.192 g) was dissolved in anhydrous chloroform (10 ml) and left to stir overnight to ensure a complete dissolution of PIM-1 and formation of a homogenous solution. The PIM-1 solution was filtered through glass wool into a level glass Petri dish (7 cm in diameter) and placed inside a desiccator. Then, the membrane was allowed to form by solvent evaporation over 3-5 days.

4.2.2 Preparation of PIM-1/ MPN-1 and MPN-2 membranes

Mixed matrix membranes based on PIM-1 with microporous polyimide networks fillers (NP-1 and NP-2) were prepared as follows: PIM-1 was dissolved in anhydrous chloroform (5 ml) and stirred overnight. In the meantime, the network polyimide fillers were dispersed in anhydrous chloroform (5 ml) and left to stir overnight. Then, the network polyimide particles were sonicated for 15 min using a bench top sonicator supplied by Scientific Supplies before filtering the PIM-1 solution through glass wool into the network polyimide suspension. The resulting PIM-1/filler solution was stirred overnight. After that, the solution was sonicated for 15 min, cast into a level glass petri dish (7 cm in diameter) and placed inside a desiccator. The membrane was allowed to form through solvent evaporation over 3-5 days. Table 4-2 shows the amount of PIM-1 and network polyimide fillers (NP-1 and NP-2) which were utilized in the preparation of mixed matrix membranes.

Table 4-2: Amount of network polyimide fillers and PIM-1 used in the preparation of mixed matrix membranes.

Filler	PIM-1	Filler Amount Wt.%	Filler Amount (g)	PIM-1 Amount (g)	Solvent Amount (ml)	Casting Dish Diam. (cm)
-	PIM-1	0	0	0.192	10	7
MPN(1-2)	PIM-1	5	0.0095	0.1825	10	7
MPN(1-2)	PIM-1	10	0.019	0.173	10	7
MPN(1-2)	PIM-1	15	0.0285	0.1635	10	7
MPN(1-2)	PIM-1	20	0.038	0.154	10	7
MPN(1-2)	PIM-1	25	0.0475	0.1445	10	7
MPN(1-2)	PIM-1	30	0.057	0.135	10	7

4.2.3 Characterization Techniques

The Fourier transform infrared spectra of membranes were recorded on an ATI Matteson Genesis series FTIR spectrometer.

The powder X-ray diffraction (PXRD) was utilized to scan both the filler powders and MMMs. The data were collected on a Panalytical X' Pert Pro diffractometer Model PW 3040/60 using CuKα radiation at an operating voltage of 40 kV and 30 mA at room temperature. A small amount of each powder sample was put onto the sample holder and scanned between (2Θ) range of 5-40^{o}. A small piece of membrane was cut from the central region of MMM and placed in the middle of the sample holder and scanned as the powder samples.

The surface morphology of powder samples was investigated using a FEI Quanta200 ESEM. The Powder was scattered onto a carbon disc. Then, the samples were coated with gold via sputtering using an Emitech coater. The cross section of membranes was prepared by freeze fracturing after immersing the membranes in the liquid nitrogen. Then, the samples were placed onto the holder and coated in gold the same as powder samples.

The CO_2 sorption analysis of the powder samples was carried out using a Micromeritics ASAP 2050 surface area and porosity analyzer. A small amount of sample (between 0.1- 0.2 g) was weighed into the degas port. It was then degassed automatically under high vacuum at 100 ^{o}C for 16 h. After reweighing, the sample was placed in the analysis port and degassed manually for a further 2 h to ensure that all volatiles were removed completely from the sample. Then, the analysis was implemented at 298 K, in the relative pressure range from 0 to 8 bar. After completing the analysis, the sample was out-degassed for 2 h. Then, the free space was obtained using helium.

4.2.4 Gas Permeation Measurements

Time Lag Method

The measurements of gas permeability were accomplished by Dr. Johannes Jansen′s group at the Institute of Membrane Technology (ITM) in Italy. The single gas permeation measurements were performed in a fixed volume-pressure, manufactured by GKSS, Germany. The system (Figure 4-5) consists of a permeation cell, representing the heart of the system in which the flat membrane sample is placed on a sintered steel support, 8 gas cylinders were connected to the instrument with an additional liquid flask for vapour transport measurements.[33,34] The gases with purity 99.998% were tested in the following order: He, H_2, N_2, O_2, CH_4, and CO_2.[35] A Feed pressure can be used up to 1.33 bar with a resolution of 0.1 mbar and the permeate pressure can be determined between 0-13.3 mbar with a resolution of 0.001 mbar. The system is computer controlled by a series of pneumatic valves to the feed and permeate sides. Before membrane measurement, the membrane cell was evacuated for 2 h to remove dissolved gases or vapours. Before measurement of the subsequent gas, the membrane cell was first evacuated, flushed with second gas and again evacuated, to ensure the complete removal of the previous gas.[33]

The gas permeability measurements were determined using time lag mode, allowing for the diffusion coefficients of each gas to be calculated. The transient permeation for the fixed-volume pressure instrument is described by the Equation 4-6.[35, 36]

$$P_t = P_0 + \left(dp/dt\right)_0 + \frac{RT.A.l}{V_P.\,V_m}.P_f.S\left(\frac{D.t}{l^2} - \frac{1}{6} - \frac{2}{\pi^2}\sum_1^{\infty}\frac{(-1)^n}{n^2}\exp\left(-\frac{D.n^2.\pi^2.t}{l^2}\right)\right) \quad (4\text{-}6)$$

Here, P_t represents the permeate pressure at time t where P_0 is the starting pressure less than 0.05 mbar. The baseline slope $(dp/dt)_0$ is negligible if the membrane is free of defects. R is the universal gas constant, T is the absolute temperature and A is the exposed membrane area, V_p and V_m represents the permeate volume and molar volume, respectively, of a gas at standard temperature 0 ^oC and pressure 1 atm, P_f is the feed pressure, S and D are the solubility and diffusion coefficients and I represents the membrane thickness. The permeability coefficients, P, can be calculated using Equation 4-7, using the slope of the time-pressure curve in steady state condition.

$$P_t = P_0 + \left(dp/dt\right)_0 . t + \frac{RT.A}{Vp.V_m} . \frac{P_f.P}{I}\left(t . \frac{I^2}{6D}\right) \quad (4\text{-}7)$$

The diffusion coefficient can be calculated using time lag method as represented by Equation (4-8). [33]

$$D = I^2/6\theta \quad (4\text{-}8)$$

Where I represents the membrane thickness and θ is the time lag. Based on the solution-diffusion model, the solubility coefficient, S, can be obtained using Equation 4-2.

The thickness of membrane was measured using a digital micrometer (Mitutoyo). The as cast membrane samples were tested without any treatments. For alcohol treatment, the membrane samples were soaked in methanol overnight and then dried between two glass sinters overnight at room temperature.

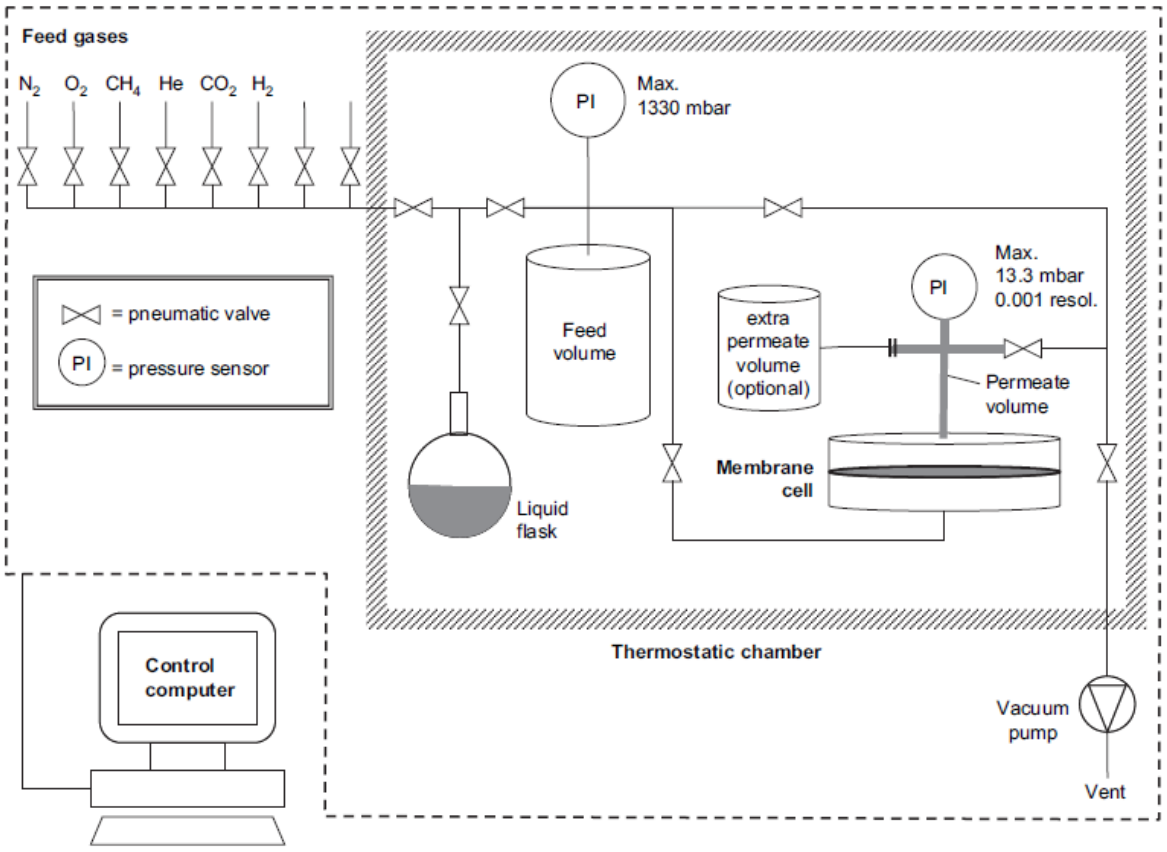

Figure 4-5: A schematic of gas permeation equipment.[34]

4.4 Results and Discussion

4.4.1.1 Preparation of PIM-1/NP-1 and NP-2 MMMs

Mixed matrix membranes were fabricated using PIM-1 with different loadings of microporous polyimide networks NP-1 and NP-2, starting with pure PIM-1 BD-2 (0 wt. % fillers) which forms a transparent bright yellow flexible membrane (Fig. 4-6.a). Homogenous membranes of PIM-1/NP-1 were formed with loadings of 10, 20, and 30 %. However, PIM-1/NP-1 membranes with 30 wt. % loading were tough and inhomogeneous on the macro scale, as can be seen in Figure 4-6, f and g. PIM-1/NP-2 membranes were cast with different loadings (10, 20, and 30 %). As shown in Figure 4-6h-n, the membranes exhibit homogeneity on the macro scale with the NP-1 particles being dispersed throughout the membrane.

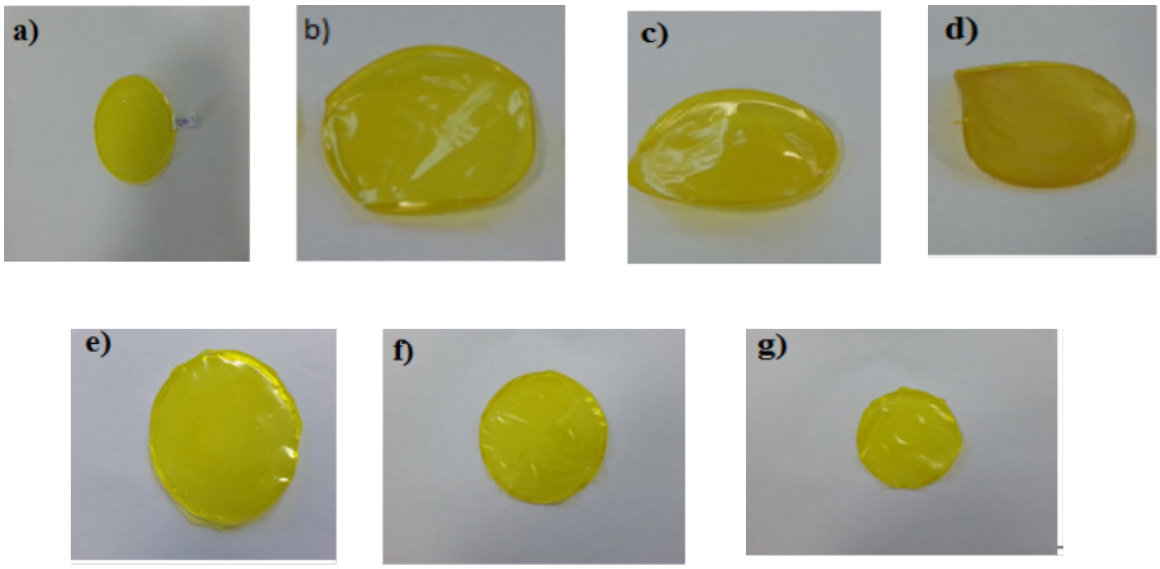

Figure 4-6: Images of PIM-1/NP-1 and NP-2 MMMs: (a) PIM-1 (BD-2), (b) PIM-1/ 10 wt.% NP-1, (c) PIM-1/ 20 wt.% NP-1, (d) PIM-1/ 30 wt. % NP-1, (e) PIM-1/ 10 wt.% NP-2, (f) PIM-1/ 20 wt.% NP-2, (g) PIM-1/ 30 wt. % NP-2.

4.4.2 Characterization of PIM-1/NP-1 MMMs

4.4.2.1 FTIR Spectroscopy

The dense membrane of PIM-1 and PIM-1/NP-1 MMMs were investigated using FTIR spectroscopy as can be seen in Figure 4-7. The absorption band at 2239 cm^{-1} is related to the nitrile group in PIM-1, whereas the band at 1263 cm^{-1} corresponds to the ether linkage. It can be noticed that the peak at 1722 cm^{-1} which belongs to asymmetric stretching of (C=O) group becomes more visible and stronger as a result of increasing NP-1 loading.

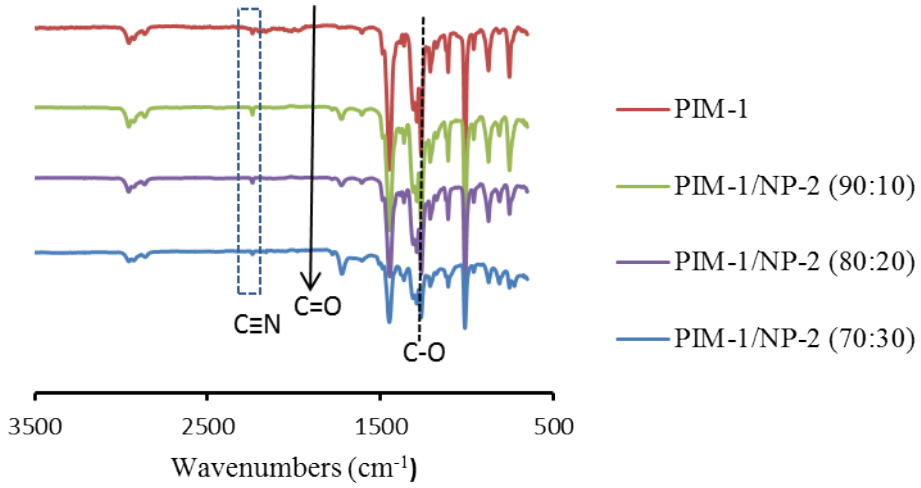

Figure 4-7: FTIR spectroscopy of PIM-1 membrane and PIM-1/NP-1 MMMs.

4.4.2.2 Powder X- Ray Diffraction (PXRD)

The PXRD patterns of PIM-1/NP-1 membranes have been compared with powder NP-1 as is presented in Figure 4-8. The NP-1 powder shows one amorphous halo located around (13-16°) consistent with Li *et al*[37]. It can be noticed that the reflection peak of NP-1 filler is seen throughout the MMMs and the intensity of peaks increases as the amount of filler increases.

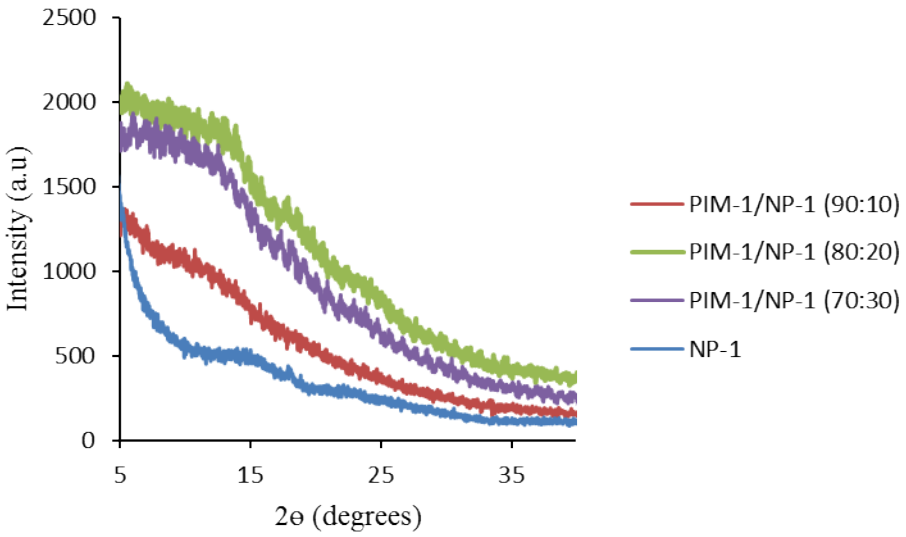

Figure 4-8: PXRD Patterns of NP-1 filler and PIM-1/NP-1 MMMs.

4.4.2.3 SEM Cross Section

The SEM images of NP-1 filler with cross section images of 10, 20, and 30 wt. % loaded of PIM-1/NP-1 MMMs is presented in Figure 4-9. As can be seen in Figures 4-9a, NP-1 consists of floppy agglomerates of tiny particles similar to that reported by Li *et al* [37]. The SEM image of (90:10) loaded PIM-1/NP-1 membrane does not show the distribution of NP-1 throughout the membrane due to low loading of filler. On the other hand, Figure 4-9c shows some loose agglomerates which might be attributed to poor dispersion of particles throughout the membrane. For higher loaded PIM-1/NP-1 membrane, a homogenous distribution of filler can be seen through the membrane.

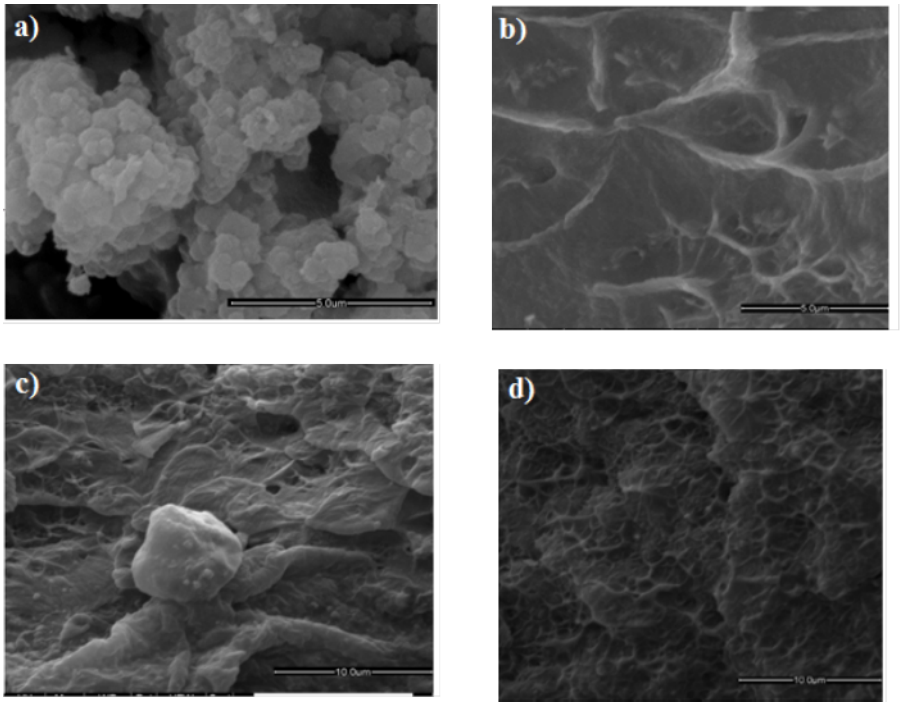

Figure 4-9: SEM image of NP-1 at 25,000 x magnification (a). SEM images of the cross sections of PIM-1/NP-1 (90:10) at 20,000 x magnification (b), (80:20) at 10,000 x magnification (c), (70:30) at 10,000 x magnification (d).

4.4.3 Characterization of PIM-1/NP-2 MMMs

4.4.3.1 FTIR Spectroscopy

The PIM-1 membrane and PIM-1/NP-2 MMMs were examined using FTIR spectroscopy as shown in Figure 4-10. The absorption band at 2239 cm^{-1} is attributed to the nitrile group in PIM-1, while the band at 1263 cm^{-1} relates to ether linkage. It can be seen that the absorption bands at 1724 cm^{-1} which correspond to asymmetric vibration of carbonyl group in the imide rings become more visible and stronger as the amount of NP-2 filler increases.

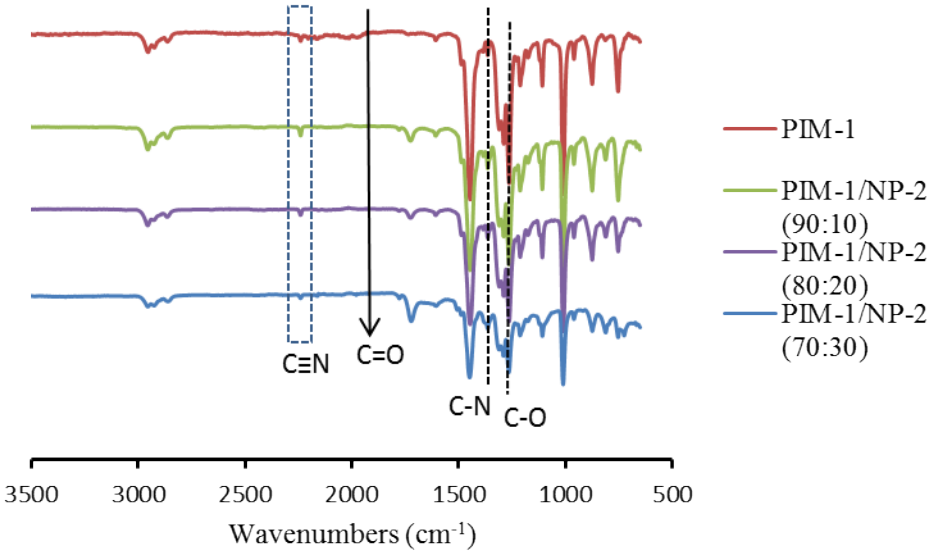

Figure 4-10: FTIR spectroscopy of PIM-1 membrane and PIM-1/NP-2 MMMs.

4.4.3.2 Powder X-Ray Diffraction (PXRD)

The PXRD patters of PIM-1/NP-2 membranes have been compared with powder NP-2. As is shown in Figure 4-11, NP-2 shows three broad halos. The peak at higher angles (5.4 Aº) can be attributed to chain-to chain distance of space efficient packed chains, whereas the peak at 7.2 Aº corresponds to loosely packed polymer chain which represents the formation of micropores between the polymer chains. The peak at 12.4 Aº is related to the distance between the spiro carbon atoms.[38] It can be seen that the reflection peak of NP-2 filler is shown throughout the MMMs and the intensity of peaks increases as the amount of filler increases.

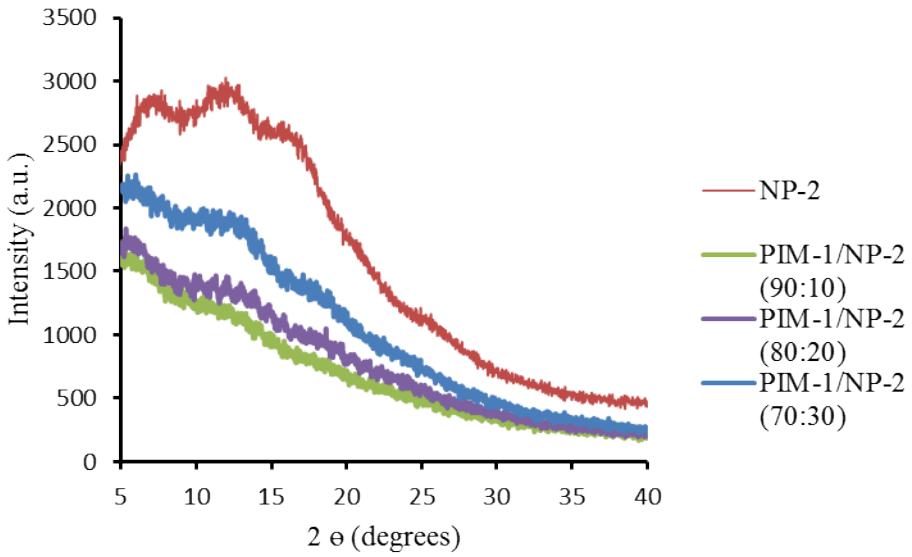

Figure 4-11: PXRD Patterns of NP-1 filler and PIM-1/NP-1 MMMs.

4.4.3.3 SEM Cross Section

Images of NP-2 with PIM-1/NP-2 MMMs are shown in Figure 4-12. It can be seen that the NP-2 is composed of agglomerates of particles with rough surface and irregular shapes. The SEM images of membranes show the good dispersion of filler throughout the membrane even at high loading. Where the polymer surrounds the particles with circular cavities. The good chemical affinity between the polymer matrix and NP-2 can be related to the presence of a spirocentre and dioxin rings in the structure of both polymer matrix and filler, which play an important role in increasing the compatibility between the two phases.

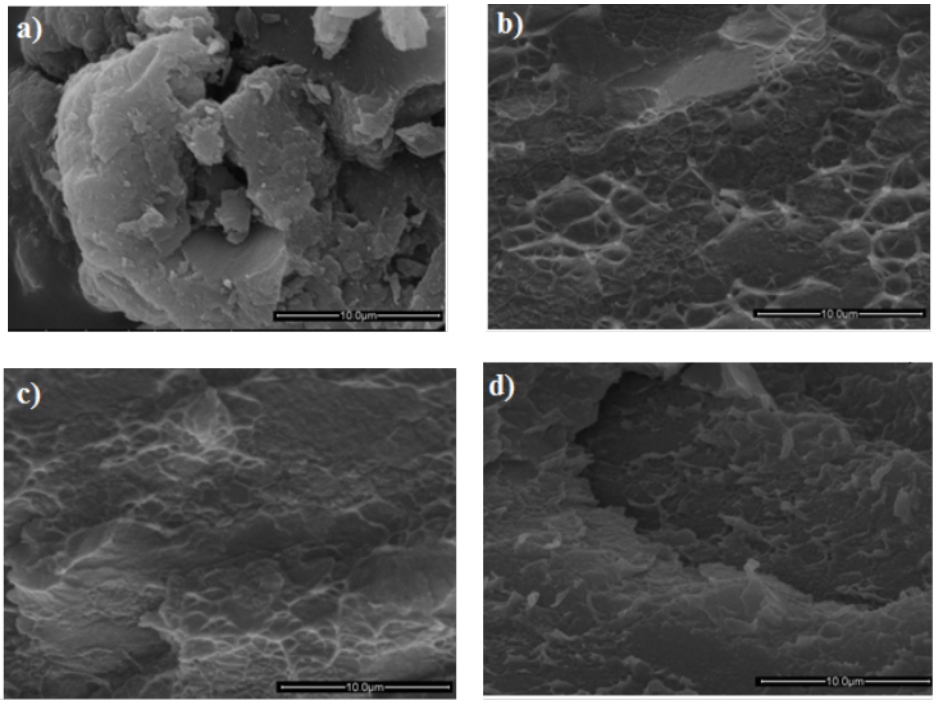

Figure 4-12: SEM image of NP-2 at 10,000 x magnification (a). SEM images of the cross sections of PIM-1/NP-1 90:10 (b), 80:20 (c), 70:30 (d) all at 10,000 x magnification.

4.4.4 CO_2 Adsorption in PIM-1 Polymer Matrix and Dispersed Fillers MPN-1 and MPN-2

The CO_2 adsorption properties of PIM-1 and network polyimides powders were measured at 298 K and in the pressure range from 0 to 8 bar as shown in Figure 4-13. It can be seen that both network polyimide fillers show high CO_2 uptake at high pressure in comparison to PIM-1, due to high surface area as described previously in chapter 3. It is expected that both fillers show high CO_2 uptake at low pressure as the network polymers contain abundant nitrogen and oxygen atoms in the form of imide heterocycles which increase the affinity towards CO_2 as a result of dipole-quadruple interactions between the pore surface and CO_2 molecules.[37-39] However, at 1 bar, the CO_2 uptake in the MPN-1 is higher than MPN-2 which might be related to the presence of very small pores (ultramicropores, < 0.7 nm). [40]

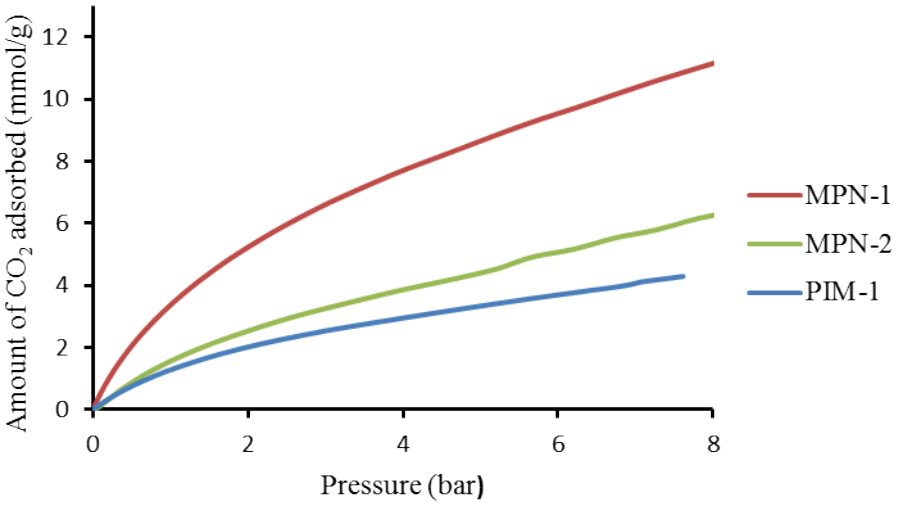

Figure 4-13: CO_2 adsorption isotherms of PIM-1 and MPNs at 298 K.

4.4.3 Gas Transport Properties of PIM-1/NP-1

The raw data of gas permeation properties (permeability and selectivity) of PIM-1 membrane and PIM-1/NP-1 MMM with ratio and treatment can be found in Appendix B.

As can be seen in Figure 4-14a, the permeability of PIM-1/NP-1 MMM decreases for all gases. The sharp decrease in the permeability of CO_2 gas for network polyimides (NPs) compared to PIM-1 can be attributed to the strong affinity between CO_2 and imide linkages. However, as can be seen in Figure 4-14b, at 20 wt.% there is an increase in the selectivity of small gases such as He, H_2 and CO_2 compared to as cast PIM-1, with the selectivity remaining stable across the MMM, which can be attributed to the presence of very small pores. After methanol treatment (Figure 4-14b), the permeability of H_2 and He gases increases 2-3 times. Whereas, the selectivity of H_2 and He over N_2 increases 13-17 times compared to PM-1. As described previously, alcohol treatment helps to flush out the residual solvent trapped inside the pores which opens up the voids. Hence, increasing the free volume.[20, 23]

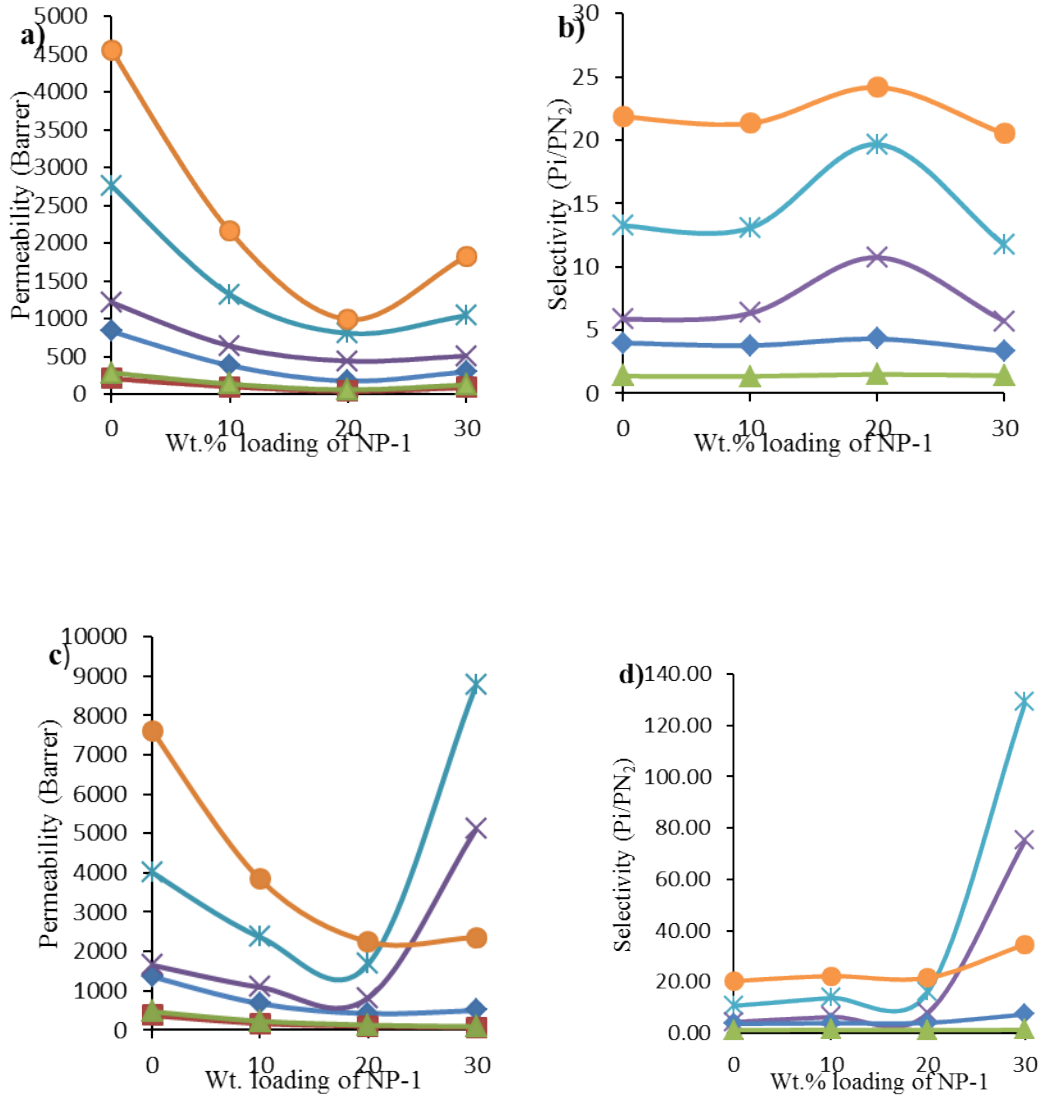

Figure 4-14: Graphs showing the permeability of gases (a and c) and selectivity of gases over N_2 (b and d) vs. wt. % loading of NP-1 in the PIM-1 membranes as cast (a and b) and after methanol treatment (c and d) for the following gases: O_2 (◆), He (×), H_2 (*), CO_2 (●), CH_4 (▲), and N_2 (■).

The raw data of gas permeation properties (diffusivity and selectivity) of PIM-1 membrane and PIM-1/NP-1 MMM with ratio and treatment can be found in Appendix B. The diffusivity and solubility of PIM-1 and PIM-1/NP-1 MMM were also investigated. In Figure 4-15, the diffusion and solubility coefficients are plotted against the wt. % of NP-1 in the membrane. As can be seen, the diffusion coefficients of N_2, O_2, CO_2, and CH_4 remain consistent. On the other hand, it can be seen that there is a decrease in the diffusivity of small gases such as He and H_2 as the amount of

filler is increased. This indicates that a decrease in the permeability of gases is affected by the decrease of diffusion. In terms of solubility, Figure 4-15b

shows a general decrease in the solubility of all gases compared to PIM-1. However, it can be observed that there is an increase in the solubility of CH_4 gas as the amount of filler increases. After methanol treatment, it can be seen that there is an increase in the diffusivity of He and H_2 gases as it is known that immersing the membrane in alcohol helps to increase the free volume of PIM-1 membrane which enhance the diffusivity as well as the permeability of gases.

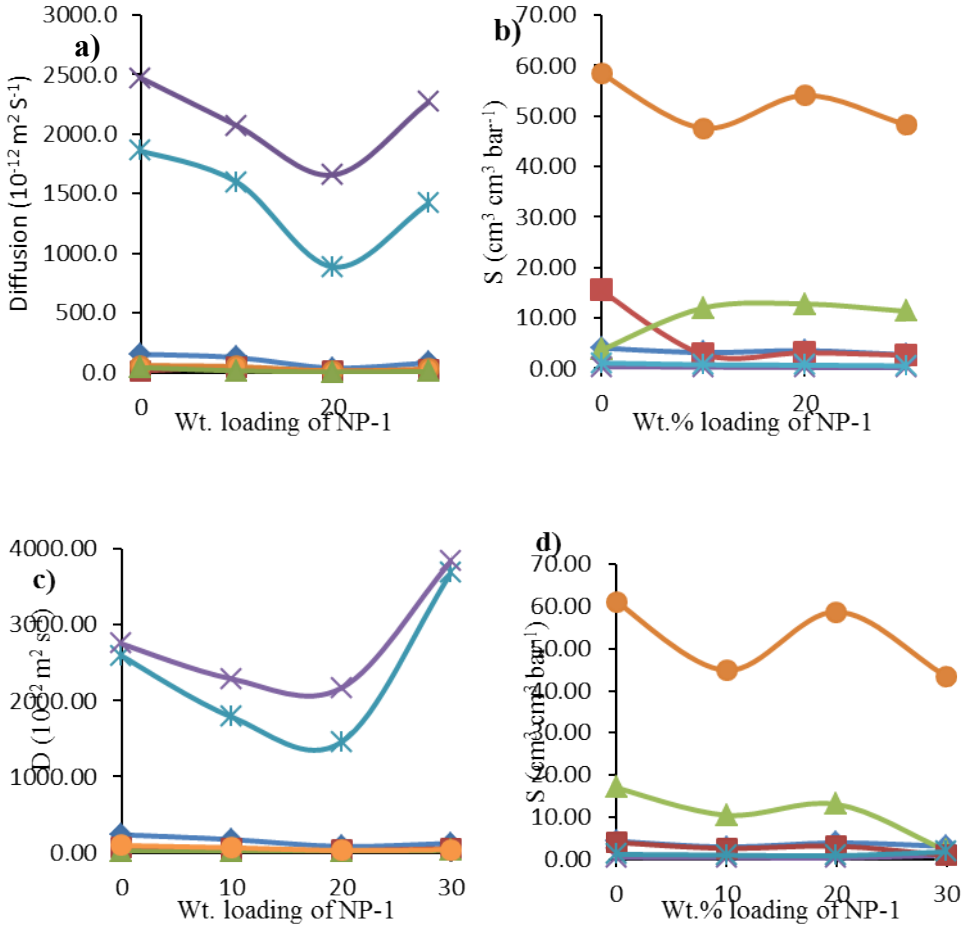

Figure 4-15: Graphs showing the diffusion of gases (a and c) and solubility of gases (b and d) vs. wt. % loading of NP-1 in the PIM-1 membranes as cast (a and b) and after methanol treatment (c and d) for the following gases: O_2 (◆), He (×), H_2 (*), CO_2 (●), CH_4 (▲) and N_2 (■).

The selectivity of PIM-1/NP-1 MMMs for different gases was plotted vs permeability and compared with Robeson's upper bounds (Figure 4-16). It can be seen that at 10 and 20 wt. % loading of NP-1 there is no improvement in the permeability of small gases such as H_2. However, an enhancement can be observed in the selectivity of H_2/CH_4, H_2/N_2, and H_2/CO_2. Furthermore, at high loading of NP-1(30 wt. %) and after treatment with methanol, it can be noticed an increase in the permeability of H_2 coupled with an extraordinary increment in the selectivity of H_2 over CH_4, N_2, and CO_2 gas, surpassing Robeson's 2008 upper bound, which as described previously can be related to the effect of small pores of NP-1 filler as a pathway for small gases. In terms of the effect of increasing the loading of NP-1 on the permeability of CO_2, it is shown that there is no improvement compared to the permeability of CO_2 gas for PIM-1 membrane. On the other hand, it is noticed an improvement in the selectivity of CO_2 over CH_4 and N_2.

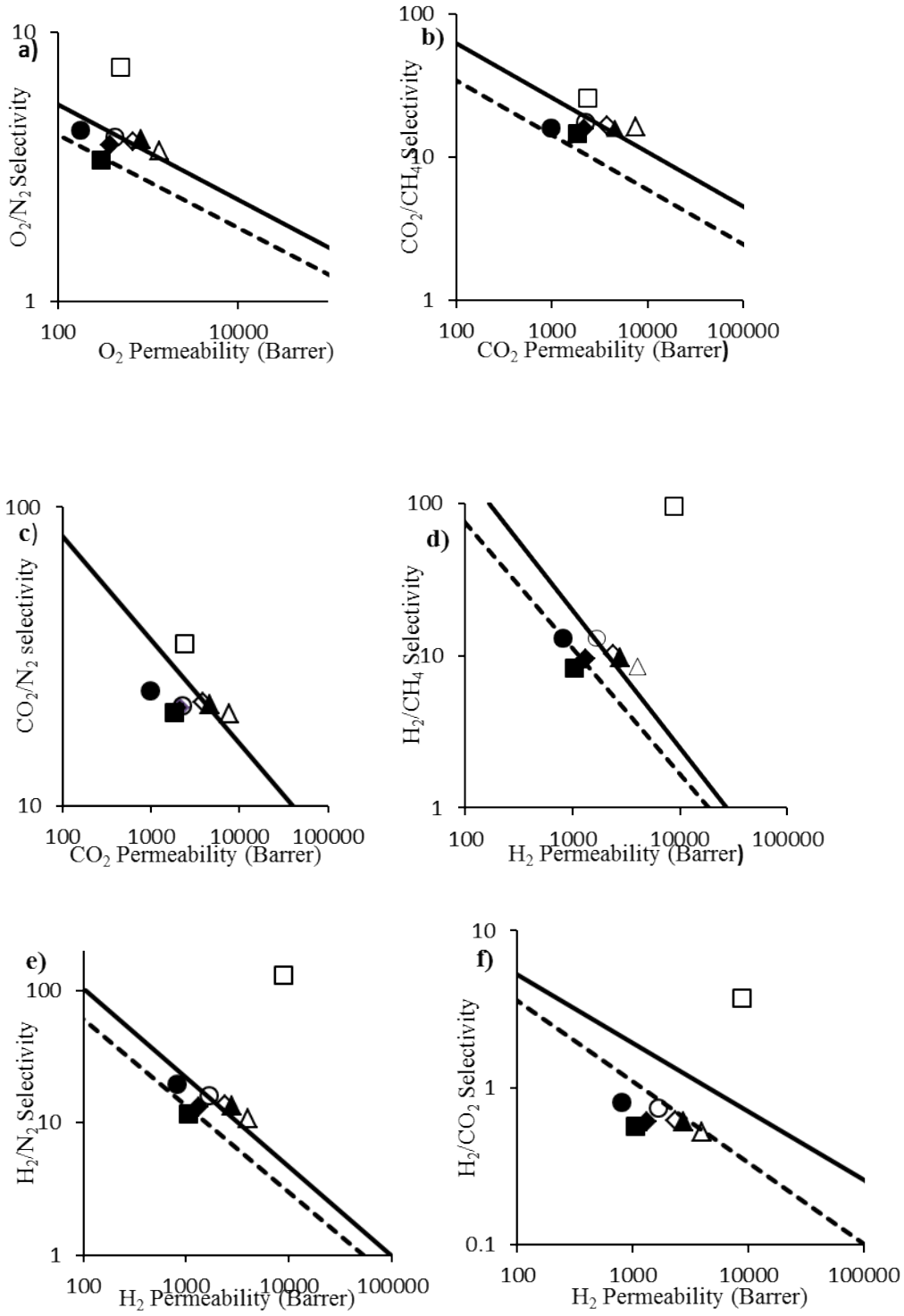

Figure 4-16: Robeson plots for important gas pairs. (a) H_2/N_2, (b) CO_2/CH_4, (c) CO_2/N_2, (d) H_2/CH_4, (e) H_2/N_2, (f) H_2/CO_2. (▲) PIM-1 as cast, (△) PIM-1 MeOH, (◆) 90:10 PIM-1/NP-1 as cast, (◇) 90:10 PIM-1/NP-1 MeOH, (●) 80:20 PIM-1/NP-1 as cast, (○) 80:20 PIM-1/NP-1 MeOH,(■) 70:30 PIM-1/NP-1 as cast, (□) 70:30 PIM-1: NP-1 MeOH. Dashed lines represent Robseon 1991 and solid lines represent Robeson 2008 upper bounds.

4.4.4 Gas Transport Properties of PIM-1/NP-2

The raw data of PIM-1 membrane and PIM-1/NP-2 MMMs for gas permeation properties (permeability and selectivity) with ratio and treatment can be seen in Appendix C. As can be seen in Figure 4-17a, at 10 and 20 wt. % loading of NP-2, the permeability of CO_2, H_2, and He gases increases 1.66 times compared to as cast PIM-1. Whereas, the permeability of CH_4, O_2, and N_2 remains consistent as the amount of filler increases. In terms of the selectivity, it is shown that the selectivity of CH_4 is constant with increasing the amount of NP-2, while the selectivity of CO_2, H_2, He, and O_2 over N_2 shows a slight increase compared to PIM-1 as the loading of NP-2 increases. (Figure 4-17b) shows that after methanol treatment, there is an increase in the permeability of CO_2, H_2, and He. The immersing of membrane in methanol have a good impact on the permeability of gases as alcohol treatment helps to remove residual solvents trapped inside the pores and voids. Thus, open a pathway for gases.

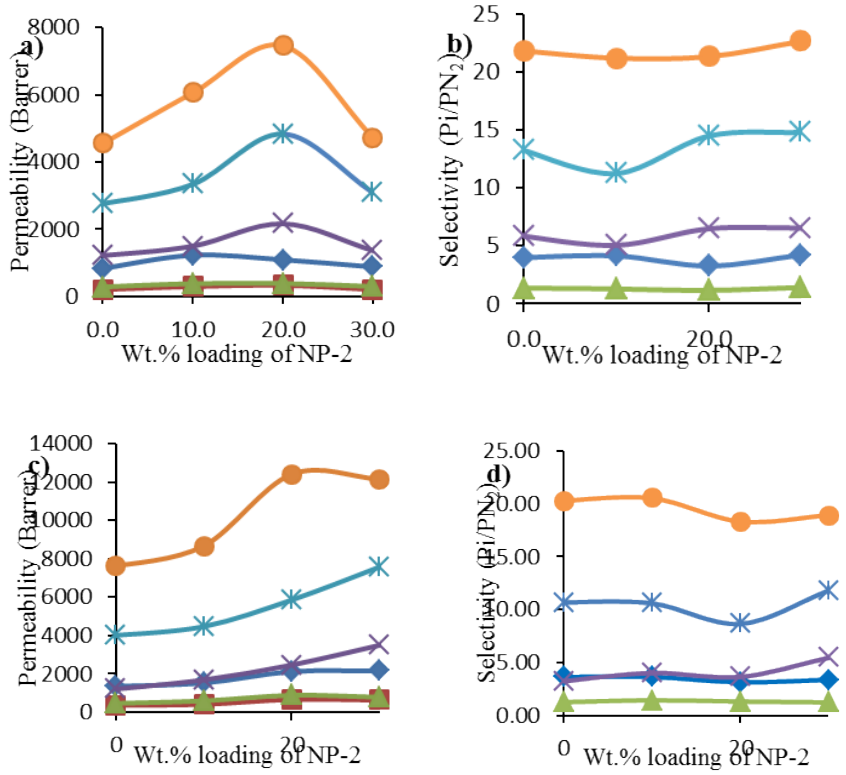

Figure 4-17: Graphs showing the permeability of gases (a and c) and selectivity of gases over N_2 (b and d) vs. wt% loading of NP-2 in the PIM-1 membranes as cast (a and b) and after methanol treatment (c and d) for the following gases: O_2 (◆), He (×), H_2 (*), CO_2 (●), CH_4 (▲), and N_2 (■).

The raw data of PIM-1 membrane and PIM-1/NP-2 MMM for gas permeation properties (diffusivity and solubility) with ratio and treatment can be seen in Appendix D. The diffusivity and solubility of PIM-1 and PIM-1/NP-1 MMMs were also examined. In Figure 4-18, the diffusion and solubility coefficients are plotted vs wt. % loading of NP-1 in the membrane. As can be seen in Figure 4-18a, there is an obvious enhancement in the diffusivity of small gases such as H_2, and He with a slight increase in the diffusion of CO_2, O_2, N_2, and CH_4 as the amount of filler increases. The diffusion coefficients of N_2, O_2, CO_2, and CH_4 remain consistent. For solubility, Figure 4-18b shows a general decrease in the solubility of all gases compared to PIM-1. After methanol treatment, it can be seen that there is an increase in the diffusivity of He and H_2 gases as it is known that immersing the membrane in alcohol helps to flush out the residual solvent, out of the membrane

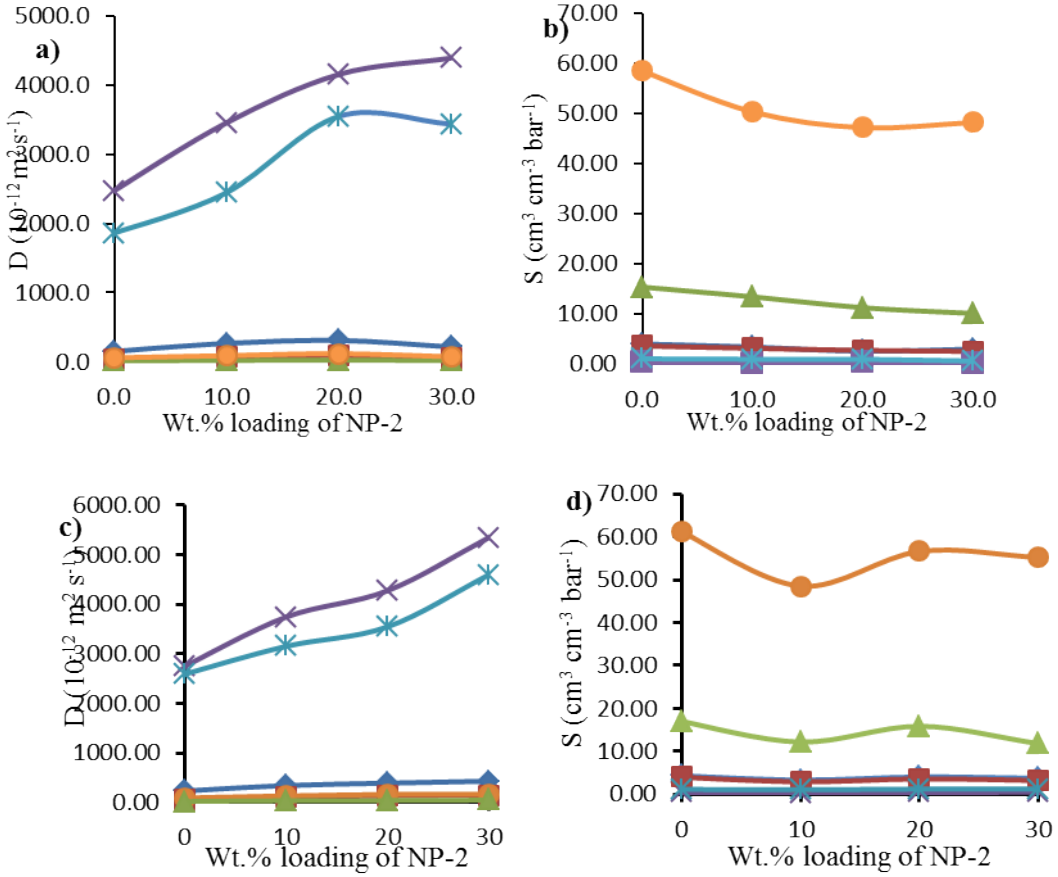

Figure 4-18: Graphs showing the diffusion of gases (a and c) and solubility of gases (b and d) vs. wt. % loading of NP-2 in the PIM-1 membranes as cast (a and b) and after methanol treatment (c and d) for the following gases: O_2 (◆), He (×), H_2 (*), CO_2 (●), CH_4 (▲), and N_2 (■).

The selectivity of PIM-1/NP-2 MMMs for different gases was plotted against permeability and compared with Robeson's upper bounds (Figure 4-19). It can be observed that at 20wt. % loading of NP-2 there is an increment in the permeability of small gases such as H_2, which surpasses the upper bound of 2008. Furthermore, it can be seen that there is an increase in the selectivity of H_2/CH_4, while, maintaining its selectivity over N_2 and CO_2. At 30 wt. % loading of NP-2, it is shown that there is no improvement in the permeability of O_2 compared to PIM-1. However, a slight increase can be noticed in the selectivity of O_2 over N_2. For permeability of CO_2, Figure 4-19b shows at 20 wt. % loading of NP-2 an increase in the permeability of CO_2 with its selectivity over CH_4 and N_2.

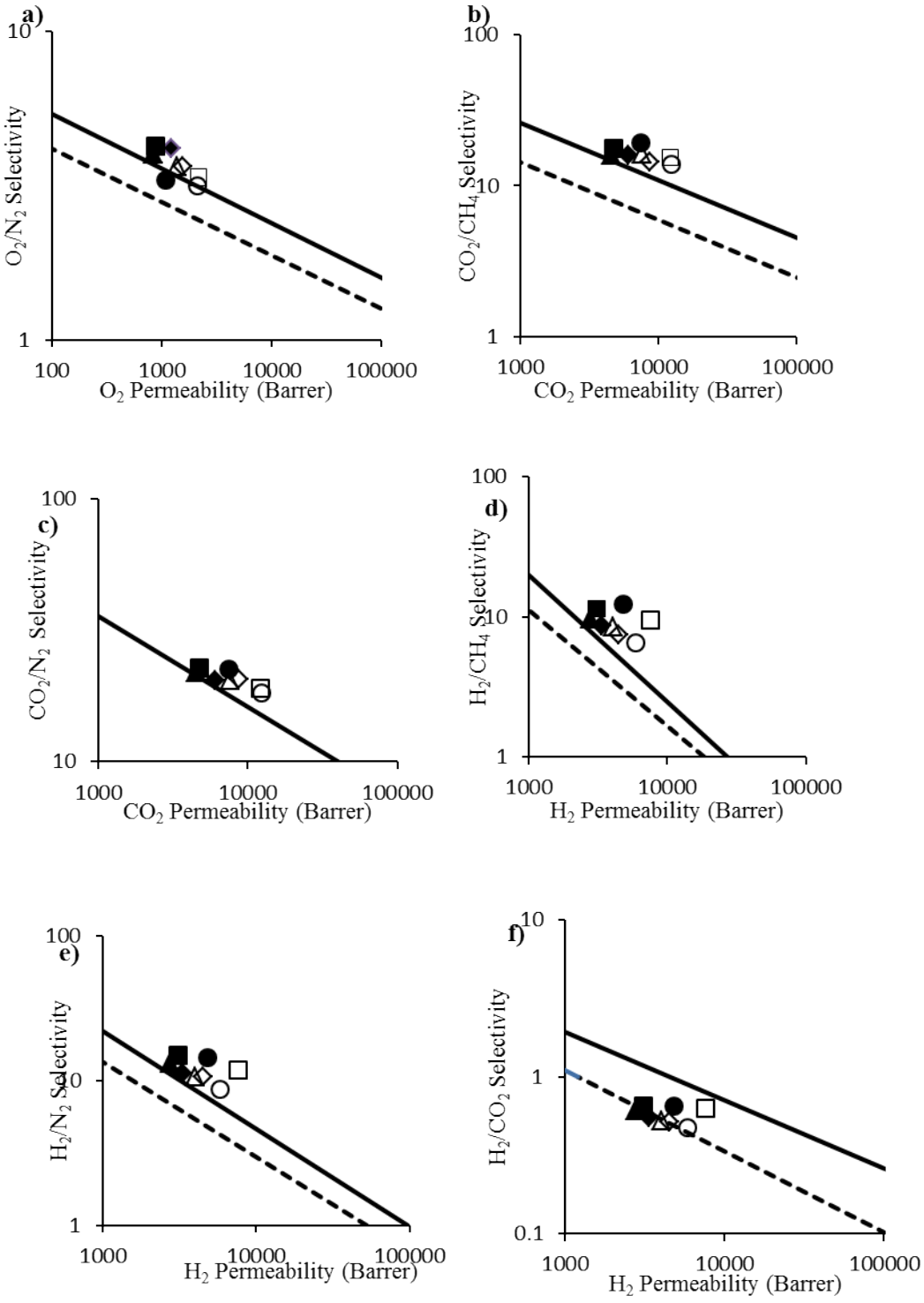

Figure 4-19: Robeson plots for important gas pair. (a) H_2/N2, (b) CO_2/CH4, (c) CO_2/N_2, (d) H_2/CH_4, (e) H_2/N_2, (f) H_2/CO_2. (▲) PIM-1 as cast, (△) PIM-1 MeOH,(◆) 90:10 PIM-1/NP-2 as cast,(◇) 90:10 PIM-1/NP-2 MeOH, (●) 80:20 PIM-1/NP-2 as cast, (○) 80:20 PIM-1/NP-2 MeOH,(■)70:30 PIM-1/NP-2 as cast, (□) 70:30 PIM-1:NP-2 MeOH. Dashed lines represent Robseon 1991 and solid lines represent Robeson 2008 upper bounds.

4.5 Summary

MMMs were fabricated using PIM-1 as polymer matrix and network polyimide fillers. The incorporation of fillers through membrane was confirmed by FTIR spectroscopy and PXRD. The SEM images showed a homogenous dispersion of NP-1. However, some agglomerates were observed at 20 wt. % loading, which can be attributed to poor distribution of filler. On the other hand, the SEM images of PIM-1/NP-2 MMMs showed a good dispersion of filler throughout the membrane due to good chemical affinity between two phases.

The fillers showed high CO_2 capacity compared to PIM-1. At low pressure (1 bar) the CO_2 uptake of NP-1 is higher than NP-2 due to presence very small pores (ultramicropores, < 0.7 nm). The gas permeation properties of MMMs were tested using time lag method. The results of PIM-1/NP-1 MMM showed a decrease in the diffusivity and permeability of gases, with an increase in the selectivity of small gases over. However, after methanol treatment, a big improvement was observed in the diffusivity and permeability of H_2 and He gases. For PIM-1/NP-2 MMM, an enhancement was observed for both the diffusivity and permeability of gases with maintaining the selectivity throughout the membrane.

4.6 References

1. T-S. Shung, S. S. Chan, R. Wang, Z. lu and C. He, Characterization of permeability and sorption in Matrimid/ C_{60} mixed matrix membranes, *J. Membr. Sci*., 2003, **211**, 91-99.
2. T-S. Chung, L. Y. Jiang, Y. Li and S. Kulprathipanja, Mixed matrix membranes (MMMs) comprising organic polymers with dispersed inorganic fillers for gas separation, *Prog. Polym. Sci.*, 2007, **32**, 483-507.
3. E. R. Rangel, E. M. Maya, F. Sánchez, J. D. Abajo and J. G. de la Campa, Gas separation properties of mixed-matrix membranes containing porous polyimides fillers, *J. Membr. Sci*., 2013, **447**, 403-412.
4. H. Mushardt, V. Kramer, D. Hülagü, T. Brinkmann and M. Kraume, Development of solubility selective mixed matrix membranes for gas separation, *Chemie. Ingenieur. Technik*., 2014, **86**, 83-91.
5. O. Bakhiari and N. Sadeghi, The formed voids around the filler particles impact on the mixed matrix membranes gas permeabilities, *IJCEA*., 2014, **5**, No.2.
6. M. A. Aroon and A. F. Ismail, Performance studies of mixed matrix membranes for gas separation: A review, *Sep. Purif. Technol*., 2010, 75, 229-242.
7. Y. Li, G. He, S. Wang, S. Yu, F. Pan, H. Wu and Z. Jiang, Recent advances in the fabrication of advanced composite membranes, *J. Mater. Chem. A*., 2013, **1**, 10058-10077.
8. G. Dong, H. Li and V. Chen, Challenges and opportunities for mixed-matrix membranes for gas separation, *J. Mater. Chem. A*., 2013, **1**, 4610-4630.
9. P. Li, Z. Wang, Z. Qiao, Y. liu, X. Cao, W. Li, J. Wang, S. Wang, Recent developments in membranes for efficient hydrogen purification, *J. Membr. Sci*., 2015, **495**, 130-168.
10. P. M. Budd and N. B. McKeown, Highly permeable polymers for gas separation membranes, *Polym. Chem*., 2010, **1**, 63-68.
11. C. H. Lau, P. Li, F. Li, T-S. Chung and D. R. Paul, Reverse-selective polymeric membranes for gas separations, *Progress in polymer Science*, 2013, **38**, 740-766.
12. N.Du, H. B. Park, M. M. Dal-Cin and M. D. Guiver, Advances in high permeability polymeric membrane materials for CO_2 separations. *Energy Environ. Sci*., 2012, **5**, 7306.
13. M. G. Buonomenna, W. Yave and G.Golemme, Some approaches for high performance polymer based membranes for gas separation: block copolymers, carbon molecular sieves and mixed matrix membranes, *RSC Adv*., 2012, **2**, 10745-10773.

14. H. Shamsipur, B. A. Dawood, P. M. Budd, P. Bernaido, G. Clarizia and j. C. Jansen, Thermally rearrangeable PIM-1 Polyimides for gas separation membranes, *Macromolecules*, 2014, **47**, 5595-5606.
15. C. E. powell and G. G. Qiao, polymeric CO2/N2 gas separation membranes for the capture of carbon dioxide from power plant flue gases, *J. Membr. Sci*., 2006, **279**, 1-49.
16. M. L. Jue, R. P. Lively, Targeted gas separations through polymer membrane functionalization, *Reactive & Functional Polymers*., 2015, **86**, 88-110.
17. N. N. Li, A. G. Fane, W. S. W. Ho and T. Matsuura, Advanced membrane technology and applications, John Wiley & Sons, Inc., Hoboken, New Jersey, 2008, ch.30, pp. 795-796.
18. F. Y. Li, Y. Xiao, T-S. Chung and S. Kawi, High-performance thermally self-cross-linked polymer of intrinsic microporosity (PIM-1) membranes for energy development, *Macromolecules*, 2012, **45**, 1427-1437.
19. P. M. Budd, K. J. Msayib, C. E. Tattershall, B. S. Ghanem, K. J. Reynolds, N. B. Mckeown and D. Fritsch, Gas separation membranes from polymers of intrinsic microporosity, *J. Membr. Sci*., 2005, **251**, 263-269.
20. P. M. Budd and N. B. Mckeown, Highly permeable polymers for gas separation membranes, Poly. Chem., 2012, **1**, 63-68.
21. P. M. Budd, N. B. Mckeown and D. Fritsch, Free volume and intrinsic microporosity in polymers, *J. Mater. Chem*., 2005, **15**, 1977-1986.
22. A.J. Hill, S. J. Pas, T. J. Bastow, M. I. Burgar, K. Nagai, L. G. Toy and B. D. Freeman, Influence of methanol conditioning and physical aging on carbon spin-lattice relaxation times of poly(1-trimethylsilyl-1-propyne), *J. Membr. Sci*., 2004, **243**, 37-44.
23. N. B. Mckeown, P. M. Budd, K. J. Msayib, B. S. Ghanem, H. J. Kingston, C. E. Tattershall, s. Makhseed, K. J. Reynolds and D. Fritsch, polymers of intrinsic microporosity (PIMs): Bridging the void between microporous and polymeric materials, *Chem. Eur. J*., 2005, **11**, 2610-2620.
24. P. M. Budd, N. B. Mckeown, B. S. Ghanem, K. J. Msayib, D. Fritsch, L. Starannikova, N. Belov, O. Sanfirova, Y. Yampolskii and V. Shantarovich, Gas permeation parameters and other physicochemical properties of a polymer of intrinsic microporosity: Polybenzodioxane PIM-1, *J. Membr. Sci*., 2008, **325**, 851-860.

25. S. Thomas, I. Pinnau, N. Du and M. D. Guiver, Pure-and mixed-gas permeation properties of a microporous spirobisindane-based ladder polymer (PIM-1), *J. Membr. Sci*., 2009, **333**, 125-131.
26. A. Bushell, Mixed matrix membranes of a polymer of intrinsic with crystalline porous solids, PhD Thesis, Manchester University, 2012.
27. H. A. Mannan, H. Mukhtar, T. Murugesan, R. Nasir. D. F. Mohsim and A. Mushtaq, Recent applications of polymer blends in gas separation membranes, *Chem. Eng. Technol.*, 2013, **36**, 1838-1846.
28. H. Mushardt, V. Kramer, D.Hülagü, T. Brinkmann and M. Kraume, Development of solubility selective mixed matrix membranes for gas separation, *Chemie Ingenieur Technik*., 2014, **86**, No. 1-2, 83-91.
29. E. R. Rangel, E. M. Maya, F. Sanchez, J. Abajo and J. G. Campa, Gas separation properties of mixed-matrix membranes containing porous polyimides fillers, *J. Membr. Sci.*, 2013, **447**, 403-412.
30. A. F. Bushell, P. M. Budd, M. P. Attfield, J. T. A. Jones, T. Hasell, A. I. Cooper, P. Bernardo, F. Bazzarelli, G. Clarizia and J. C. Jansen, Nonporous organic polymer/cage composite membranes, *Angew. Chem. Int. Ed*., 2013, **52**, 1253-1256.
31. C. H. Lau, P. T. Nguyen, M. R. Hill, A. W. Thornton, K. Konstas, C. M. Doherty, R. J. Mulder, L. Bourgeois, A.C.Y.Liu, D.J. Sprouster, J.P. Sullivan. T.J .Bastow, A. J. Hill, D.L.Gin and R. D. Noble, Ending aging in super glassy polymer membranes, *Angew. Chem. Int. Ed.*, 2014, **53**, 1-6.
32. C. H. Lau, K. Konstas, A. W. Thornton, A. C. Y. Liu, S. Mudie, D. F. Kennedy, S. C. Howard, A. J. Hill and M. R. Hill, Gas-separation membranes loaded with porous aromatic frameworks that improve with age, *Angew. Chem*., 2015, **127**, 1-6.
33. G. Clarizia, C. Algieri and E. Drioli, Filler-polymer combination: a route to modify gas transport properties of a polymeric membrane, Polymer., 2004, **45**, 5671-5681.
34. M. Macchione, J. C. Jansen, G. De Luca, E. Tocci, M. Longeri and E. Drioli, Experimental analysis and simulation of the gas transport in dense Hyflon AD60X membranes: Institute of residual solvent, *Polymer*, 2007, **48**, 2619-2635.

35. C. R. Mason, L. M. Atem, N. M. Al-Harbi, P. M. Budd, P. Bernardo, F. Bazzarelli, G. Clarizia and J. C. Jansen, polymer of intrinsic microporosity incorporating thioamide functionality: Preparation and gas transport properties, *Macromolecules*, 2011, **44**, 6471-6479.
36. J. C. Jansen, K. Friess and E. Drioli, Organic vapour transport in glassy perfluoropolymer membranes: A simple semi-quantitative approach to analyze clustering phenomena by time lag measurements, *J. Membr.Sci*., 2011, **367**, 141-151.
37. G. Li and Z. Wang, Microporous polyimides with uniform pores for adsorption and separation of CO_2 gas and organic vapors, *Macromolecules*, 2013, **46**, 3058-3066.
38. N. Du, G. P. Robertson, J. Song, I. Pinnau, S. Thomas and M. D. Guiver, polymers of intrinsic microporosity contain trifluoromethyl and phenylsulfone groups as materials for membrane gas separation, *Macromolecules*, 2008, **41**, 9656-96622.
39. G. Li and Z. Wang, Naphthalene-based microporous polyimides: Adsorption behaviour of CO2 and toxic vapors and their separation from other gases, *J. Phys. Chem*., 2013, **11**7, 24428-24437.
40. 20.K. V. Rao, R. Haldar, T. K. Maji and S. J. George, Porous polyimides from polycyclic aromatic linkers: selective CO_2 capture and hydrogen storage, *Polymer*, 2014, **55**, 1452-1458.
41. C. R. Mason, L. M. Atem, K. W. J. Heard, B. Satilmis, P. M. Budd, K. Friess, M. Lanc, P. Bernardo, G. Clarizia and J. C. Jansen, Enhancement of CO_2 affinity in a polymer of intrinsic microporosity by amine modification, *Macromolecules*, 2014, **47**, 1021-1029.

Chapter 5

Synthesis and Characterization of Hyperbranched Polyimides

5.1 Introduction

This chapter explores the synthesis and characterization of aromatic hyperbranched polyimides using different molar ratios. It also investigates the effect of end-capping modification on the properties of polyimides. The tetraamine used in the synthesis of polymers is (*p*-aminophenyl) methane (TAPM), which was previously discussed in chapter 3, and the dianhydride used is pyromellitic dianhydride (PMDA). The polymers are characterized using various techniques, including FTIR, NMR spectroscopy and TGA. Following this, their CO_2 uptake and solubility are also examined.

5.1.1 Hyperbranched Polyimides

Recently, hyperbranched polymers (HBPs) have attracted great attention due to their unique and distinctive properties which can be related to their highly branched structures.[1-5] Hyperbranched polyimides (HBPIs) are a new type of polymer based on hyperbranched polymers and polyimides. They have a highly branched structure with a large number of terminal functional groups. Furthermore, they possess the properties of both hyperbranched polymers and polyimides, such as high glass transition temperatures and excellent solubility. As a result of their unique characteristic structure with excellent physical and chemical properties, hyperbranched polyimides have drawn a considerable interest in many applications.[6, 7]

5.1.2 Synthesis of Hyperbranched Polyimides Based on $A_2 + B_3$ Polymerization

Hyperbranched polyimides can be easily and successfully prepared by one-step polymerization of bifunctional anhydride (A_2) and trifunctional amine (B_3) monomers.[7, 8] The kind and ratio of end groups can be determined by the ratio of anhydride and amine monomers.[8] It is known that one-step polymerization of A_2 and B_x (x is higher than 2) results in crosslinking, which can be distinguished during the polymerization by the occurrence of gelation. The gel is related to the formation of an infinite network as the polymer molecules are crosslinked to each other to form macroscopic molecules. In the process of gelation, there is a dramatic physical change which can be determined by the transformation of the reaction mixture into a polymer of infinite viscosity.[9] Therefore, to avoid gelation in the condensation polymerization of A_2+B_3, controlled reaction conditions are required. For instance, low monomer concentrations, slow addition rates and molar ratio of monomers.[10]

In 2000, Fang *et al*. [10] prepared a series of aromatic hyperbranched polyimides by condensation polymerization of tris(4-aminophenyl)amine (TAPA) as B_3 monomer with a series of commercially available dianhydride monomers, such as 2,2-bis(3,4-dicarboxyphenyl)hexafluoropropane dianhydride (6FDA), 3,3',4,4'-diphenylsulfonetetracarboxylic dianhydride (DSDA) and pyromellitic anhydride (PMDA), as A_2 monomers. In the first step of reaction, the dianhydrides and triamine monomers were polymerized in dimethylacetmaide (DMAc) solvent at room temperature for 3 h to obtain hyperbranched polyamic acid, followed by chemical or thermal imidization.

To avoid gelation, Fang *et al*.[10] controlled the reaction conditions of polymerization through many factors such as monomer addition, molar ratio of monomers and concentration. Two different kinds of monomer addition orders, named manner 1 and manner 2, were utilized for condensation polymerization of dianhydrides and triamine monomers. Manner 1 involved the addition of dianhydride solution to triamine solution with the monomer molar ratio of 1:1 to form amine-terminated hyperbranched polyimide, whereas manner 2 was the vice versa with the molar ratio between the anhydride and amine 2:1, yielding anhydride-terminated hyperbranched polyimide. Furthermore, it was found that the slow addition of monomer plays an important factor to avoid gelation. The monomer was dissolved in DMAc solvent and

added slowly so that the concentration of dianhydride (manner1) or triamine (manner 2) approached zero to avoid any high local concentration. It was noted that gelation occurred immediately when monomer solids were added directly or even if the addition of monomer solution was not slow enough.

The monomer concentration is also an important factor for preventing gelation. It was found that the total solid content should be kept below 0.2 mol/L for manner 1 and 0.075 mol/L for manner 2. It was observed that any high concentration can cause in the formation of insoluble gel.

The 6FDA-based polyimides showed good solubility in DMAc, NMP and DMSO solvents and were partially soluble in acetone, THF and 1,4-dioxane. However, PMDA and DSDA-based polyimides were insoluble in the tested solvents.

In 2002, Chen *et al*. [11] prepared hyperbranched polyimides by condensation polymerization of 1,3,5-tris(4-aminophenoxy)benzene (TAPOB) as triamine monomer with 4,4'-(hexafluoroisopropylidene)diphthalic anhydride (6FDA), 4,4'-oxydiphthalic anhydride (ODPA) and 3,3',4,4'-benzophenonetetracarboxylic dianhydride (BTDA) as dianhydride monomers. Different monomer addition orders, molar ratios and concentration were utilized as described by Fang *et al*[10], resulting in amino or anhydride terminated groups. The dianhydride and triamine monomers were first reacted in NMP at 40 ^{o}C, obtaining a solution of polyamic acid, which was then thermally polymerized at 170 ^{o}C for 5 h, resulting in amino-terminated hyperbranched polyimide, or converted chemically using a mixture of triethylamine and acetic anhydride at 40 ^{o}C for 12 h, yielding anhydride-terminated hyperbranched polyimide. It was found that the hyperbranched polyimides showed good solubility in common organic solvents. However, the thermally imidized amino-terminated polyimides were more difficult to dissolve compared with anhydride-terminated polyimides.

Hao *et al*.[12] prepared hyperbranched polyimides based on polymerization of 1,4-phenylenediamine (as A_2 monomer) with triphthalic anhydride (as B_3 monomer) in a 1:1 molar ratio. It was found that gelation can be obtained as a result of high reaction temperature, high monomer concentration or if the addition of monomer was not slow enough. The reaction involved synthesis of polyamic acid in DMAc at 0 ^{o}C, followed by chemical imidization using a mixture of acetic anhydride and pyridine. The

resulting anhydride-terminated hyperbranched polyimide was soluble upon heating in high boiling point solvents such as NMP, DMF, DMSO and DMAc.

In 2015, Li *et al*. [5] prepared a series of hyperbranched polyimides by polymerization of 1,3,5-tri[4-(4-nitrophenoxy)phenyl]benzene with commercially available dianhydrides such as 4,4'-(4,4'isopropylidenediphenoxy)bis(phthalic anhydride) (BPADA), 4,4'-oxydiphthalic anhydride (ODPA) and 3,3',4,4'-tetracarboxylic acid (BTDA). The dianhydride and triamine were first polymerized in NMP solvent at 0 ^{o}C with different monomer addition order and molar ratios to give polyamic acid, which was then polymerized by thermal or chemical imidization, producing amino and anhydride terminated hyperbranched polyimides, respectively. The hyperbranched polyimides showed good solubility in organic solvents due to the presence of ether bonds in both triamine and dianhydride monomers, which improved the flexibility, thus increasing the solubility of the polyimides. However, the hyperbranched polyimides prepared from BTDA monomer showed less solubility in comparison with other hyperbranched polyimides.

The end-capping modification is an important method which has been utilized to introduce reactive functional groups at the end of polymer structure. Moreover, it can be employed to control the molecular weight of polymers or blocking the reactive functional groups at the ends. Furthermore, it can be used to modify some properties of polymers.[13]

Chen *et al*. [11] utilized the end capping method to improve some properties of the hyperbranched polyimides in terms of molecular weight, thermal stability and solubility. As described previously, the dianhydride and triamine monomers were first polymerized in NMP at 40 ^{o}C, obtaining a solution of polyamic acid with different terminal functional groups depending on the addition order and molar ratio of monomers. Two different types of end-cappers were used. In the case of amine-terminated polyamic acid, phthalic anhydride was added as end-capper at 40 ^{o}C and stirred for 5 h, followed by chemical imidization using a mixture of triethylamine and acetic anhydride at 40 ^{o}C for 12 h, resulting in modified amino-terminated hyperbranched polyimide. Aniline was added as end capper to the solution of anhydride-terminated polyamic acid at 40 ^{o}C for 5h, followed by chemical imidization in the presence of triethylamine and acetic anhydride at 40 ^{o}C for 12 h, producing chemically modified anhydride-terminated hyperbranched polyimide. It was found

that both anhydride and amino modified polyimides showed an increase in their molecular weights. The thermal stability of 6FDA-based hyperbranched polyimides was further improved after the chemical modification using end cappers, which can be related to the introduction of imide structure at the ends of polymer. In terms of solubility, it was found that the chemically modified hyperbranched polyimides showed better solubility compared to their parent polymers as a result of decreased interaction between macromolecules.

Later on, Chen *et al*. [14] prepared a series of autophotosensitive hyperbranched polyimides with excellent solubility and good thermal stability using a series of ortho-alkyl anilines as end-cappers. A solution of TAPOB was first slowly added to the reaction system containing BTDA in NMP solvent with molar ratio of 1:2 to obtain anhydride-terminated hyperbranched polyamic acid, which was end-capped using four ortho-alkyl anilines such as 2-methylaniline, 2, 6-dimethylaniline, 2-ethylaniline and 2-tert-butylaniline, followed by chemical imidization using a mixture of triethylamine and acetic anhydride, producing autophotosensitive hyperbranched polyimides which showed excellent solubility in the strong polar solvents such as NMP, DMF, DMAc and DMSO. However, the end-capped hyperbranched polyimides with 2-ethylaniline and 2-tertbutylaniline showed better solubility in cyclic ethers such as THF.

In this research, we aimed to increase the solubility of microporous polyimide network MPN-1 by decreasing the extent of network formation. As mentioned previously, hyperbranched polyimide has a highly branched structure with a large number of terminal functional groups, resulting in good solubility. Furthermore, the end-capping reaction can also improve the solubility of hyperbranched polyimides. As a result, two strategies have been utilized. First, using different molar ratios and, second, using end-capping modification. To the best of our knowledge, modification of the properties of hyperbranched polyimides based on A_2+B_4 polymerization using tetra(*p*-aminophenyl)methane (TAPM) as B4 monomer and pyromellitic anhydride (PMDA) as A_2 has never been studied before.

5.2 Experimental

5.2.1 Chemicals

Pyromellitic dianhydride (97%, Aldrich), acetic anhydride (≥ 98.0%, Sigma-Aldrich), anhydrous dimethylacetamide (99.8%, Sigma-Aldrich), anhydrous pyridine (99.8%, Sigma-Aldrich), aniline (≥ 99.5%, Sigma-Aldrich) 2-ethylaniline (98%, Aldrich), 2-tert-butylaniline (98%, Aldrich).

5.2.2 Apparatus

^{1}H and ^{13}C NMR spectra were recorded on a Bruker 400 MHz spectrometer. ^{1}H NMR samples were prepared by dissolving 10 mg of sample in 1 ml of deuterated chloroform ($CDCl_3$) or deuterated dimethyl sulfoxide (DMSO) as solvents. Due to the low sensitivity of ^{13}C compared to ^{1}H, 20 mg of sample was dissolved in 1 ml of deuterated chloroform or deuterated dimethylsulfoxide. High powered decoupling (Hpdec) magic angle spinning (MAS) solid state ^{13}C NMR spectra were collected using a Bruker Avance lll 400 MHz instrument using adamantane as a reference. Powder samples were packed into a 4 mm zirconia rotor and run at a spinning rate of ~ 12000 Hz. The spectra were collected with 6000 scans, using a repetition time of 10 seconds and a spectral width of 600 ppm.

The Fourier transform infrared spectra of solids were recorded on a Bio-Rad FTS 6000 spectrometer equipped with an ATR setup, and annexed to a Whatman FTIR purge gas generator. The spectra were recorded in the attenuated total reflection (ATR) mode, with a resolution of 0.25 cm-1, a sensitivity of 1, and 16 scans in the range 4000 – 500 cm^{-1}.

The CO_2 sorption analysis of the samples was carried out using a Micromeritics ASAP 2050 surface area and porosity analyzer. A small amount of sample (between 0.1- 0.2 g) was weighed into the degas port. It was then degassed automatically under high vacuum at 100 ^{o}C for 16 h. After reweighing, the sample was placed in the analysis port and degassed manually for a further 2 h to ensure that all volatiles were removed completely from the sample. Then, the analysis was implemented at 298 K, in the relative pressure range from 0 to 8 bar. After completing the analysis, the sample was out-degassed for 2 h. Then, the free space was obtained using helium.

The thermogravimetric analysis (TGA) curves were recorded using a Mettler Toledo Star @ System. The samples were heated to 800 ^{o}C, under N_2 with a flow rate of 10 ^{o}C/min.

5.2.3 Synthetic Procedures

Tetra(p-aminophenyl)methane (TAPM) as shown in Figure 5-1 was used in the synthesis of hyperbranched polyimides. The synthesis steps of TAPM were described previously in chapter 3.

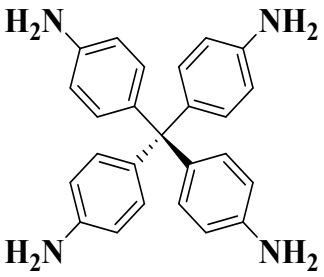

Figure 5-1: Structure of TAPM.

5.2.3.1 Synthesis of Anhydride-Hyperbranched Polyimide AD-HBPI-1

The schematic synthesis of AD-HBPI-1 is presented in Figure 5-2.

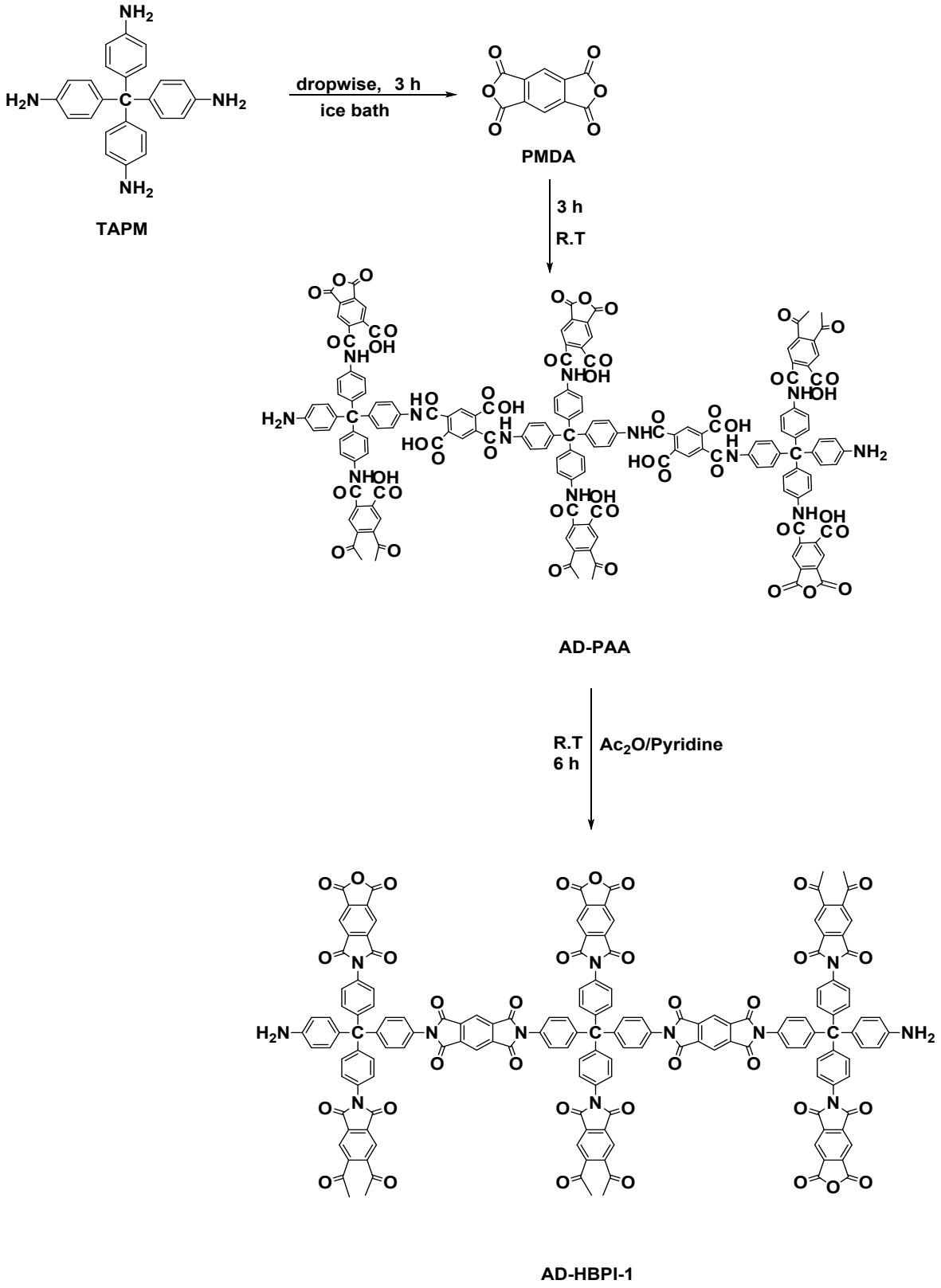

Figure 5-2: Synthesis of AD-HBPI-1.

Under nitrogen atmosphere, to a three-neck round bottom flask fitted with a mechanical stirrer, a condenser, in an ice-bath, was added pyromellitic dianhydride (PMDA) (0.2908 g, 1.33 mmol) dissolved in dimethylacetamide (DMAc) (30 ml). Then, a solution of tetra(*p*-amino phenyl)methane (TAPM) (0.1902 g, 0.5 mmol) in DMAc (30 ml) was added dropwise via syringe over 3 h. After the addition was completed, the mixture was stirred at room temperature for 3 h. Then, acetic anhydride (1.2 ml) and pyridine (0.6 ml) was added and the reaction mixture was left to stir for a further 6 h. After that, the reaction mixture was poured into chloroform. The precipitate was then filtered off, washed thoroughly with chloroform, and finally dried in vacuum.

5.2.3.2 Synthesis of Modified-Hyperbranched Polyimide M-HBPI-1

The schematic synthesis of M-HBPI-1 is shown in Figure 5-3.

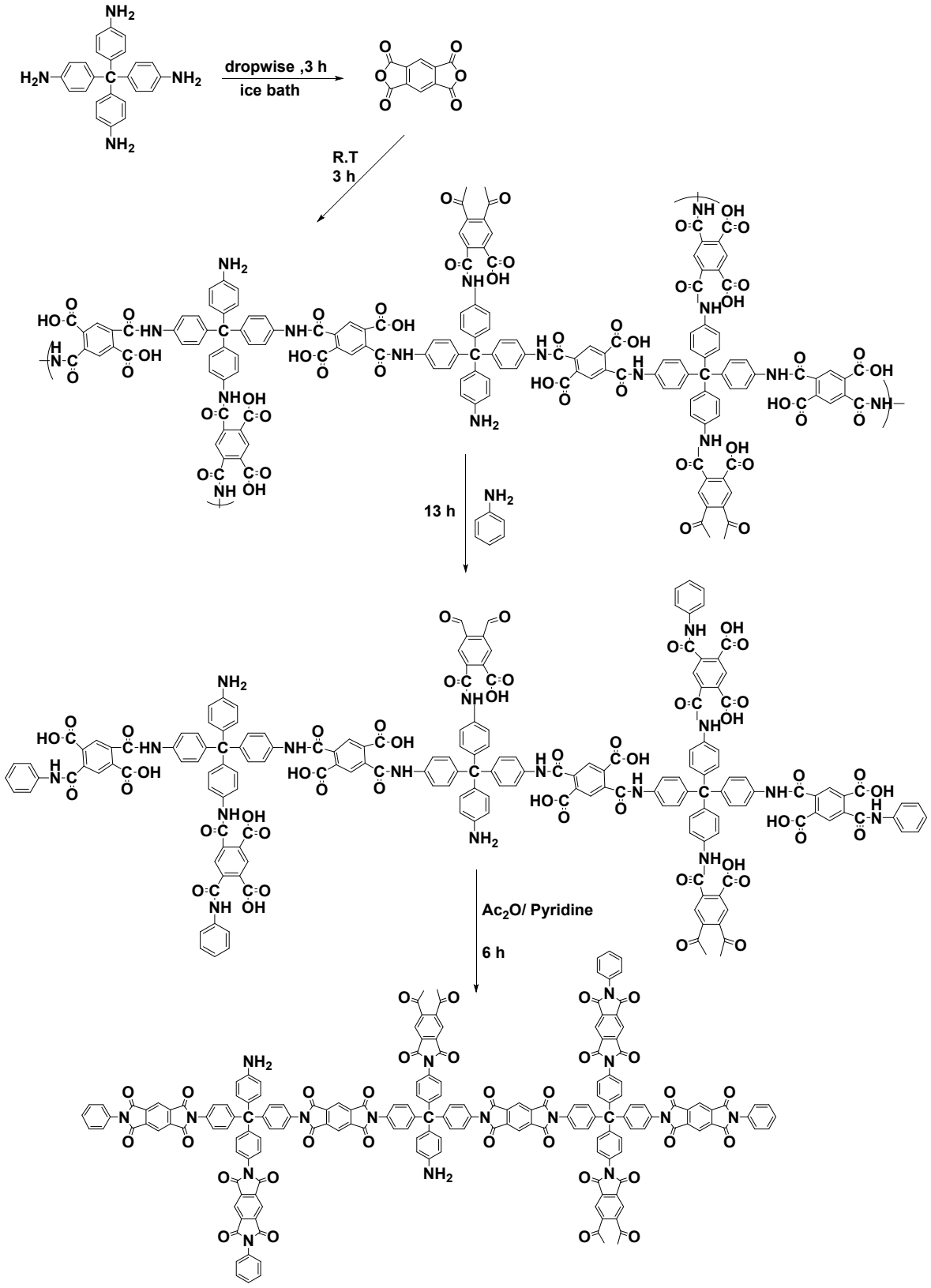

Figure 5-3: Synthesis of M-HBPI-1.

To a three-neck round bottom flask equipped with a mechanical stirrer, a condenser, in an ice-bath and under a flow of nitrogen, was added pyromellitic dianhydride (PMDA) (0.2907 g, 1.33 mmol) dissolved in dimethylacetamide (DMAc) (30 ml). A solution of tetra(*p*-amino phenyl) methane (TAPM) (0.1902 g, 0.5 mmol) in DMAc (30 ml) was added to the mixture dropwise through a syringe over 3 h. After the addition of solution was completed, the mixture was stirred at room temperature for 3 h. Then, aniline (0.66 mmol, 0.062 g) was added and the reaction mixture was stirred for 13 h. After that, acetic anhydride (1.2 ml) and pyridine (0.6 ml) were added and the reaction mixture was left to stir for a further 6 h. The solution was then precipitated in chloroform, filtered and washed thoroughly with chloroform and dried at 100 ^{o}C under vacuum overnight.

5.2.3.3 Synthesis of Modified-Hyperbranched Polyimide M-HBPI-2

The schematic synthesis of M-HBPI-2 is presented in Figure 5-4.

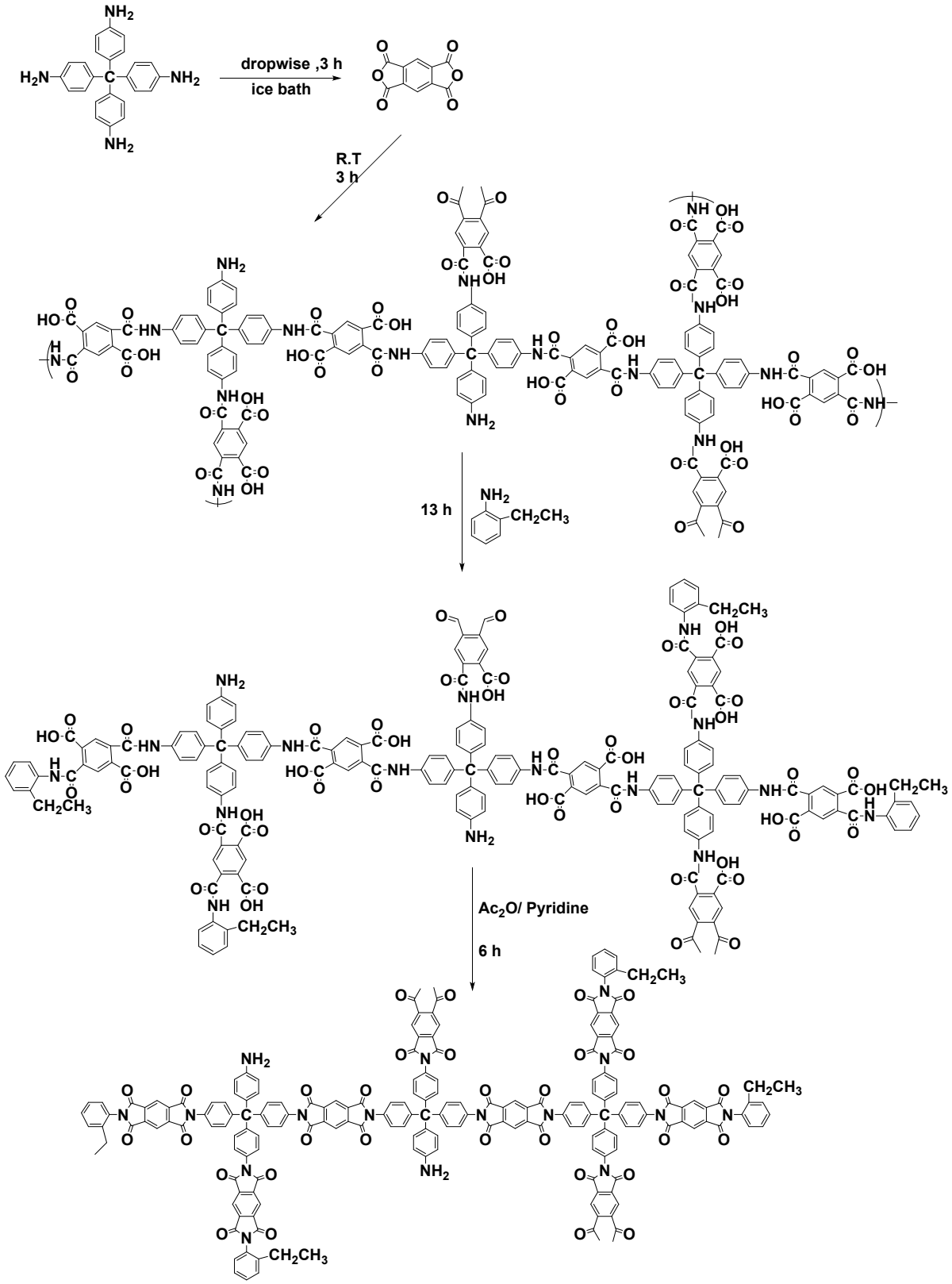

Figure 5-4: Synthesis of M-HBPI-2.

Under a nitrogen atmosphere, in a three-neck round bottom flask equipped with a mechanical stirrer and condenser, in an ice bath, was added pyromellitic dianhydride (PMDA) (0.2907 g, 1.33 mmol) in dimethylacetamide (DMAc) (30 ml). Then, a solution of tetra(p-amino phenyl)methane (TAPM) (0.1902 g, 0.5 mmol) in DMAc (30 ml) was added dropwise through syringe over 3 h. After completion of the addition, the mixture was stirred at room temperature for 3 h. Then, 2-ethylaniline (0.0807 g, 0.66 mmol) was added and the reaction mixture was further stirred for 13 h. After that, acetic anhydride (1.2 ml) and pyridine (0.6 ml) were added and the reaction mixture was left to stir for a further 6 h. Finally, the solution was poured into chloroform, filtered, washed again with chloroform and dried at 100 ^{o}C under vacuum overnight.

5.2.3.4 Synthesis of Modified-Hyperbranched Polyimide M-HBPI-3

The schematic synthesis of M-HBPI-3 is shown in Figure 5-5.

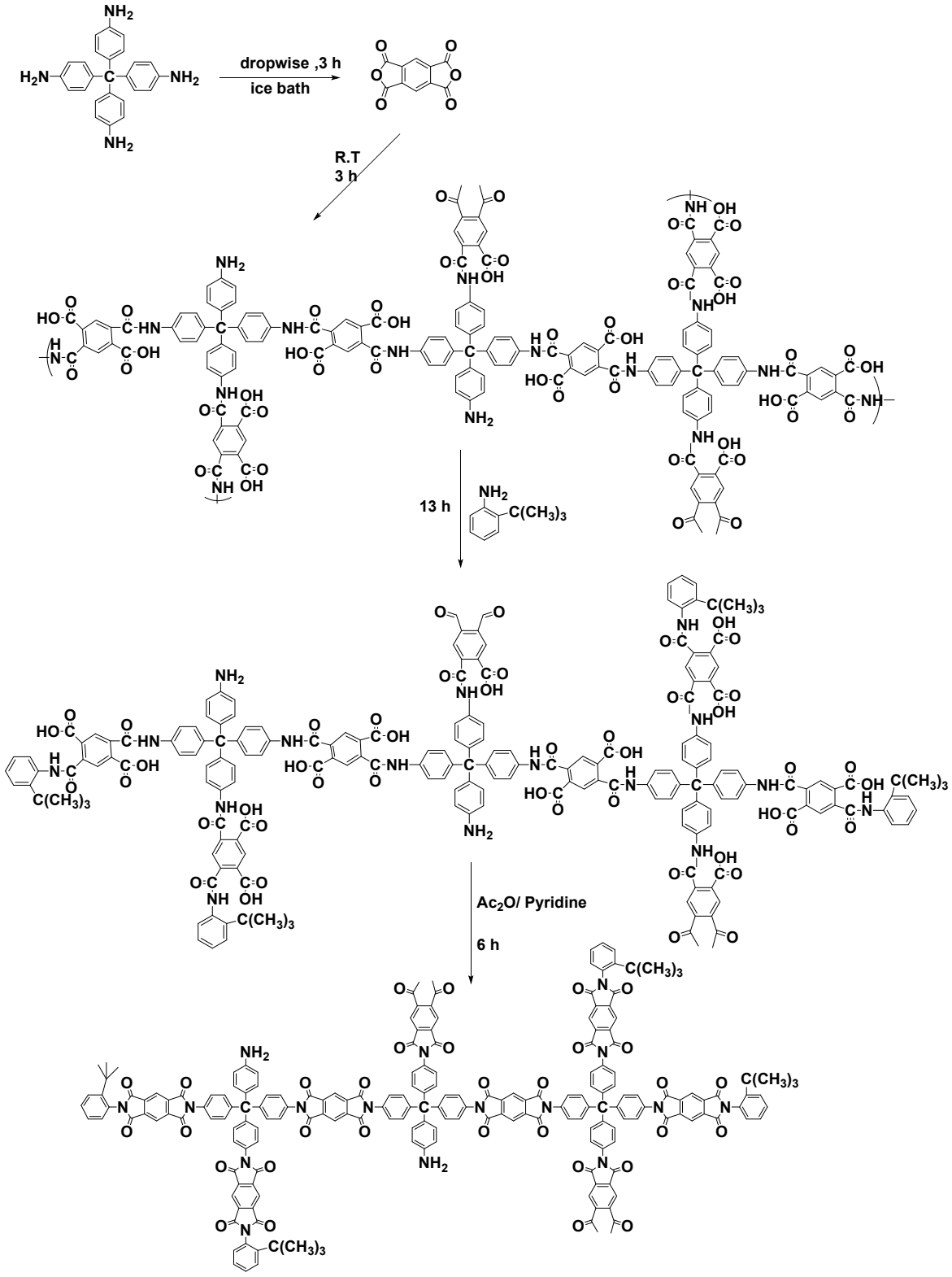

Figure 5-5: Synthesis of M-HBPI-3.

To a three-neck round bottom flask fitted with a mechanical stirrer and condenser, in an ice bath and under a flow of nitrogen, was added pyromellitic dianhydride (PMDA) (0.2907 g, 1.33 mmol) in dimethylacetamide (DMAc) (30 ml). Then, a solution of tetra(*p*-amino phenyl)methane (TAPM) (0.1902 g, 0.5 mmol) in DMAc (30 ml) was added drop by drop via syringe over 3 h. After the addition was completed, the mixture was stirred at room temperature for 3 h. 2-tert-butylaniline (0.0994 g, 0.66 mmol) was added and the reaction mixture was left to stir for 13 h. Then, acetic anhydride (1.2 ml) and pyridine (0.6 ml) were added to the reaction mixture and stirred for a further 6 h. The solution was precipitated into chloroform, filtered, washed again with chloroform, and dried at 100 ^{o}C under vacuum overnight.

5.2.3.5 Synthesis of Anhydride-Hyperbranched Polyimide AD-HBPI-2

The schematic synthesis of AD-HBPI-2 is shown in Figure 5-6.

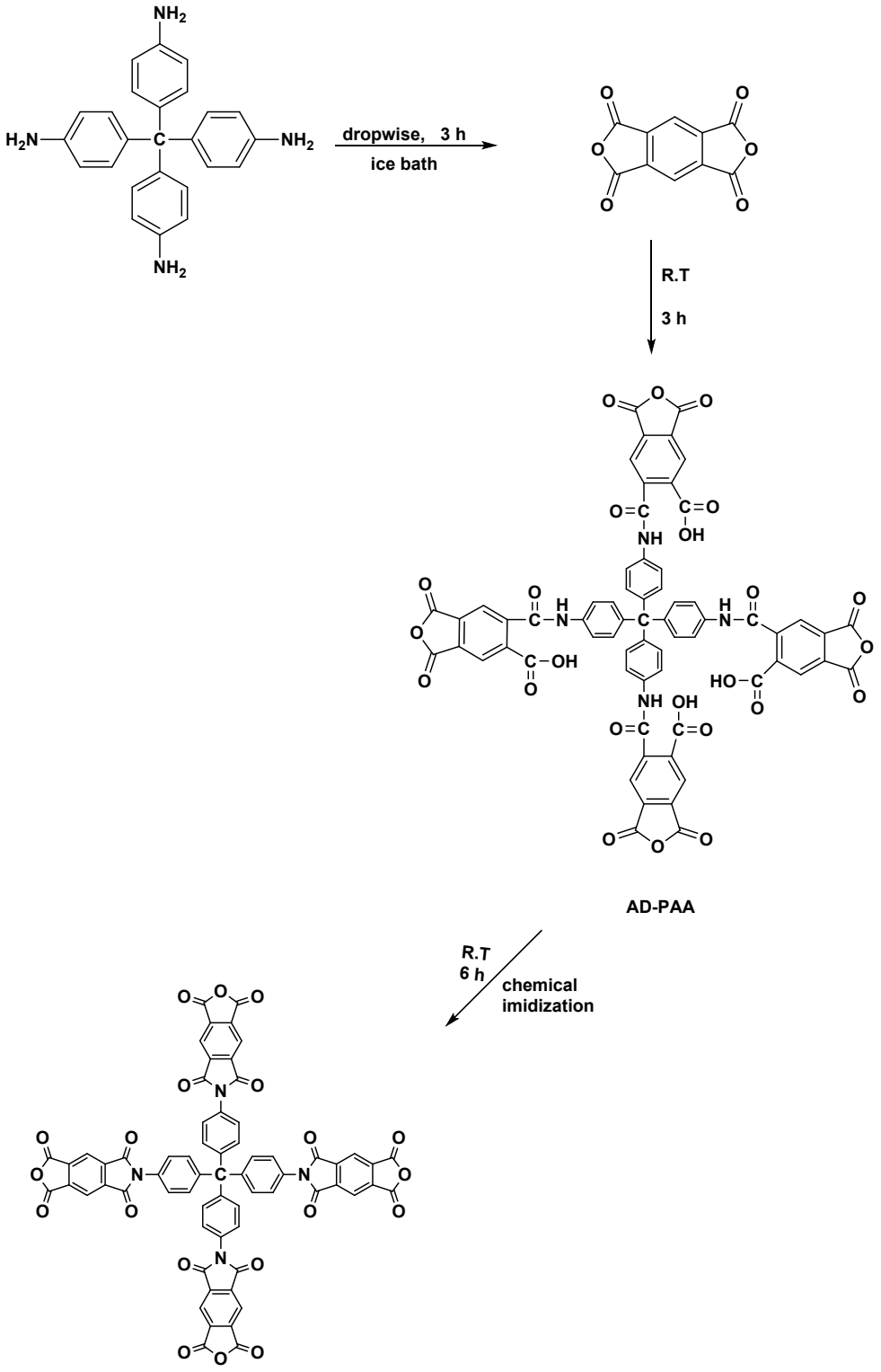

Figure 5-6: Synthesis of AD-HBPI-2.

Under a flow of nitrogen, in a three-neck round bottom flask equipped with a mechanical stirrer and condenser, in an ice bath, was added pyromellitic dianhydride (PMDA) (0.4362 g, 2 mmol) dissolved in dimethylacetamide (DMAc) (41 ml). Then, a solution of tetra(*p*-amino phenyl)methane (TAPM) (0.1902 g, 0.5 mmol) in DMAc (41 ml) was added dropwise via syringe over 3 h. After that, the mixture was stirred at room temperature for 3 h. Then, acetic anhydride (1.2 ml) and pyridine (0.6 ml) was added and the reaction mixture was stirred for a further 6 h. Then, the reaction mixture was precipitated in chloroform, filtered off, washed thoroughly with chloroform, and finally dried in vacuum.

5.3 Results and Discussion

5.3.1 AD-HBPI-1

In the aim of synthesising hyperbranched polyimides based on A_2 + B_4 polymerization, it was important to take into consideration the factors that prevent the formation of gelation. Fang *et al*.[10] found that the monomer concentration below 0.075 mol/L should be used to prevent the formation of insoluble gel. However, for A_2+B_4 polymerization, it was found that gelation was obtained at monomer concentration of 0.075 mol/L, which can be attributed to the fact that the polymerization of dianhydride and tetraamine is more complicated than the polymerization of dianhydride and triamine. As a result, it was noted that the total solid content for PMDA and TAPM should be kept at 0.03 mol/L. Furthermore, high mechanical stirring, slow addition and ice bath were utilized to prevent the formation of insoluble gel. As can be seen in Figure 5-2, a solution of TAPM in DMAc solvent was added slowly to a solution of PMDA dissolved in DMAc solvent over 3 h with monomer molar ratio of 2:0.75 (the molar ratio of anhydride groups to amine groups was 4:3) to form anhydride-terminated polyamic acid as a transparent homogenous solution, which was then chemically converted to anhydride-terminated polyimide using a mixture of acetic anhydride and pyridine.

5.3.1.1 FTIR Spectroscopy

The formations of anhydride-terminated polyamic acid (AD-PAA) and anhydride-terminated hyperbranched polyimide (AD-HBPI-1) were confirmed by FTIR spectroscopy, as can be seen in Figure 5-7. The absorption band at 1714 cm^{-1} is related to stretching of the carbonyl group of carboxylic acid, while the band at 1667 cm^{-1} corresponds to carbonyl amide stretching, which are the characteristic peaks reported for hyperbranched polyamic acid based on A_2+B_3 polymerization[15, 16]. The absorption bands at 1853 and 1782 cm^{-1} are assigned to asymmetric and symmetric vibration of carbonyl of terminal anhydride group in the anhydride-terminated polyamic acid, respectively. The complete conversion of amic acid to imide ring was proved with the appearance of bands at 1781 cm^{-1} (asymmetrical C=O stretching), 1725 cm^{-1} (symmetrical C=O stretching), and 1371 cm^{-1} (C-N stretching). Furthermore, the band at 1861 cm^{-1} is related to stretching of carbonyl of the anhydride terminated group, as reported for anhydride-terminated hyperbranched polyimides.[1, 4, 10, 11, 15]

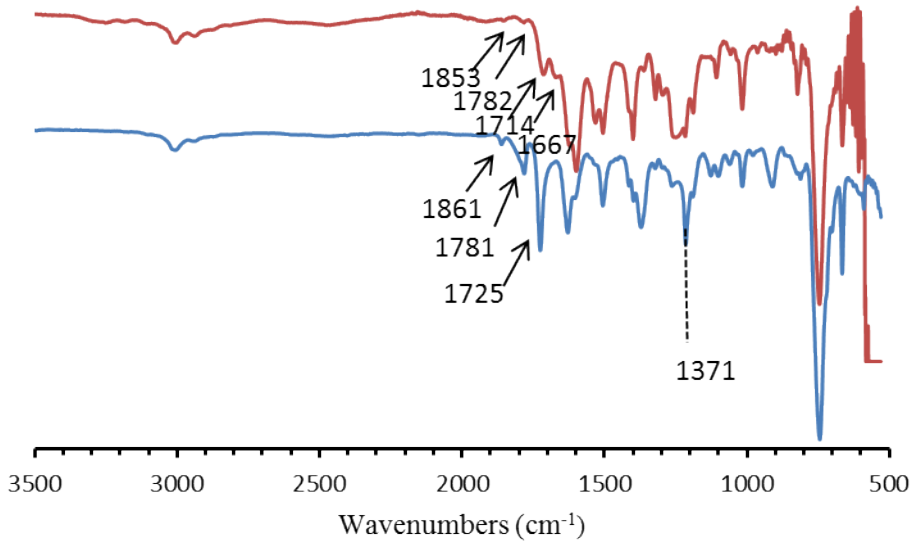

Figure 5-7: FTIR spectrum of AD-PAA (top, red) and AD-HBPI-1(bottom, blue).

5.3.1.2 Solid State ^{13}C-NMR Spectroscopy

Due to insolubility of AD-HBPI-1 in any solvents, solid-state ^{13}C NMR was utilized to provide further indication about the chemical structure of the polymer, as is shown in Figure 5-8. The peak at 64 ppm is attributed to the aliphatic carbon of the tetrahedral core, while the peaks at 145 and 165 ppm are related to the N-substituted phenyl carbon and carbonyl carbon of the imide ring, respectively. These characteristic peaks indicate the complete polymerization and formation of imide ring as suggested by FTIR spectroscopy. The overlapping peaks at 118, 129 and 136 ppm correspond to other aromatic carbon atoms in the polymer structure.

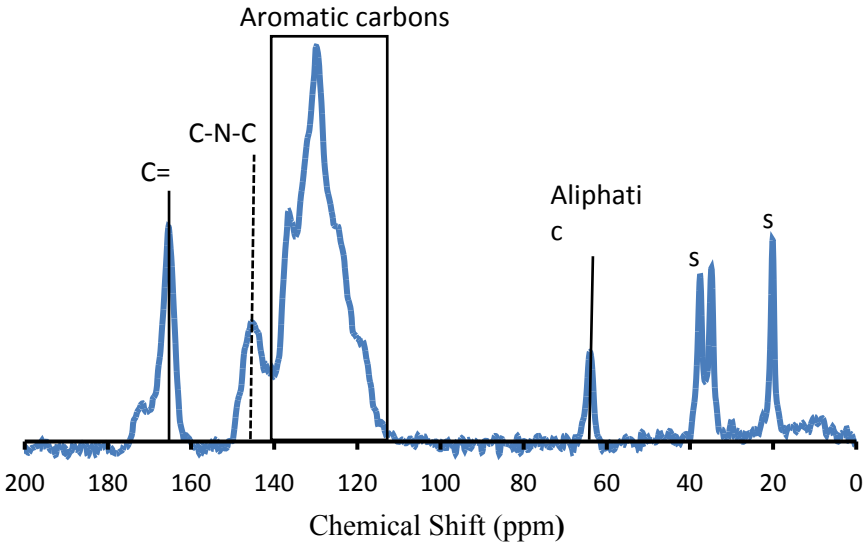

Figure 5-8: Solid-state ^{13}C NMR spectra of AD-HBPI-1.

5.3.1.3 Thermogravimetric Analysis (TGA)

The thermal stability of AD-HBPI-1 was examined by thermogravimetric analysis (TGA) under nitrogen atmosphere. As can be seen in Figure 5-9, the weight loss below 100 °C is due to the removal of moisture during heating.[17] The small weight loss between 150-392 °C can be attributed to residual solvent as observed in ^{13}C solid-state NMR spectra. It can also be related to the decomposition of terminated groups. The thermal decomposition around 400 °C is mainly related to the decomposition of imide units in the polymer structure.[5] It also indicates complete polymerization and formation of fully imidized polymer, as confirmed previously by FTIR and solid-state ^{13}C NMR spectroscopy. The remaining weight of AD-HBPI-1 at 800 °C is 60% (as shown in Fig 5-9) which is comparable to the reported anhydride-terminated hyperbranched polyimides based on A_2+B_3 polymerization,[5,10] indicating the good thermal stability of AD-HBPI-1.

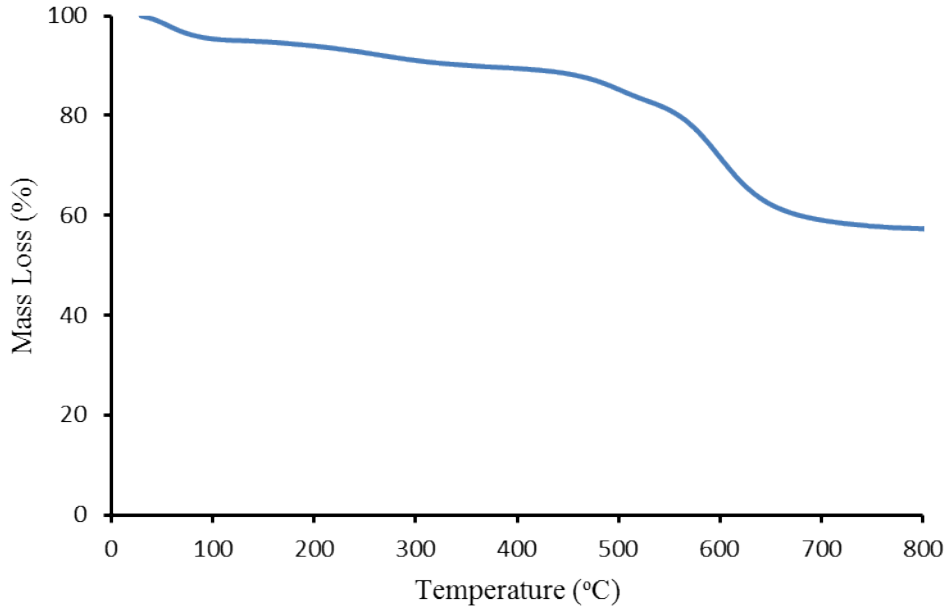

Figure 5-9: TGA of AD-HBPI-1.

5.3.2 M-HBPIs (M-HBPI-1, M-HBPI-2 and M-HBPI-3)

End-capping modification has been utilized to improve the solubility of AD-HBPI-1 by terminating the anhydride end groups. The reaction conditions of the synthesis of M-HBPIs were similar to AD-HBPI-1 in terms of monomer concentration (0.03 mol/L), slow addition, high mechanical stirring and low temperature reaction (0 ^{o}C) to avoid the formation of insoluble gel. As can be seen in Figures (5-3), (5-4) and (5-5), a solution of TAPM dissolved in DMAc solvent was added dropwise into the reaction system containing PMDA in DMAc at 0 ^{o}C over 3 h with the monomer molar ratio of 2:0.75 (the molar ratio of anhydride groups to amine groups was 4:3), resulting in anhydride-terminated polyamic acid. After that, an excess amount of aniline, 2-ethylaniline and 2-tert-butylaniline were added to the reaction mixture. It was noted that once the addition of end-cappers was completed, the color of reaction mixture transformed from yellow to colorless. Then, the polymer was chemically converted to polyimide at room temperature using a mixture of acetic anhydride and pyridine, yielding M-HBPI-1, M-HBPI-2 and M-HBPI-3, respectively.

5.3.2.1 FTIR Spectroscopy

The formation of anhydride-terminated polyamic acid (AD-PAA) as intermediate precursor was first confirmed by FTIR spectroscopy as is shown in Figure 5-10. The band at 1714 cm^{-1} is attributed to stretching of the carbonyl group of carboxylic acid, whereas the band at 1667 cm^{-1} relates to carbonyl amide stretching, which are the characteristic peaks reported for hyperbranched polyamic acid based on A_2+B_3 polymerization.[15, 16] Furthermore, the absorption bands at 1853 and 1782 cm^{-1} correspond to asymmetric and symmetric vibration of carbonyl of the anhydride-terminated group in the AD-PAA, respectively. The formation of imide ring for all polymers was indicated by the appearance of the bands at 1777 and 1718 cm^{-1} relating to asymmetric and symmetric vibration of carbonyl group of imide ring, respectively. The band at 1360 cm^{-1} corresponds to C-N stretching of the five-membered imide ring. The disappearance of the band around 1860 cm^{-1} relating to carbonyl stretching of anhydride terminal groups confirms that the end-capping modification using

aniline, 2-ethylaniline, and 2-tert-butylaniline was achieved successfully, as reported for end-capped polyimides based on A_2+B_3.[1, 11, 14, 18]

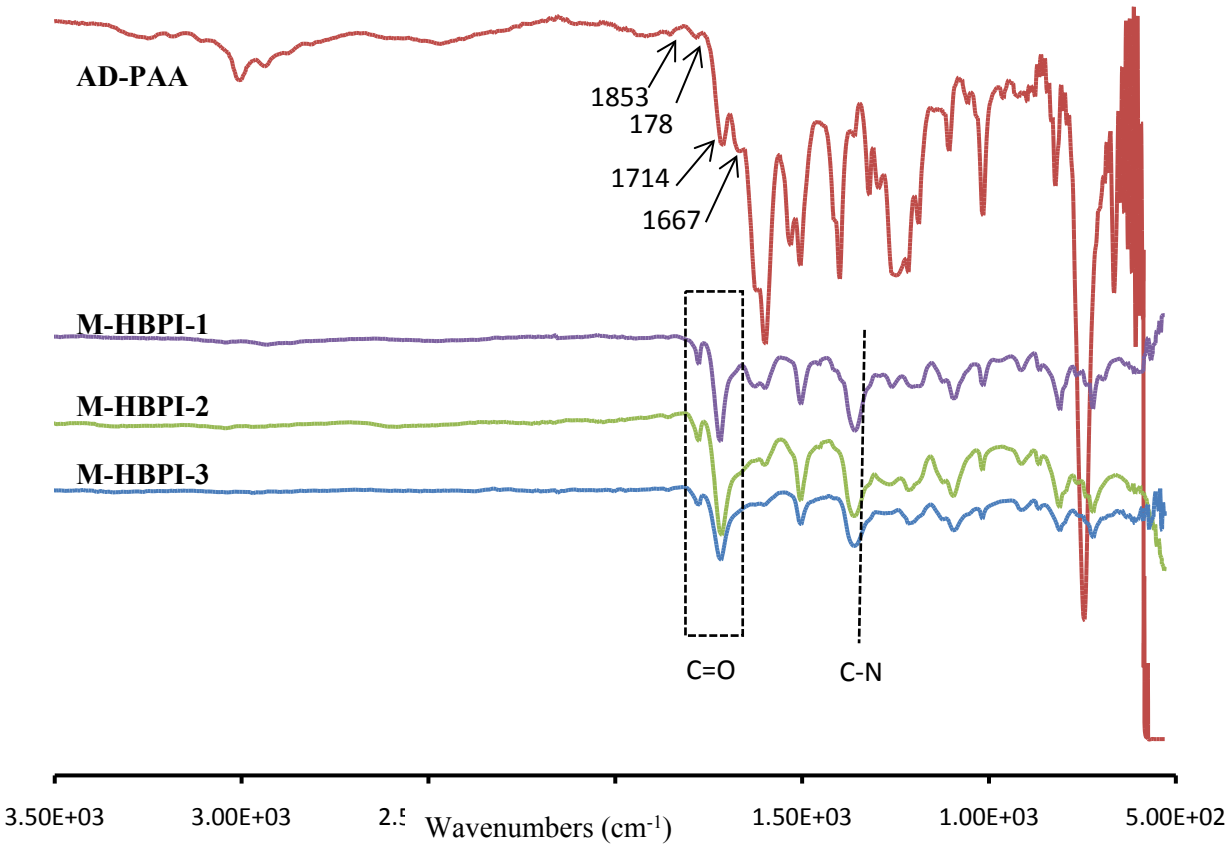

Figure 5-10: FTIR Spectroscopy of AD-PAA and M-HBPIs.

5.3.2.2 Solid State ^{13}C-NMR Spectroscopy

As a result of insolubility of M-HBPIs in any solvents, solid-state ^{13}C NMR spectroscopy was utilized to provide proof of chemical struture of end-capped polyimides. As can be seen in Figure 5-11, for all the modified polyimides, the peak at 63 ppm relates to the quaternary carbon of the tetrahedral center, while the peaks at 144 and 165 ppm are attributed to the N-substituted phenyl carbon and carbonyl carbon of the imide ring, respectively, indicating the formation of imide ring in the all end-capped polymers as proved by FTIR spectroscopy. The broad peaks in the range of 119-136 ppm are assigned to other aromatic carbon atoms in the polymer backbone. The M-HBPI-2 shows peaks at 12 and 22 ppm corresponding to the CH_2 and CH_3 groups of 2-ethylaniline, whereas M-HBPI-3 exhibits two peaks at 31 and 35 ppm relating to the CH_3 and tertiary carbon of 2-tert-butylaniline, confirming that the funtionalizations of anhydride terminated groups using 2-ethylaniline and 2-tert-butylaniline were achieved completely. For M-H-BPI-1, the end-capping modification using aniline gives peaks around 128 ppm, which is difficult to distinguish by solid state ^{13}C-NMR spectroscopy as it appears in the aromatic region. However, FTIR spectroscopy indicated the disappearance of anhydride terminated group, confirming the complete modification.

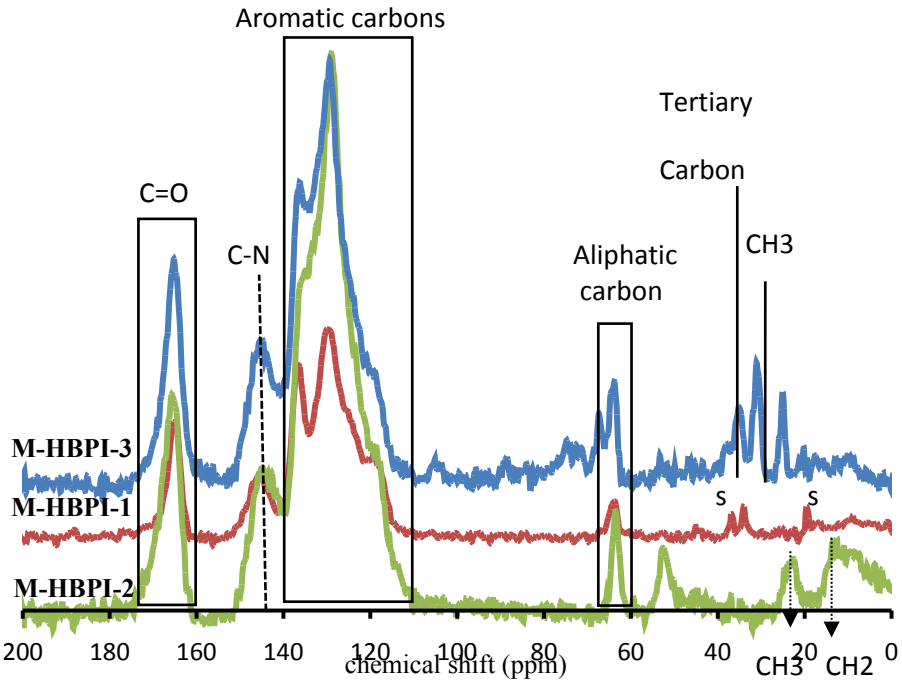

Figure 5-11: ^{13}C Solid-state NMR spectra of M-HBPIs.

5.3.2.3 Thermogravimetric Analysis (TGA)

The thermal stability of M-HBPIs was evaluated using thermogravmetric analysis (TGA) under nitrogen atmosphere as is presented in Figure 5-12. All the modified polyimides show a small degradation step below 100 °C relating to the removal of moisture upon heating.[15] For M-HBPI-1 and M-HBPI-2, the second degradation step can be seen between 150-300 °C, which might be attributed to the remaining solvent and degradation of residual end groups, while the third degradation step above 400 °C is related to presence of high temperature resistant imide units in the structure of polymers.[5] It also indicates that the M-HBPIs were well imidized. However, the incorporation of alkyl groups at the periphery of M-HBPI-3 might cause a decrease in the thermal stability of the polymer.

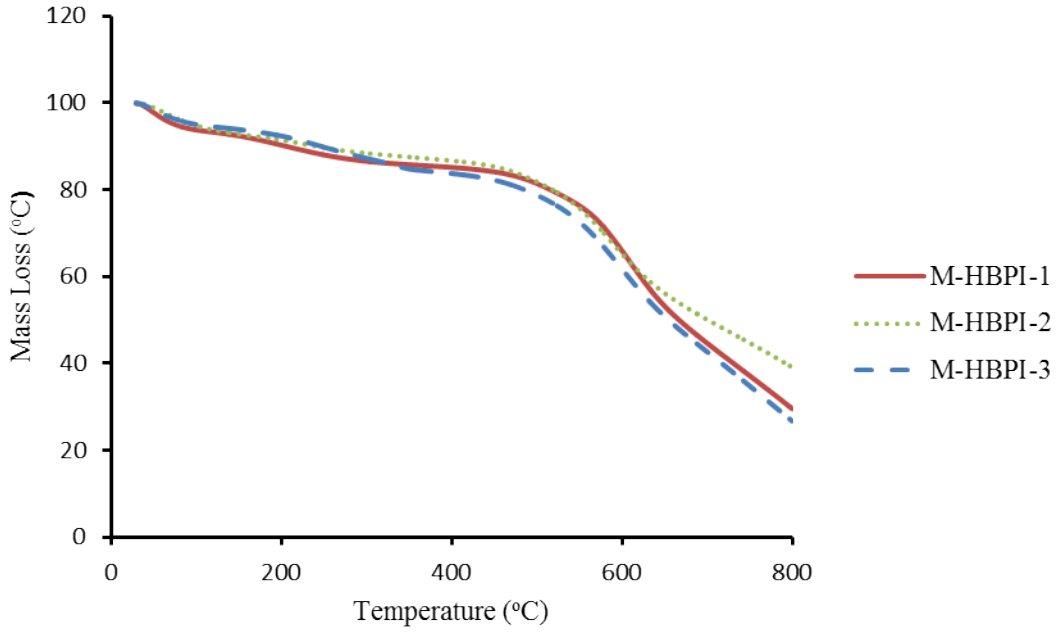

Figure 5-12: Thermal stability of M-HBPIs.

5.3.3 AD-HBI-2

Due to insolubility of AD-HBPI-1 and M-HBPIs in common organic solvents, AD-HBI-2 was prepared with the monomer molar ratio of 2:0.5 between PMDA and TAPM (the molar ratio of anhydride groups to amine groups was 4:2), aiming to decrease the extent of polymer structure. Thus, enhancing the solubility. The same reaction conditions were followed as described previously in the synthesis of AD-HBPI-1 and M-HBPIs in terms of low monomer concentration (0.03 mol/L), slow addition, high mechanical stirring and low temperature (0 ^{o}C). As can be seen in Figure 5-6, a solution of TAPM in DMAc was added slowly to a solution of PMDA dissolved in DMAc over 3 h, yielding anhydride-terminated polyamic acid (AD-PAA). Then, the polymer was imidized chemically to anhydride-terminated imide compound using a mixture of acetic anhydride and pyridine.

5.3.3.1 FTIR Spectroscopy

The FTIR spectroscopy was utilized to characterize the structure of AD-PAA and AD-HBI-2 (Fig. 5-13). The absorption band at 1713 cm^{-1} relates to stretching of the carbonyl group of carboxylic acid, whereas the peak at 1677 cm^{-1} corresponds to carbonyl stretching of amide group. The bands at 1853 and 1782 cm^{-1} are attributed to asymmetric and symmetric stretching of carbonyl of the anhydride-terminated group, respectively, confirming the formation of anhydride-terminated polyamic acid as intermediate precursor. The appearance of bands at 1779 and 1718 cm^{-1} are assigned to asymmetric and symmetric stretching from imide carbonyl groups. The band at 1361 cm^{-1} relates to imide C-N group, indicating the formation of imide ring in the structure of compound. The band at 1860 cm^{-1} is attributed to the stretching of carbonyl of the terminated anhydride group.

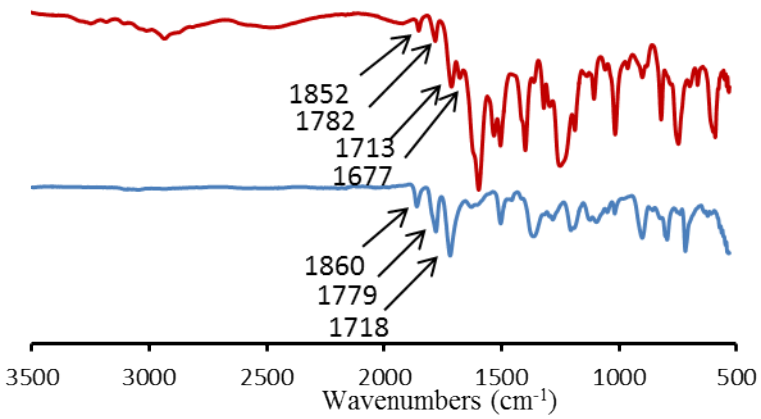

Figure 5-13: FTIR spectrum of AD-PAA-2(top, red) and AD-HBI-2(bottom, blue).

5.3.3.2 ^{1}H NMR Spectroscopy

The chemical structure of AD-HBI-2 was further characterized using ^{1}H NMR spectroscopy as is shown in Figure 5-14. It is expected that there should be two doublet peaks in the range 7-7.30 ppm corresponding to protons in the phenyl rings of TAPM monomer. However, due to overlapping peaks, a broad peak appeared in the range 7.53-7.56 ppm that relates to protons in the phenyl rings of tetrahedral core, whereas the peak around 8.15 ppm corresponds to protons in the phenyl rings of PMDA monomer.

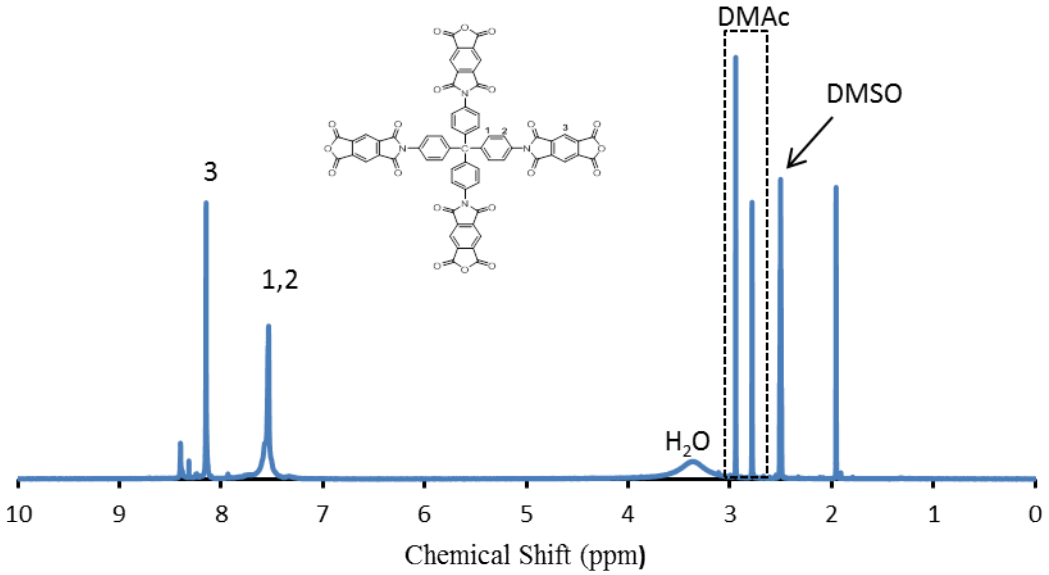

Figure 5-14: ^{1}H-NMR Spectrum of AD-HBI-2.

5.3.3.3 Thermogravimetric Analysis (TGA)

The thermal stability of AD-HBI-2 was investigated using thermogravimetric analysis (TGA) under nitrogen atmosphere. As is shown in Figure 5-15, AD-HBI-1 shows high thermal stability up to 450 ^{o}C, retaining about 57% of weight at 800 ^{o}C, which is comparable to the reported anhydride-hyperbranched polyimides based on A_2+B_3 polymerization.[5, 10] The good thermal stability of AD-HBI-1 can be related to the presence of rigid tetrahedral shape and high temperature resistant imide units in the polymer backbone. The weight loss between 150-300 ^{o}C can be attributed to the remaining solvent and residual end groups.

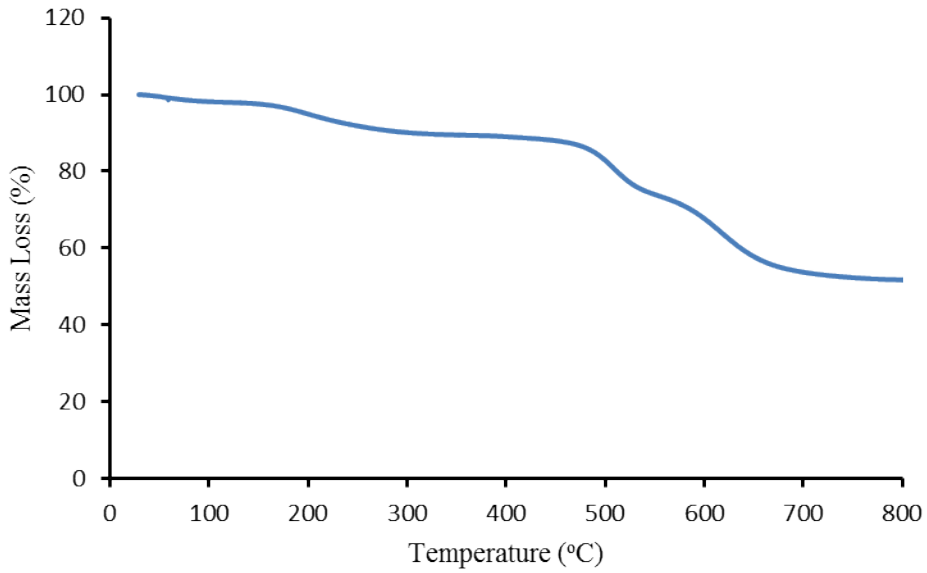

Figure 5-15: TGA of AD-HBI-2.

5.3.3.4 CO_2 Adsorption in AD-HBPIs and M-HBPIs

The CO_2 adsorption properties of AD-HBPIs and M-HBPIs were measured at 298 K and in the pressure range from 0 to 8 bar, as are presented in Figure 5-16. It is known that the introduction of nitrogen and oxygen atoms can enhance the uptake capacity of CO_2 due to dipole-quadruple interaction between CO_2 and nitrogen sites in the polymer skeleton.[19, 20] AD-HBPI-1 shows high CO_2 uptake of 4.43 mmol g^{-1} compared to AD-HBI-2, which might be attributed to the difference in the molar ratio of amine, as for AD-HBPI-1 the molar ratio between PMDA and TAPM is 2:0.75 whereas for AD-HBI-2, the molar ratio between PMDA and TAPM monomers is 2:0.5. As a result, AD-HBPI-1 contains more nitrogen and oxygen atoms. Thus, increasing the affinity of polymer skeleton towards CO_2. It was expected that the end-capping modification using aniline, 2-ethylaniline and 2-tert-butylaniline should increase the capacity of CO_2 adsorption as the contents of nitrogen increases. However, it is found that there was no improvement in the uptake of CO_2.

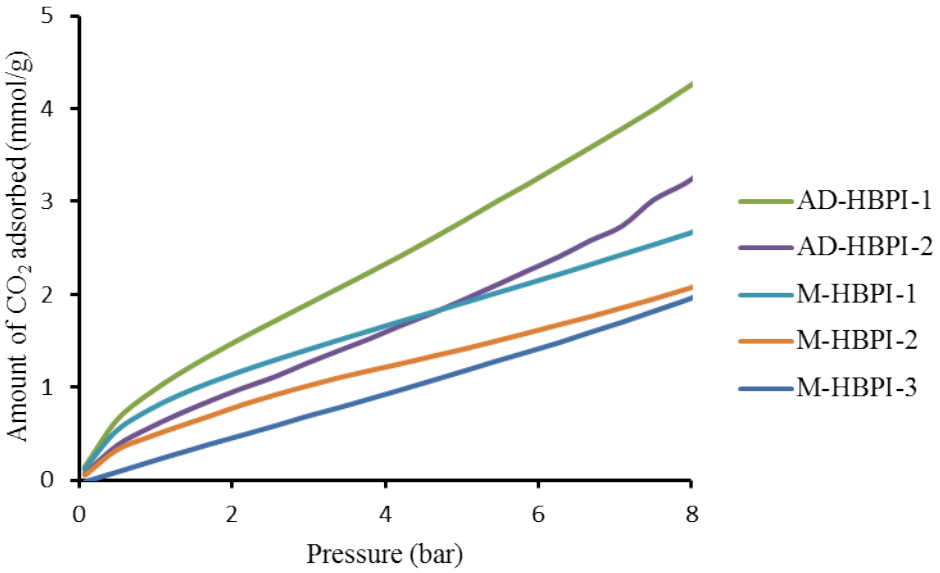

Figure 5-16: The CO_2 adsorption isotherms of AD-HBPIs and M-HBPIs at 298K.

5.3.3.5 Solubility of AD-HBPIs and M-HBPIs

The solubility of prepared samples was tested using a range of organic solvents by dissolving 10 mg of polymer in 5 mL of solvent at room temperature and upon heating. The results are shown in Table 5-1 and determined by visual observation. It was found that AD-HBPI-1 was insoluble in common polar aprotic solvents such as DMAc, NMP, DMF and DMSO at room temperature and upon heating. Furthermore, it was insoluble in cyclic ethers solvents such as THF and chlorinated solvents such as chloroform, both at room temperature and even upon heating. On the other hand, AD-HBI-2 was soluble in polar aprotic solvents such as DMAc, NMP, DMF and DMSO at room temperature, but was insoluble in chloroform and THF solvents. It can be attributed to the difference in the molar ratio between anhydride and amine as AD-HBPI-1 contains more of TAPM as a rigid tetrahedral core linked with four phenyl rings, which might increase the stiffness of polymer chains, decreasing the solubility of polymer. For AD-HBPI-1 the molar ratio between PMDA and TAPM is (2:0.5), resulting in a structure which contains less TAPM. For M-HBPIs, the introduction of aniline, 2-ethylaniline and 2-tert-butylaniline at the end of polymer chains showed no improvement.

Table 5-1: Solubility of AD-HBPIs and M-HBPIs. (-) shows that the polymer is insoluble at room temperature and upon heating, (+) shows the polymer soluble at room temperature.

Polymer	Solvent					
	THF	$CHCl_3$	DMAc	NMP	DMF	DMSO
AD-HBPI-1	-	-	-	-	-	-
M-HBPI-1	-	-	-	-	-	-
M-HBPI-2	-	-	-	-	-	-
M-HBPI-3	-	-	-	-	-	-
AD-HBI-2	-	-	+	+	+	+

5.4 Summary

In this chapter, anhydride-terminated hyperbranched polyimide (AD-HBPI-1) was prepared from PMDA (A_2) with TAPM (B_4) by changing the molar ratio. No gelation was observed during the polymerization due to low monomer concentrations, high mechanical stirring, slow addition and low temperature. FTIR spectroscopy confirmed the conversion of amic acid to imide ring and formation of anhydride-terminated end groups. The formation of imide ring was further indicated by solid state ^{13}C-NMR spectroscopy. AD-HBI-1 showed good thermal stability up to 400 ^{o}C. However, it was insoluble in common organic solvents. Then, end-capping modification was performed to increase the solubility of AD-HBPI-1 using aniline, 2-ethylaniline, and 2-tert-butylaniline as end-cappers. FTIR and solid State ^{13}C-NMR Spectroscopy confirmed successful modification. Though, the M-HBPIs were insoluble in polar aprotic solvents. A polymerization was carried out with monomer molar ratio of 2: 0.5 between PMDA and TAPM. The resulting was an organic compound as confirmed by ^{1}H NMR spectroscopy. The compound was terminated with anhydride as indicated by FTIR spectroscopy. It showed a good solubility at room temperature in the common aprotic solvents. However, AD-HBPI-1 showed high CO_2 uptake compared to AD-HBI-2 and M-HBPIs.

5.5 References

1. H. Chen, J. Yin and H. Xu, Synthesis of Arenesulfonated hyperbranched polyimide from A_2 + B_3 monomers*, Polymer Journal*, 2003, **35**, 280-285.
2. S-J. Park, K. Li and F-L. Jin, Synthesis and characterization of hyperbranched polyimides from 2,4,6-triaminopyrimidine and dianhydrides system, *Materials Chemistry and Physics*, 2008, **108**, 214-219.
3. Y. Chen, Q-Y. Zhang, N. Ali, J. Ren and J-L. Sun, Synthesis and properties of hyperbranched polyimides from A_2+B ʹB_2 monomers and A_2+ B ʹB_2 +B_2 monomers with various commoner ratios., *J Polym Res*., 2012, **19**, 9858.
4. Y. Chen, Q. Zhang, W. Sun, X. Lei and P. Yao, Synthesis, characterization and properties of TAP-6FDA hyperbranched polyimides with different branching degrees, *Polym Int*., 2014, **63**, 788-795.
5. Q. Li, H. Xiong, L. Pang, Q. Li, Y. Zhang, W. Chen, Z. Xu and C. Yi, Synthesis and characterization of thermally stable, hydrophobic hyperbranched polyimides derived from a novel triamine High Performance, *Polymers*, 2014, **27**, 426-438.
6. Y. Chen, Q. Zhang, W. Sun, X. Lei and P. Yao, Synthesis and gas permeation properties of hyperbranched polyimides membranes from a novel (A_2+ B_2 ʹB + B_2)-type method, *J. Membr. Sci.*, 2014, **450**, 138-146.
7. Y. Yin, L. Yang, M.Yoshino, J. Fang, K. Tanaka, H. Kita and K-I. Okamoto, Synthesis and gas permeation properties of star-like poly(ethylene oxide)s using hyperbranched polyimide as central core, *Polym. J.*, 2004, **36**, 294-302.
8. E. Minko, P. Sysel, M. Spergl and P. Slapakova, Hyperbranched polyimides prepared from 4,4',4"- triaminotriphenylmethane and mixed matrix materials based on them, In Tech., 2012, DOI: 10.5772/2834.
9. G. Odian, Principles of polymerization, John Wiley & Sons, Inc., New Jersy, 2004.
10. J. Fang, H. Kita and K-I. Ohamoto, Hyperbranched polyimides for gas separation applications.1. Synthesis and characterization, *Macromolecules*, 2000, **33**, 4639-4646.
11. H. Chen and J. Yin, Synthesis and characterization of hyperbranched polyimides with good organosolubility and thermal properties based on a new

triamine and convensional dianhydride, *J. Polym Sci, A:Polym Chem*., 2002, **40**, 3804-14.

12. J. Hao, M. Jikei and M-A. Kakimoto, Preparation of hyperbranched aromatic polyimides via A_2+B_3 appraoch, *Macromolecules*, 2002, **35**, 5372-5381.
13. S. B. Mhaske, R. V. Bhingarkar, M.B. Sabne, R. Mercier, S. P. Vernekar, Synthesis and characterization of end-capped polyimides and their gas permeability properties, *J. Appl. Polym. Sci*., 2000, **77**, 627-635.
14. H. Chen and J. Yin, Synthesis of autophotosensitive hyperbranched polyimides based on 3,3',4,4'-benzophenonetertracarboxylic dianhydride and 1,3,5-tris(4-aminophenoxy)benzene via end capping of the terminal anhydride groups by ortho-alkyl aniline, *J. Polym Sci., A:Polym Chem*., 2003, **41**, 2026-2035.
15. W. Chen, W. Tan, S. Wu, Z. Xu, k. W. K. Yeung and C. Yi, Preparation and properties of novel triphenylpyridine-containing hyperbranched polyimides derived from 2,4,4-tris(4-aminophenyl)pyridine under microwave irradiation, *Macromol. Chem. Phys,* 2010, **211**, 1803-1813.
16. J. Shen, Ying, Zhang, W.Chen, W. Wang, Z. Xu, K. Yeung and C. Yi, Synthesis and properties of hyperbranched polyimides derived from novel triamine with prolonged chain segments, *J. Poly. Sci. A: Polym. Chem*., 2013, **51**, 2425-2437.
17. P. Arab, M. Gulam. Rabbani, A. K. Sekizkardes, T. islamoglu and H. M. El-Kaderi, Copper (I)-catalysed synthesis of nanoporous azo-linked polymers: Impact of textural properties on gas storage and selective carbon dioxide capture, *Chem, Mater*., 2014, **26**, 1385-1392.
18. H. Chen and J. Yin, Synthesis and characterization of negative-type photosensitive hyperbranched polyimides with excellent organosolubility from an A_2+B_3 monomer system, *J. Polym Sci, A: Polym Chem*., 2004, **42**, 1735-1744.
19. G. Li and Z. Wang, Naphthalene-based microporus polyimides: Adsorption behavior of CO2 and toxic vapors and their separation from other gases, *J. Phys. Chem*., 2013, **117**, 24428-24437.
20. K. V. Rao, R. Haldar, T. K. Maji and S. J. George, Porous polyimides from polycyclic aromatic linkers: selective CO_2 capture and hydrogen storage, *Polymer*, 2014, **55**, 1452-1458.

Chapter 6

Conclusions and Recommendations for Future Work

6.1 Conclusions

The work set out to prepare MMMs using PIM-1 as a continuous phase with network polyimide fillers, to investigate their effects on the gas transport properties of MMMs. PIM-1 has been prepared successfully using two different synthetic methods. Both methods gave structurally similar polymers as proved by FTIR spectroscopy and ^{1}H NMR spectroscopy. The N_2 sorption analysis revealed that both polymers showed comparable surface areas. However, PIM-1 prepared by high temperature method has higher molecular weight in comparison to low temperature method relating to reaction conditions.

MPN-1 was synthesized using previously reported procedure. However, a change in polymerization conditions, such as concentration, might have an effect on the surface area of the polymer. MPN-2 was prepared for the first time using two different methods. The data revealed that the chemical structure and BET surface area of MPN-2 prepared by both methods were comparable.

MMMs were fabricated using 10, 20, and 30 wt. % loadings of MPN-1 and MPN-2. The presence of fillers in the membranes was confirmed by PXRD as well as FTIR spectroscopy. The SEM images indicated a homogenous dispersion of PIM-1/MPN-1 was achieved throughout the membrane. However, at 20 wt. %, some agglomerates was seen which might be attributed to poor dispersion of filler. The SEM images of PIM-1/NP-2 MMMs showed a good dispersion of filler even at high loadings due to good chemical affinity between two organic filler and polymer matrix.

The CO_2 uptake was measured for both fillers. It was found that at low pressure (1 bar), MPN-1 showed high CO_2 uptake compared to MPN-2 due to presence very small pores (ultramicropores, < 0.7 nm). The gas transport properties of MMMs were measured using time lag method. The MMMs were tested before and after alcohol treatment. The data showed a large enhancement in both the permeability and diffusivity of gases as alcohol treatment flush out any residual solvents as well as swelling the polymer. Thus, creating more free volume.

Anhydride-terminated hyperbranched polyimide (AD-HBPI-1) was prepared from PMDA (A_2) with TAPM (B_4) by changing the molar ratio. No gelation was observed during the polymerization as a result of low monomer concentrations, high mechanical stirring, slow addition rate and low temperature. However, AD-HBPI-1

was insoluble in common polar aprotic solvents. End-capping modification was performed to increase the solubility of AD-HBPI-1 using aniline, 2-ethylaniline, and 2-tert-butylaniline as end-cappers. FTIR and solid State ^{13}C-NMR Spectroscopy confirmed successful modification. Though, the M-HBPIs were insoluble in polar aprotic solvents. A polymerization was carried out with monomer molar ratio of 2: 0.5 between PMDA and TAPM. The resulting was an organic compound as confirmed by ^{1}H NMR spectroscopy. It showed a good solubility in the common aprotic solvents. However, The CO_2 uptake of AD-HBPI-1 was higher compared to M-HBPIs.

6.2 Recommendations for Future Work

Further work can be done to study the effect of MPN-2 on the aging process of PIM-1. It is expected that the good chemical affinity between PIM-1 and MPN-2 offer the opportunity to freeze the structure. Thus, stopping the physical aging of PIM-1 over time with increasing the permeability and selectivity.

The synthesis of hyperbranched polyimides with terminated amine groups can be investigated to study the effect of amine end groups on CO_2 sorption properties and to examine their effect on the enhancing the solubility of polymer. Fabrication of MMMs can be explored utilizing PIM-1 as polymer matrix with anhydride and amine-terminated polyimide as dispersed phase using different molar ratios to investigate the effect of end groups on the gas sorption and permeation properties of MMMs.

Appendix A: PIM-1 membrane and PIM-1/NP-1 MMMs data

PIM-1 membrane, PIM-1/NP-1 MMMs ratio and treatment	Permeability (Barrer)						Selectivity				
	N_2	CH_4	O_2	He	H_2	CO_2	P_{CH4}/P_{N2}	P_{O2}/P_{N2}	P_{He}/P_{N2}	P_{H2}/P_{N2}	P_{CO2}/P_{N2}
PIM-1 membrane as cast	208.00	286	833	1217	2760	4551	1.37	4	5.85	13.26	21.87
PIM-1 membrane methanol treatment	375	472	1362	1653	4011	7616	1.25	3.63	4.4	10.69	20.3
PIM-1/NP-1 MMM 90:10 as cast	101	138	383	641	1322	2156	1.36	3.79	6.34	13.08	21.34
PIM-1/NP-1 MMM 90:10 methanol treatment	172	231	676	1093	2365	3833	1.34	3.93	6.35	13.75	22.28
PIM-1/NP-1 80:20 as cast	41	62	177	441	807	992	1.51	4.31	10.75	19.68	24.19
PIM-1/NP-1 MMM 80:20 methanol treatment	104	129	423	821	1678	2249	1.24	4.06	7.89	16.13	21.62
PIM-1/NP-1 MMM 70:30 as cast	89	126	299	509	1044	1826	1.41	3.35	5.71	11.73	20.51
PIM-1/NP-1 MMM 70:30 methanol treatment	68	92	502	5111	8777	2361	1.35	7.38	75.16	129.07	34.72

Appendix B: PIM-1 membrane and PIM-1/NP-1 MMMs data

PIM-1 membrane, PIM-1/NP-1 MMMs, ratio and treatment	Diffusion (10^{-12} m^2 s^{-1})						Solubility (cm^3 cm^{-3} bar^{-1})					
	N_2	CH_4	O_2	He	H_2	CO_2	N_2	CH_4	O_2	He	H_2	CO_2
PIM-1 membrane as cast	13.90	42.4	153.1	2472.1	1859.9	58.4	15.41	3.68	4.08	0.37	1.11	58.45
PIM-1 membrane methanol treatment	70.42	20.82	235.77	2472.1	1859.9	58.4	4	16.99	4.33	0.45	1.16	61.15
PIM-1/NP-1 MMM 90:10 as cast	39	14	125	2071	1598	49	2.83	12.02	3.18	0.28	0.78	47.63
PIM-1/NP-1 MMM 90:10 methanol treatment	50	17	172	2290	1788	64	2.59	10.46	2.94	0.36	0.99	44.85
PIM-1/NP-1 MMM 80:20 as cast	9.75	3.63	37.24	1658.6	885.87	13.75	3.15	12.82	3.56	0.2	0.68	54.12
PIM-1/NP-1 MMM 80:20 methanol treatment	24.82	7.43	80.72	2171.3	1458.2	28.71	3.14	13.06	3.93	0.28	0.86	58.75
PIM-1/NP-1 MMM 70:30 as cast	25.32	8.35	81.62	2275.9	1424.1	28.34	2.75	11.34	2.75	0.17	0.55	48.31
PIM-1/NP-1 MMM 70:30 methanol treatment	54.23	33.56	122.43	3851.2	3698.5	40.83	0.94	2.05	3.07	1	1.78	43.36

Appendix C: PIM-1 membrane and PIM-1/NP-2 MMMs data

PIM-1 membrane, PIM-1/NP-1 MMMs ratio and treatment	Permeability (Barrer)						Selectivity				
	N_2	CH_4	O_2	He	H_2	CO_2	P_{CH4}/P_{N2}	P_{O2}/P_{N2}	P_{He}/P_{N2}	P_{H2}/P_{N2}	P_{CO2}/P_{N2}
PIM-1 membrane as cast	208.00	286	833	1217	2760	4551	1.37	4	5.85	13.26	21.87
PIM-1 membrane methanol treatment	375	472	1362	1217	4011	7616	1.25	3.63	3.24	10.69	20.3
PIM-1/NP-1 MMM 90:10 as cast	296	383	1230	1498	3338	6057	1.29	4.15	5.06	11.27	21.24
PIM-1/NP-1 MMM 90:10 methanol treatment	422	605	1533	1698	4475	8676	1.43	3.63	4.02	10.6	20.55
PIM-1/NP-1 80:20 as cast	333	390	1093	2165	4835	7460	1.17	3.28	6.5	14.51	21.37
PIM-1/NP-1 MMM 80:20 methanol treatment	676	892	2126	2471	5858	12403	1.31	3.14	3.65	8.66	18.34
PIM-1/NP-1 MMM 70:30 as cast	208	296	881	1366	3085	4723	1.42	4.23	6.56	14.83	22.7
PIM-1/NP-1 MMM 70:30 methanol treatment	641	792	2161	3504	7583	12144	1.23	3.37	5.46	11.82	18.94

Appendix D: PIM-1 membrane and PIM-1/NP-2 MMMs data

PIM-1 membrane, PIM-1/NP-1 MMMs, ratio and treatment	Diffusion (10^{-12} m^2 s^{-1})						Solubility (cm^3 cm^{-3} bar^{-1})					
	N_2	CH_4	O_2	He	H_2	CO_2	N_2	CH_4	O_2	He	H_2	CO_2
PIM-1 membrane as cast	42.40	13.9	153.1	2472.1	1859.9	58.4	3.68	15.41	4.08	0.37	1.11	58.45
PIM-1 membrane methanol treatment	70.42	20.82	235.77	2752	2594	93.42	4	16.99	4.33	0.45	1.16	61.15
PIM-1/NP-1 MMM 90:10 as cast	69.21	21.34	267.3	3454.2	2443.7	90.38	3.21	13.47	3.45	0.33	1.02	50.27
PIM-1/NP-1 MMM 90:10 methanol treatment	108.1	37.3	344.2	3745	3154.4	134.2	2.93	12.18	3.34	0.37	1.06	48.51
PIM-1/NP-1 MMM 80:20 as cast	89.4	25.9	310.2	4151.2	3546.5	118.7	2.79	11.3	2.64	0.93	1.02	47.13
PIM-1/NP-1 MMM 80:20 methanol treatment	141	42	393	4276	3547	164	3.61	15.85	4.06	0.43	1.24	56.59
PIM-1/NP-1 MMM 70:30 as cast	60.12	19.87	216.58	4388.3	3433.3	73.51	2.6	10.16	3.05	0.23	0.67	48.19
PIM-1/NP-1 MMM 70:30 methanol treatment	148.94	50.23	432.42	5348.9	4598.4	165.07	3.23	11.82	3.75	0.49	1.24	55.18